ISSN 2074-272X

науково-практичний журнал 2017/5

Електротехніка і Електромеханіка

Electrical Engineering & Electromechanics

Електротехніка. Визначні події. Славетні імена
Електротехнічні комплекси та системи. Силова електроніка
Теоретична електротехніка та електрофізика
Техніка сильних електричних та магнітних полів. Кабельна техніка
Електричні станції, мережі і системи
Ювілеї

За 2015р. журнал отримав індекс 83.98 від міжнародної наукометричної бази Index Copernicus

«ELECTRICAL ENGINEERING & ELECTROMECHANICS»

SCIENTIFIC & PRACTICAL JOURNAL

Journal was founded in 2002

Founders:

National Technical University «Kharkiv Polytechnic Institute» (Kharkiv, Ukraine)

State Institution «Institute of Technical Problems of Magnetism of the NAS of Ukraine» (Kharkiv, Ukraine)

ISSUE 5/2017

TABLE OF CONTENTS

Editorial office address: Dept. of Electrical Apparatus, NTU «KhPI», Kyrpychova Str., 2, Kharkiv, 61002, Ukraine
phones: +380 57 7076281, +380 67 3594696, **e-mail:** a.m.grechko@gmail.com (**Grechko O.M.)**

ISSN (print) 2074-272X
ISSN (online) 2309-3404

Printed 20.10.2017. Format 60 x 90 ⅛. Paper – offset. Laser printing. Edition 200 copies. Order no.66/172-05-2017.

Printed by Printing house «Madrid Ltd» (11, Maksymilianivska Str., Kharkiv, 61024, Ukraine)

UDC 621.3: 537.8: 910.4 **doi: 10.20998/2074-272X.2017.5.01**

M.I. Baranov

AN ANTHOLOGY OF THE DISTINGUISHED ACHIEVEMENTS IN SCIENCE AND TECHNIQUE. PART 40: THE SCIENTIFIC OPENING OF THE METHOD OF EXPLOSIVE IMPLOSION FOR THE OBTAINING ABOVE CRITICAL MASS OF NUCLEAR CHARGE AND UKRAINIAN «TRACK» IN THE «MANHATTAN» AMERICAN ATOMIC PROJECT

Purpose. *Preparation of short scientifically-historical essay about the prominent American scientist-chemist and physicist George Bogdan Kistiakowsky, having the Ukrainian «roots» and bringing in a considerable scientific and technical contribution to development and creation of the first atomic bombs in the USA.* ***Methodology.*** *Scientific methods of collection, analysis and analytical treatment of the opened scientific and technical information of world level in area of atomic and nuclear physics, physics of hyperpessure, applied electrophysics, modern experimental physics, atomic science and technology.* ***Results.*** *The state-of-the-art review of the state of basic scientific and technical problems, arising up before scientists and engineers at development and creation within the framework of the «Manhattan» American atomic project of the first standards of atomic bombs of the USA is resulted. Two basic methods of receipt in the a-bomb of above critical mass of the divided nuclear material of military load are described: method of «cannon-shot» and method of «explosive implosion». Basic information is resulted about the declassified scheme and construction decisions, applied scientists and specialists in the first atomic bombs of the USA. Technical information is indicated about basic ordinary hard chemical explosive matters (EM), atomic bombs of the USA of implosend type utillized in the first.* ***Originality.*** *Systematization of the scientific and technical materials devoted the basic results of pioneer nuclear researches in the USA and USSR in the period of 1940-th on a capture above all things for soldiery aims by intranuclear energy and to the offensive on a planet Earth of nuclear era known from the opened sources is executed. The important role of the scientific ukrainian origin of G.B. Kistiakowsky in development and creation in the National nuclear center of the USA − Los-Alamos of laboratory of the first implosend atomic bombs of the USA. The large deposit of the American scientist is marked in area of physical chemistry, of theory and practice chemical EM G.B. Kistiakowsky in a fight for stopping in the world of race of armaments and nuclear disarmament.* ***Practical value.*** *Popularization and deepening for students, engineer and technical specialists and research workers of scientific and technical knowledges in area of nuclear physics, modern experimental physics, atomic science and technology, extending their scientific range of interests and further development of scientific and technical progress in human society.* References 21, figures 10.

Key words: **history of creation in the USA and USSR of the first standards of nuclear weapon, atomic bomb, critical mass of nuclear explosive, nuclear explosion, methods of «cannon-shot» and «explosive implosion» for an atomic bomb, chemical explosive matter**, **scientific achievements, nuclear disarmament**.

Приведен научно-исторический очерк о выдающемся американском ученом-химике и физике Джордже Богдане Кистяковском, имевшем украинские «корни» и внесшем огромный вклад в разработку и создание первых атомных бомб США. Благодаря его научным достижениям в области изобретения новых химических взрывчатых веществ и успешному развитию им метода взрывной имплозии в 1945 году была реализована на практике теория ядерного взрыва. Отмечены усилия этого ученого в последние десятилетия его жизни в борьбе за прекращение в мире гонки вооружений и ядерное разоружение. Библ. 21, рис. 10.

Ключевые слова: **история создания в США и СССР первых образцов ядерного оружия, атомная бомба, ядерный взрыв, метод взрывной имплозии и бомба, научные достижения, ядерное разоружение.**

Introduction. The world history of mastery in the first half of the 20th century by outstanding scientists and engineers of the genus of human intranuclear energy and its further military-strategic use, because of its specificity and closeness, contains more than one dozen little-known, interesting and interesting for the general reader scientific and technical facts. One of such facts in 2015 was reported by our metropolitan newspaper «Zerkalo Nedeli» [1, 2]. It dealt essentially with Ukraine (then in the early 20th century from the Russian Empire) George Bogdan (Georgy Bogdanovich) Kistiakowsky, an outstanding American expert in the field of physical chemistry and solid explosives, who made a huge contribution to the creation of the first US atomic bombs and practical implementation of the theory of nuclear explosion [3]. What exactly did the Ukrainian G.B. Kistiakowsky (Fig. 1), so valuable and important for the onset of the atomic era on our planet, do? We will try to follow below with the use of exclusively open sources and messages from the World Wide Web in a concentrated form of a brief scientific and historical essay to trace the milestones of the life and creative path of this legendary scientist of the United States, who stood at the very origins of the creation and creation of the most terrible weapons in the history of mankind.

1. The beginning of the way. George Kistiakowsky was born on November 18, 1900 in the family of Professor of law at Kiev University Bogdan Aleksandrovich Kistiakowsky and his wife Maria (nee Berenshtam) [4]. He received his secondary education in private schools in Kiev. In the autumn of 1918 he joined the White Army and until the autumn of 1920 participated in military operations. After the defeat of Wrangel's

forces in the Crimea, he first came to Turkey, and then to Germany. In 1921 he entered the University of Berlin on Chemical Faculty, which he graduated from in 3.5 years. In 1925, under the scientific guidance of Prof. M. Bodenstein he successfully defended a Doctoral Thesis at this University on the topic of the problem of the decomposition of chlorine oxide with the help of a flux of light radiation [3]. In 1926, as a scholar of the International Committee for Education in Physical Chemistry, he was sent to the Princeton University (USA) for scientific internship [4].

Fig. 1. Prominent American chemist and physicist George Bogdan Kistiakowsky (1900-1982), one of the main inventors and creators of the first atomic bombs of the USA of implosive type [3]

According to the results of the research, in 1928 he published his first scientific monograph «*Photochemical Processes*» in the United States, which brought the young scientist to fame in the field of photochemistry. Since 1930, as a Professor, he began teaching chemistry at Harvard University (Boston, USA), with whom he was associated for the rest of his life. In 1933 G.B. Kistiakowsky accepted US citizenship and began to bear a new name - George Bogdan Kistiakowsky. During the Second World War he dealt exclusively with military scientific and technical issues [3, 4]. He had an active civil position and was an ardent opponent of German fascism. Therefore, in those war years, this scientist concentrated all his physical, moral and creative forces on works directly aimed at the victory over Germany. Since 1941 G. Kistiakowsky became a member of the Committee on Atomic Energy of the National Academy of Sciences of the United States. In this Academy of Sciences of the USA he was elected for scientific merits in the field of studying chemical explosive matters (EM). In 1942, he headed the Department for the development and testing of conventional chemical explosives at the National Defense Research Committee of the United States [3, 4].

2. Manhattan Project of the USA. It is known that the pioneers of the nuclear era on the planet Earth were the two most powerful countries in the world - the US and the USSR. For this purpose, their most outstanding physicists, at first, developed theoretical models of nuclear-physical processes and nuclear warheads of a new type of weapons of enormous destructive power. Their scientists and engineers have conducted numerous experiments on physical and technical stands to determine a number of nuclear constants. Historically, in the practical creation of the first nuclear weapons (at the stage of work on the production of atomic bombs), large-scale issues have come to the fore, connected with the organization in these developed countries of a fundamentally new type of industry - the nuclear industry, which requires huge capital investments and completely new technologies for the production of fissionable nuclear materials, and other necessary for the realization of the unprecedented enormous scientific and military tasks of the accompanying materials of nuclear (super high) purity [5].

In the United States, to achieve this goal in the shortest time (with the first persons from the political leadership of the country and the outstanding physicists of the world on its territory constantly remembered similar searches in Germany for the creation of such a superweapon) after the signing by President Franklin Roosevelt on January 19, 1942 the American government, in complete secrecy, launched a decree on the conduct of work on the creation of an atomic bomb in the United States by the US «Manhattan» Atomic Project widely known to many of us [1-6]. Since the autumn of 1942, to intensify the whole complex of closed works and transfer them to a practical plane, this scientific and technical project of a huge military purpose was transferred directly to the American army. His administrative leader was appointed Brigadier General of the US Army 46-year-old Leslie Groves [5-7]. As a scientific supervisor of the project, from the autumn of 1943, at the request of L. Groves, a 39-year-old theoretical physicist from the University of California (Berkeley, USA), Professor Robert Oppenheimer (1904-1967) [5-8]. This scientist-physicist was simultaneously appointed director of the new National Nuclear Center of the United States, a super-secret Los Alamos Scientific Laboratory located in the desert area of New Mexico, which deals exclusively with the development and creation of the first atomic bombs in the USA [5-8]. In the Manhattan project, in fact, an international team of leading physicists and specialists from all over the world (naturally except physicists in the USSR and Germany), including 12 Nobel Prize Laureates in physics and chemistry, took part [7, 9]. More than 130 thousand people were involved in the work of this project. All financial costs of the project were written off to the virtually existing Manhattan engineering district, whose command was General L. Groves (hence, obviously, according to the cover secret developed by the US secret services, and the name of this super-secret project took place). The incurred monetary costs for the implementation of this superproject for the period 1942-1945 amounted to a huge for those times the amount -

about 2 billion USD (in current prices it is about 63 billion USD) [9]. Note that in 1944, the United States gross domestic product (GDP) was about 1499 billion USD [9]. For comparison, it should be noted that during this period Germany's GDP was about 437 billion USD, the USSR's GDP was 362 billion USD, Britain's GDP was 346 billion USD and Japan's was 189 billion USD. From these economic data it is clear that in 1944 the US GDP exceeded the GDP of Germany, the USSR, Great Britain and Japan combined. To this, it is necessary to add that the United States, after the occupation by the German troops of France in 1940 (before this event, France, with its world-famous school of nuclear physicists headed by Frederic Joliot-Curie, occupied the leading position in the scientific world on the Uranium problem) Concentrate from the Belgian Congo (countries in Central Africa) in the volume of about 1200 tons, as well as serious calculations by the UK on its own nuclear project «Tub Alloys» (supervisor of the work - Professor of physics J. Thompson) [9]. Here it is necessary to point out that the scientific group of J. Thompson, which included the French nuclear physicists H. Halban and L. Kovarski, the famous students of F. Joliot-Curie, already in July 1941 sent to the British government deeply developed materials on the creation of uranium atomic bomb, including the calculation of the critical mass of its nuclear explosive - the uranium isotope ${}_{92}{}^{235}U$ [9]. Given the complex military situation in Britain (the constant German bombing and the danger of German invasion) and the shortage of «financial resources» for expensive scientific projects on the «foggy Albion», the leaders of the Western Allies in the anti-Hitler coalition in the war against Germany, F. Roosevelt and W. Churchill agreed to those severe the war years about the mutual exchange of secret information on the atomic superbomb. The proud British, figuratively speaking, «gritting their teeth» and realizing that by voluntary transfer to the Americans of their data on the new superweapons, they lose the «key» to world domination, after all, under pressure from external and internal circumstances, they were forced to give the US their developments of own nuclear weapons.

As for the German Atomic Project (the scientific supervisor of the works is the outstanding German theoretical physicist, Nobel Prize Laureate in physics for 1932 Werner Heisenberg (1901-1976)), despite her capture in 1940 at the concentrator in Oolen under the occupation of 1200 tons of uranium concentrate by Belgium [9], the shortage of highly qualified specialists (many hastily left the country) and the extremely inadequate financing of these works (about USD 10 million [9]) led to the collapse of their obsessive ideas on mastering the world's first intranuclear energy, the creation of the first atomic superbomb and victory over the USSR [7].

Concerning nuclear research of a military nature, bleached with heavy human and material and technical losses of the USSR, during this period, for several years, «to death» by belligerent conventional weapons against Germany with its considerable own and European resources, it is necessary to say that the Atomic Project of the USSR (the scientific supervisor of the work - Professor Igor Kurchatov (1903-1960), which started with the instruction of the State Defense Committee of the USSR No. 2352 of September 28, 1942 «On the organization of work on uranium», due to poor financing and underestimation by the government of the strategic importance of this work till 20 August 1945 was carried out slowly. After this date, and the organization of the Special Committee of the USSR Council of Ministers (chairman - Marshal of State Security L.P. Beria, deputy chairman - People's Commissar of Ammunition Colonel-General B.L. Vannikov, Colonel-General A.P. Zavenyagin, members - Academicians of the USSR Academy of Sciences P.L. Kapitsa and I.V. Kurchatov) atomic work in the USSR acquired unprecedented in scope and intensity [5, 7].

Therefore, taking into account the other political, economic and scientific-technical data mentioned above and known to the author in general terms, it is quite possible to conclude that the United States during the military period of 1942-1945, in comparison with the opposing sides-parties of the Second World War, had the most favorable chances of succeeding first in the development and creation of the first atomic bombs. American scientists and experts, as pioneers in the nuclear arms race, went the hard way: they simultaneously created two fundamentally different models of atomic bombs - «*uranium*» based on the fissile uranium isotope ${}_{92}{}^{235}U$ and «*plutonium*» based on the fissile isotope of plutonium ${}_{94}{}^{239}Pu$ [2- 9].

2.1. The «gun shot» method to detonate the uranium nuclear charge of an atomic bomb. The basic scheme for constructing a uranium atomic bomb based on ***the «gun shot» method*** was set forth in the English report of the Thompson Committee, transmitted by the United States in the autumn of 1941 [9]. Its author was physicist William Parsons. This scheme provided for the creation of a critical mass (of the order of 60 kg [9]) in the neutron-fissioning isotope of uranium ${}_{92}{}^{235}U$ with the flow of an explosive chain nuclear reaction in it [10]. For this purpose, two cylindrical parts with subcritical masses were used in the uranium charge: «shell» and «target» [6, 11]. Uranium «shell» (a solid assembly of individual rings of a cylindrical bar from 90% enriched uranium ${}_{92}{}^{235}U$) with a conventional cannon barrel and a smokeless powder charge at a speed of about 350 m/s was sent inside a hollow cylindrical uranium «target» (a composite structure of separate hollow cylinders from enriched to 80% of uranium ${}_{92}{}^{235}U$) [9, 11]. With the full flight of the uranium «projectile» into the uranium «target», a supercritical mass of nuclear explosive was formed, in which a chain nuclear reaction of an explosive nature was initiated by means of a neutron fuse (external source of neutrons). For example, in the first American uranium atomic bomb «Little Boy» with a capacity of TNT equivalent of about 15 kilotons, exploded in the morning (at 09:16 am) on August 6, 1945 at an altitude of about 580 meters above the city of Hiroshima, Japan, the

uranium «shell» of the nuclear charge (160 mm long and 100 mm in diameter) had a mass of about 26 kg (enriched to 89% of uranium $_{92}^{235}$U), and the uranium target of the nuclear charge (160 mm in length, 100 mm in internal diameter and outer 160 mm in diameter) had a mass of about 38 kg (enriched to 80% of uranium $_{92}^{235}$U) [9, 11]. By the way, the neutron fuse in the first US uranium atomic bomb «Little Boy» was made on the basis of beryllium-polonium initiators emitting a neutron flux at the time of the supercritical mass of the fissioning uranium isotope $_{92}^{235}$U in the cylindrical nucleus of the bomb [9, 11]. To reflect the supercritical mass of the uranium isotope $_{92}^{235}$U in the compressed state to reflect the neutron flux into the inner region of the bomb and retain it for the required time (of the order of 500 ns [5]) in order to allow at least 70 chain links of nuclear fission to occur in it [5], the cylindrical nucleus of this uranium The bombs were surrounded from the outside by massive cylindrical shells made of tungsten carbide (for immediately adjacent to nuclear explosives) and hardened steel (for the outer shroud) [9, 11]. The total mass of such shells was about 2300 kg. The cannon barrel, about 2000 mm in length, firmly fixed on a thick carbide sheath, together with the breech part, had a mass of about 450 kg. Uranium «projectile» in a cannon barrel of the bomb developed speeds of up to 300 m/s [9, 11]. As a result, the first US uranium atomic bomb «Little Boy» with a diameter of 0.7 m and a length of 3 m had a total weight of about 4,100 kg [5, 9, 11]. Experimental data from the US confirmed that when the first uranium atomic bomb «Little Boy» was blasted, which killed about 170,000 residents and destroyed 62,000 buildings in Hiroshima for a moment, the energy released by the passage of a chain in the uranium isotope $_{92}^{235}$U nuclear reaction, «inflates» the nuclear assembly of the bomb at a speed of about 1000 km/s [7, 11]. Therefore, when it undermined, only up to 1.4% of 64 kg of the critical mass of the $_{92}^{235}$U enriched to not less than 80% of uranium had managed to react [11].

2.2. The method of «explosive implosion» to undermine the plutonium nuclear charge of an atomic bomb. Undermining the plutonium nuclear bomb of an atomic bomb based on the weapons-grade isotope of plutonium $_{94}^{239}$Pu (Fig. 2), synthesized and isolated in 1941 by a group of American nuclear scientists led by Glenn Seaborg (for this important discovery in 1951, he was awarded the Nobel Prize for chemistry) [5, 12], with a subcritical mass of up to 6.2 kg using the «gun shot» method described in subsection 2.1 proved to be fundamentally impossible [9, 11].

The main reason for this was that the weapons-grade plutonium $_{94}^{239}$Pu which is currently being produced commercially in the fuel elements of nuclear reactors in the long-term irradiation with neutrons of the natural uranium isotope $_{92}^{238}$U contained in them [5, 10], is significantly larger (about 100 times [6, 11]) by the neutron background (this fissile nuclear material is strongly «fonite» or «glows»).

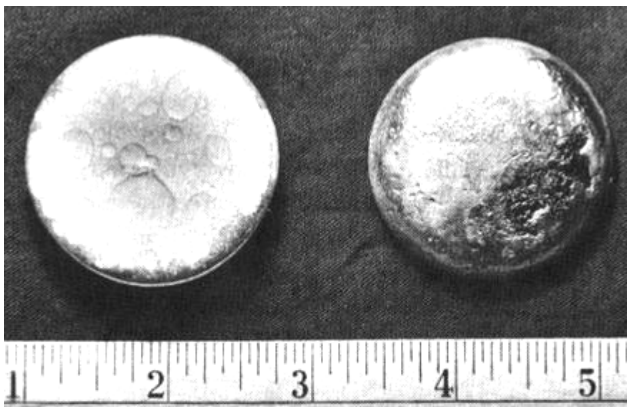

Fig. 2. The unique view of two hemispherical blanks cast in a special metallurgical furnace is silver-white (on the left with a flat inner part, and on the right with a rounded outer part) of the subcritical mass of fissile nuclear material from weapons-grade plutonium $_{94}^{239}$Pu used in the first US implosive atomic bombs «Trinity» and «Fat Man» [6]

Because of such a relatively large background neutron flux, even when the plutonium «projectile» approaches the plutonium «target» between them, a chain nuclear reaction starts prematurely, leading to inefficient separation of intranuclear energy in the zone of their «meeting». It is interesting to note the fact that I remembered for a lifetime the fact of the Soviet period from my own scientific biography, when at one time the author, while staying at the secret scientific center of the USSR at the world level - VNIITPh (Chelyabinsk-70), now called the Russian Federal Nuclear Center No. 2 (Snezhinsk), it was possible at one of the unique nuclear installations to see firsthand the controlled course of the chain nuclear reaction between two vertically approaching in the open air inside the thick lead detachable casings by massive uranium discs. Moreover, this reaction was accompanied by a visually visible intense sizzling (well, just like an electric corona!) glow of bluish-blue color in the section of the interdisk air gap up to 30 mm in length (now one can only guess at the intensity of neutron radiation in the zone of this air gap). Then, in order to avoid neutron irradiation, all observing this impressive nuclear-physical phenomenon were at a distance of about 10 m from the core behind a thick (thickness more than 100 mm) leaded glass, providing our radiation protection. Returning again to the scientific subject of our nuclear physical examination, we point out that, from the practical application of such a scheme of detonation in a nuclear bomb of a plutonium nuclear charge, one nuclear «fizzle» was obtained [11]. For an effective nuclear «detonation» of the plutonium charge in an atomic bomb, using the «cannon shot» method, the speed of the connection of its (charge) parts should have been technically unattainable (more than 1 km/s) [11]. It should not be forgotten that the uranium isotope $_{92}^{235}$U is better than the isotope of plutonium $_{94}^{239}$Pu withstanding strong mechanical loads [11]. By the way, according to modern data, to improve the stability of physical properties and increase the compressibility (plasticity), the isotope of plutonium $_{94}^{239}$Pu is doped with a small

amount of gallium $_{31}{}^{70}$Ga [11]. That is why at the end of 1943 the work on the creation of the plutonium atomic bomb in the USA was at an impasse. And as it turned out in the future, it was the plutonium type of nuclear charge that determined the world's main path for the creation of all nuclear (atomic and thermonuclear) weapons. Scientists needed a fundamentally new technical solution to create and undermine the supercritical mass of the nuclear charge of an atomic bomb from weapons-grade plutonium $_{94}{}^{239}$Pu [9, 11].

And such a new scientific and technical solution in the Los Alamos Laboratory of the United States was first discovered in 1944. Its author was the American physicist Seth Neddermeyer [9]. He proposed a ***method of «explosive implosion»*** (this term derives from the English word «*implosion*» [5, 13]), which involves, by compressing an explosive wave converging toward the center of the bomb from the explosive of chemical EM of plutonium nuclear explosives supercritical mass. According to this method of detonation of nuclear explosives from weapons-grade plutonium $_{94}{}^{239}$Pu, explosive charges from conventional chemical explosives (for example, from trinitrotoluene (TNT) or hexagen) are exploded from the outside all along the perimeter of this fissile nuclear material [5, 9, 11]. Numerous charges with chemical EM are activated by means of a system of electric detonators, triggered by a single trigger device. It was one thing to propose an implosive scheme for detonating the nuclear charge of an atomic bomb (yes, this was then certainly a revolutionary step in the field of atomic science and technology), and it is another thing to implement it practically. There were months of laboratory tests of such a scheme for building a plutonium atomic bomb, but there were no acceptable results.

And here, in the spring of 1944, the scientific leader of the «Manhattan» American Atomic Project R. Oppenheimer, and draws in full to the creation of an implosive atomic bomb of the leading US scientist in the development and testing of conventional chemical EM, Professor at Harvard University G. Kistiakowsky [9]. It should be noted that even before the above-mentioned period, practically since 1943, this American chemist has already performed some work in the framework of this superproject. In the spring of 1944, G. Kistiakowsky became the head of the Department G in the Los Alamos Laboratory, engaged in EM and responsible for solving the problem of implosion reduction of plutonium nuclear charge of an atomic bomb [4, 9]. On the special importance, the scientific and technical level and the amount of work performed in this Department can be indicated by the fact that by the beginning of 1945, in the submission of G. Kistiakowsky, the collective was tense and with full dedication to working like-minded people, including about 600 scientists and engineers [2, 4].

Despite strict secrecy in all countries of the world, the devices of nuclear munitions, thanks to some declassified data on the construction of the first US atomic bombs, we can correctly from the positions of ultrahigh-pressure physics, nuclear and nuclear physicists and, as it turned out, electrophysics, to state the basic principles of their circuit-structural construction and operation [6, 11]. G. Kistiakowsky and his Department G had to develop a new spherical explosive shell and detonation system for its explosion to implosion the plutonium charge of the bomb, based on solid chemical EM which would provide a directed and growing to the center of the bomb, where a spherical charge was placed from weapons-grade plutonium $_{94}{}^{239}$Pu with a subcritical mass, a spherical shock gas-dynamic wave [6]. Estimates made by G. Kistiakowsky showed that in order to achieve this goal, it is necessary to use both explosive and slow brisant chemical explosives in the explosive shell developed by him at the Los Alamos Laboratory of the USA. To do this, they created a new «slow» brisant chemical explosives (mixture of TNT (33%), barium nitrate (66%) and binder wax (1%)), called «baratol» and having a stable detonation velocity (propagation velocity in EM process of chemical decomposition [5, 13]) about 4 km/s [3, 6]. The use of composition B (mixture of hexagene (60%), TNT (39%), and binder wax (1%)), which has a detonation velocity of up to 9 km/s, was suggested as a «fast» brisant chemical explosive in a plutonium atomic bomb [5, 6]. A «slow» brisant chemical EM was used in the outer part of a massive explosive shell, and a «fast» brisant chemical explosive was used in its inner part adjacent to a spherical massive aluminum pusher (neutron absorber) [3, 6]. For the completeness of the complex gas-dynamic problem solved by G. Kistiakowsky 's team from the chemical-physical field of explosives, we note that the accuracy of assembling individual cast brizant lens parts of a spherical explosive shell was less than 1 mm. In order to avoid inhomogeneities in the shock wave directed to the inside of the bomb, special requirements were imposed on the accuracy of spherical surfaces in individual cast brisant lens parts weighing up to 100 kg of this explosive shell with a total mass of up to 2600 kg [6, 11]. A massive explosive shell with its outer (outer subshell) and internal (internal subshell) parts together with its massive spherical aluminum pusher and its massive spherical uranium body (a neutron reflector made from a natural uranium isotope of $_{92}{}^{238}$U) had to perform a strictly symmetrical reduction small (up to 100 mm in diameter) and made in the form of hemispheres of nuclear charge from weapon plutonium $_{94}{}^{239}$Pu separated by a thin gold layer (up to 100 microns thick) u with a subcritical mass located inside such a spherical nuclear-chemical «puff» and containing a miniature neutron beryllium-polonium initiator of a spherical shape inside itself [6, 7, 11].

As a result of scientific research, G. Kistiakowsky together with his colleagues at the Los Alamos Laboratory in the USA in February 1945 proposed the final design of the explosive shell for the first plutonium atomic bomb forming the spherical shock gas-dynamic wave growing to its center. The outer and inner subshells of this explosive shell were made of 32 explosive cast lenses, 20 of which were hexagonal, and 12 were pentagonal [6, 11]. These lenses, made by precise casting

from the molten «slow» and «fast» brisant chemical EM described above, joined together on the basis of the manufacturing of the leather shell of all the known football for us, forming a spherical explosive assembly with a thickness of up to 420 mm and an outer diameter of up to 1300 mm [6, 7, 11]. The total weight of such an explosive shell of a plutonium atomic bomb was about 2500 kg [6, 11]. A hollow aluminum pusher with a boron content of $_5{}^{11}$B (up to 40%), designed to absorb neutrons emitted from the plutonium-uranium assembly and to reduce the pressure drop behind the front of the detonation wave in the explosive shell (this solution increased the pressure of the gas-dynamic wave that passed to the center) diameter of 460 mm had a thickness of about 115 mm and weighed up to 120 kg [6]. With this explosive shell design, the hollow uranium body of a plutonium atomic bomb from a natural uranium isotope $_{92}{}^{238}$U designed to reflect and retain neutrons in its center, with a wall thickness of 70 mm, had an outer diameter of 230 mm and a mass of about 120 kg [6]. The uranium body and the plutonium charge of the bomb formed its subcritical system. Therefore, with its up to 20% of the released intranuclear energy was accounted for by the fission reactions in the uranium shell of the bomb [6, 7]. Note that during the implosion explosion of the shell of these brisant chemical EM which creates pressure in the hundreds of thousands of atmospheres in the central part of the bomb, a decrease in the diameter of the spherical plutonium charge (the «core» of the bomb) occurred 2.5 times, which led to an increase to five times taking into account the mass loss due to the evaporation of fissionable nuclear material) of the density of weapons-grade plutonium $_{94}{}^{239}$Pu and to the appearance in it of a corresponding decrease in its critical mass, up to five critical masses [6, 7, 11]. We point out that the initial diameter of the subcritical spherical parts of the plutonium charge of the bomb was 90 mm, which ensured the presence of a subcritical mass of up to 6.2 kg [6, 7, 11]. To trigger nuclear fission reactions in weapons-grade plutonium $_{94}{}^{239}$Pu with the supercritical mass obtained, a neutron flux initiating them was needed. For this purpose, a spherical cavity with a diameter of 25 mm was made inside the hemispheres of the plutonium charge to accommodate a neutron initiator containing a hollow spherical beryllium shell 20 mm in diameter with a wall thickness of 6 mm, inside of which was a beryllium liner 8 mm in diameter [6, 7, 11]. On the outer surface of the beryllium liner and the wedge-shaped slits made on the inner surface of the beryllium shell, first layers of nickel and gold were deposited, and then a thin layer of radioactive polonium $_{84}{}^{210}$Po with a total mass of up to 11 mg [6, 7, 11]. Thin layers of nickel and gold before implosive explosion of the shell from chemical EM protected the hollow sphere and the liner sphere of beryllium $_4{}^9$Be from the action of α particles (helium isotope nuclei $_2{}^4$He [10]) emitted by the polonium nuclei $_{84}{}^{210}$Po. The neutron initiator was activated when a converging shock gas-dynamic wave was reached from an implosive explosion outside the chemical EM center of the plutonium charge of the bomb. At this moment, the neutron initiator was extremely rapidly destroyed and the mixing of the polonium $_{84}{}^{210}$Po atoms with beryllium $_4{}^9$Be. The alpha particles emitted by the nuclei of $_{84}{}^{210}$Po were absorbed in the beryllium $_4{}^9$Be formed in the center of the charge of the radioactive mixture, the nuclei of which began to actively emit neutrons that acted on the fissionable weapons grade plutonium $_{94}{}^{239}$Pu with supercritical mass [6, 7]. As a result, a chain nuclear reaction of explosive type began to flow in the plutonium nuclear charge of the bomb.

2.3. Application of electric explosion of thin conductors for detonation of chemical EM in the first atomic bombs of the USA. In the first American plutonium atomic bombs, thin electrically exploding conductors (EEC) were used to accurately synchronize the detonation of electric detonators of their explosive shells (see subsection 2.2) [6, 7, 11]. The electric explosion of short segments of thin EEC, carried out with an allowance of up to ±10 ns and causing the simultaneous operation of 32 electric detonators and the corresponding detonation of all 64 lenses from the chemical explosives of the outer and inner explosive subshells of the bomb, was produced by supplying, through numerous electrical cables, from one charged high-voltage capacitor bank of a pulse of a large damped sinusoidal current [6, 15]. The weight of such a starting electrical device, together with a capacitor bank, was about 200 kg [6, 7].

3. A great physical experiment of US nuclear scientists in the Alamogordo desert. Given the colossal scientific and technological complexity of developing reliable designs and manufacturing the world's leading nuclear weapons in the «metal», it can be argued quite reasonably that this kind of sinister (diabolical) weapons of mass destruction of everything on our planet is the result of the world's prior development of science and technology. And now the paradoxical apotheosis of the scientific and technical achievements of mankind in the 20th century by the will of the objective process of the development of our civilization should be the great physical experiment of American scientists and engineers, demonstrating for the first time to all the nuclear explosion in the desert region of the Earth the first experimental US plutonium atomic bomb «Trinity» and, accordingly, the release of huge energy reserves, enclosed in the microcosm of matter.

Undoubtedly, this unique demonstration was not for everyone, but only for 425 elected scientists and specialists who arrived on the eve of this historic event at the US military training ground in the Alamogordo Desert (New Mexico) where a steel tower (Fig. 3) was installed and the first prototype of a plutonium atomic bomb, code-named «Trinity», was prepared for the explosion [7]. We will point out that in a number of sources this bomb is also called «Gadget» [14]. We will stop in our narrative on the first name of this bomb [5, 9].

Fig. 3. The general view of the epicenter of a future nuclear explosion with a steel tower up to 30 m high, on top of which the first American plutonium atomic bomb «Trinity» (US military probe in the Alamogordo Desert, New Mexico) was moved there with the help of lifting equipment, July 15, 1945) [7]

In my opinion, our attention deserves the reigning atmosphere among the authors-developers of this terrible from the universal positions and values of the American atomic bomb, as well as the leading scientists and specialists gathered at the US proving ground. Many of them intuitively realized that they were in step or from an unprecedented scientific discovery, or from an unprecedented catastrophe. For example, the Nobel Prize Laureate in physics for 1938, Enrico Fermi, who worked at the Los Alamos Laboratory on the creation of the first US atomic bombs, 5 believed that after the explosion of this atomic bomb from the present developers in a reinforced concrete bunker 10 miles away from its epicenter will not survive anybody [9]. G. Kistiakowsky argued with R. Oppenheimer for his monthly salary (USD 700) that the developed implosive explosion mechanism will work successfully and all will remain alive [9]. When declaring a 10-second readiness, all those who were in the team bunker began to pray furiously, as last time, praying and remembering the words from the Gospel [9]: «*...I believe! Lord, help my unbelief!*» At that moment R. Oppenheimer could not take himself in hand: he was shaking with nervous tension [9]. Immediately after the explosion of the bomb and when a huge column of gas and smoke rose above the desert, on which a «nuclear mushroom» opened like a parachute (Fig. 4), R. Oppenheimer, violating the «grave» silence, exclaimed [8, 9]: «*It's working!*». Most of those present with him in the bunker were simply depressed and overwhelmed by this grandiose explosion and just remained silent. Then quickly came to life, G. Kistiakowsky loudly said [9]: «*I am sure that when the end of the world comes, in the last millisecond of the Earth's existence, mankind will see exactly what we have just witnessed*».

Fig. 4. External view of the «nuclear fungus» from the explosion of the first experimental plutonium atomic bomb of the United States «Trinity» (the US military training ground in Alamogordo, New Mexico, 05:30 am, July 16, 1945) [7]

In Fig. 4, to the left of the «nuclear fungus», winding «paths» of numerous channels of air electrical discharges accompanying the first nuclear explosion (NE) in the history of mankind are clearly visible. The formation of such electrical discharges in the air atmosphere is associated with the intensive separation of electric charges of both polarities in the zone of NE leading to the emergence of a high-ionized gas medium adjacent to the «nuclear fungus» of a high-power electromagnetic pulse, which along with penetrating radiation, light and shock wave is one of the main striking factors of nuclear weapons [11].

After the nuclear explosion of July 16, 1945, the first US experimental implosive atomic bomb «Trinity» with a plutonium «filling» subcritical mass of up to 6.2 kg with a trotyl equivalent of about 18 kt from the steel tower (see Fig. 3), only a part of its melted reinforced concrete base remained (Fig. 5) [2, 5].

Fig. 5. Scientific and administrative leaders of the «Manhattan» US Atomic Project Robert Oppenheimer (left) and Leslie Groves (right) at the site of the nuclear explosion of the first implosive plutonium atomic bomb «Trinity» (the US military range 400 km south of Los Alamos, New Mexico, September 1945) [7]

From the memories of the witness of the first in the modern history of mankind to test in the uninhabited area of the Earth nuclear weapons, the US Army General T. Farrell [7, 9]: *«... This was something unprecedented. During the explosion, there was a stunningly beautiful and terrible game of gold, purple, purple, gray and blue colors. We felt ourselves to be small blasphemous creatures, swinging at the taming of forces that until then were subordinate only to the Most High.* « In the radius of 1.5 km from the epicenter of the explosion of the first implosive plutonium atomic bomb «Trinity», the upper layer of sand melted, turning on the surface into a vitreous substance of greenish color - trinitite (this name was firstly artificially obtained on Earth substance, from the name of the American bomb that «gave birth» to it) [5-7]. The destructive power of the nuclear explosion carried out by the Americans so influenced the human psyche that no festive events and even parties were held for the successful testing of the first plutonium atomic bomb at the National Nuclear Center of the USA (Los Alamos) [9].

4. Awe-inspiring atomic bombing of the United States in 1945 in Japanese cities. April 12, 1945, Franklin Roosevelt died and Harry Truman became the new President of the United States. The next day, April 13, 1945, US Secretary of Defense Henry Stimson was forced to report to the new US President and commander in chief of the US Army about the «Manhattan» superproject (surprisingly, as Vice-President, Truman did not know anything about him!) [6, 16]. It was to this US president's share that fate had the right to make an important political decision about the first military use of nuclear weapons. On May 11, 1945, the Pentagon leadership, with the approval of its commander in chief, US President G. Truman, made a decision to deploy the first nuclear weapons attacks on peaceful Japanese cities - Hiroshima, Kokure and Nagasaki [16]. An obligatory condition for carrying out atomic bombardment of these objects was the presence of a clear sky above them (first, for better aiming at a high altitude of the flight of an airplane (10-12 km), and, secondly, for photographing the results of unique bombardments). These bombardments were to take place on August 4, 1945. However, due to bad weather, the first of them (a nuclear strike in Hiroshima city) was postponed to August 6, 1945 [9, 16]. On the tragic consequences of the atomic bombing of August 6, 1945, Hiroshima, when the first uranium atomic bomb «Little Boy» was used with a power of TNT equivalent of about 15 kt, was mentioned above in Subsection 2.1 and [17]. In August 9, 1945, from the American B-29 strategic bomber (Fig. 6), to the Japanese city of Nagasaki, the plutonium atomic bomb «Fat Man» with a capacity of TNT equivalent of about 21 kt, due to the expansion in all directions at a speed of up to 1000 km/s of its plutonium-uranium assembly, only 20% of the approximately 6.2 kg of the initial mass of the charge of weapons-grade plutonium ${}_{94}{}^{239}\mathrm{Pu}$ in it had reacted (to share the nuclear image) [6, 18].

Fig. 6. The US B-29 strategic bomber used by the United States in 1945 to inflict eerie nuclear strikes on Japanese peaceful cities [7, 18]

Due to the fact that the plutonium atomic bomb «Fat Man» having a length of 3.25 m, a diameter of 1.5 m and a total weight of up to 4600 kg, was blown up at an altitude of about 500 m on the outskirts of Nagasaki (the nuclear strike on the original goal - Kokurye was canceled due to the large cloudiness above it), the number of dead inhabitants of this peaceful city immediately after the nuclear explosion over it of this bomb (Fig. 7) was only about 90 thousand people [6, 18]. The population and the government of Japan, after these two historical cases of the first US military use of nuclear weapons with horrific human losses and devastating consequences, were in an inexpressible shock. August 14, 1945 (recall that on August 9, 1945 the USSR declared war on Japan and with its victorious lightning-fast operations in the Far East practically compelled the land forces of the Kwantung Army of Japan with the number of up to 1 million soldiers and officers to surrender), the Emperor of Japan Hirohito after visiting the places nuclear bombing of the US Japanese cities begged for peace and said [9, 18]: «*... Japan is forced to accept the conditions of the Potsdam Declaration*». After that, on Sept. 2, 1945, on the American battleship «Missouri» authorized representatives of the USSR, the USA and Japan signed the Act of unconditional surrender and put a «fat point» in World War II [9, 18].

Fig. 7. The unique photograph by a Japanese amateur photographer who captured the explosion of the American plutonium atomic bomb «Fat Man» for history (11:02 am, August 9, 1945, Nagasaki, Japan) [7, 18]

5. Some recent information about the «leakage» of US atomic secrets in the USSR. All works on the US «Manhattan» Atomic Project were given the highest degree of secrecy [5, 6, 9]. The USSR from the very beginning of these works began to create a branched reconnaissance network around this superproject [9, 11]. Not only Soviet agents worked for the USSR, but also American, British and Italian scientists and specialists involved in the implementation of a number of works on this project [5, 9]. It is believed that, thanks to the active efforts of the intelligence agencies, the USSR foreign intelligence extracted about 12,000 sheets of A4 format from the US Atomic Project Manhattan with detailed information on the designs of the first US atomic bombs, information on the properties of the fissile and other radioactive materials used in them, and technologies the production of the fissile isotope of uranium $_{92}^{235}$U and the fissile isotope of plutonium $_{94}^{239}$Pu [5]. Therefore, certainly, not without reason, in the 1950s, trials took place in the USA against the spouses Julius and Ethel Rosenberg, David Greenglass (brother of E. Rozenberg) and Donald MacLeod, who gave the secret information about the US Atomic Project Manhattan [9] to the USSR. The United States established that an important agent recruited by the Soviet secret services was the English theoretical physicist Klaus Fuchs, who in September 1944 had become a direct participant in the development and creation of the first American atomic bombs [5, 9]. Over time, new names have sprung to the troubled «surface» of espionage in favor of the USSR: John Kernkross (from the famous «Cambridge Five») and Ted Hall, who «merged» US atomic secrets with Soviet intelligence [9]. Recently (in the spring of 2007) Russian President V.V. Putin appropriated the title of the Hero of Russia (posthumously) to the Soviet patriot-chemist Georges Koval, who graduated from the D.I. Mendeleyev Moscow Institute of Chemical Technology after the war who worked legally in the United States from the 1940s in the specialty and transmitted to the USSR valuable information about the activities in the closed nuclear cities of the USA Oak Ridge and Hanford on the production of fissile isotopes of uranium $_{92}^{235}$U and plutonium $_{94}^{239}$Pu [5, 9].

It is generally believed that it was the data of G. Koval who helped the scientific leader of the Atomic Project of the USSR Academician of the USSR Academy of Sciences I.V. Kurchatov in the beginning of 1945 to take a strategically correct decision on the development and creation in the USSR of the first plutonium atomic bomb under the working code name «First Lightning» [9, 11]. At that time, the USSR was not able to «pull» the creation of two types of atomic bomb (uranium and plutonium) at once. Further events in the world nuclear arms race confirmed the full truth of such a responsible decision of a strong-willed and wise Soviet nuclear physicist. On August 29, 1949 (at 10:05 am) at the Semipalatinsk nuclear test site (Southeast Kazakhstan), the USSR successfully carried out in the desert area of its territory a test of the first Soviet plutonium atomic bomb with a capacity of about 22 kt in TNT equivalent (Fig. 8). By and large, the Soviet plutonium atomic bomb under the final code name РДС-1 (this abbreviation according to the cover story of the Soviet special services came from the phrase «Stalin's Jet Propulsion» [19]) was in general a certain modification of our American nuclear plutonium atomic bomb by our nuclear physicists «Fat Man» [5, 20]. Having rechecked in the scientific laboratories the data obtained by the Soviet foreign intelligence on the construction of the first atomic bombs of the United States and convinced of their reliability, the political leadership of the Soviet country, in the person of its leader, Chairman of the USSR Council of Ministers I.V. Stalin and the scientific and administrative leadership of the Atomic Project of the USSR (represented by L.P. Beria and I.V. Kurchatov) in a narrow circle took a strictly closed decision on following the creation of the first Soviet atomic bomb by the already approved nuclear physicists and specialists in conventional EM by the US way of [19-21].

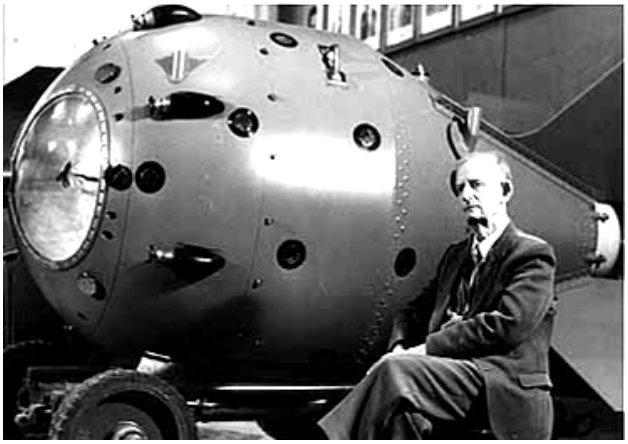

Fig. 8. External view of the first plutonium atomic bomb of the USSR, code-named РДС-1, with power of up to 22 kt in TNT developed and created under the guidance of Yulij Borisovich Khariton, Academician of the USSR Academy of Sciences (1904-1996), who is sitting with a full-scale mock-up of the bomb (museum of theVNIIEPh now called the Russian Federal Nuclear Center No. 1, Arzamas-16, now called Sarov city, 1984, RF) [5, 16]

For the Soviet Union, then, it was vital to ensure our own security by any means «gaining» time and quickly ending the US monopoly in the field of nuclear weapons. Therefore, more than 70 years after the beginning of the unprecedented in the USSR unprecedented in financial costs and the military-industrial epic for the creation of its own atomic bomb, the above-mentioned strategic decision of the USSR in the field of Soviet nuclear research and the production in the shortest possible time of the first atomic bomb samples.

6. Scientific, educational and political activities of G. Kistiakowsky after the «Manhattan» US atomic project. Immediately after the successful completion of the work at the Los Alamos Laboratory for the creation of the first atomic bombs of the United States, G. Kistiakowsky returned to the teaching and research

work at Harvard University (Fig. 9) [2-4]. From 1947 to 1950 he was Head of the Department of Chemistry at this University in the United States. In the period 1953-1958 G. Kistiakowsky was a member of the US Defense Intelligence Agency Advisory Committee on Ballistic Missiles [2-4]. In 1957 he, as a well-known scientist in the field of physical chemistry and an extremely well-proven manager in the execution of the most important work on the Atomic Project, received an invitation from the US President D. Eisenhower (Fig. 10) to join the President's Council on Science and Technology. In this work, he did not stay long in the «shadow» and already in 1959 he headed this Council in the administration of the US president. In the period 1959-1961 G. Kistiakowsky also headed the Office of the President of the US Office of Science and Technology Policy. While in the White House, this scientist actively pursued and introduced into the consciousness of the country's political elite the policy of nuclear disarmament [2, 3, 9].

Fig. 9. Professor of Harvard University G. Kistiakowsky after the successful completion of research in the Los Alamos Laboratory of the United States on the atomic problem again for his favorite scientific and pedagogical work [3]

Fig. 10. US President D. Eisenhower (right) and his special assistant on science and technology G. Kistiakowsky (left) (Washington, White House, 1958) [3, 4]

Being in the post of adviser to the US president on science and technology until 1961, G. Kistiakowsky carried out consultations of the first person of the American state on coordination among various institutions of the country of a complex of scientific research and training of scientific personnel. In 1965, for scientific merit, he was elected Vice-President of the National Academy of Sciences of the United States. This honorable position he held until 1972 [9].

After retiring, G. Kistiakowsky actively joined in the fight against the proliferation of nuclear weapons in the world. In 1977 he headed the American Council for the Preservation of Life [3, 4]. It is believed that G. Kistiakowsky was in the United States one of the most successful Ukrainian scientists. At one time his main scientific developments in the field of physical chemistry and chemical EM were compared with the famous inventions of the Swedish engineer and businessman Alfred Nobel (1833-1896) [3-5, 12]. For outstanding scientific achievements, G. Kistiakowsky in the USA was awarded the Willard Gibbs Prize (1960), the National Scientific Medal of the USA (1967), the Priestly Medal (1972) and the Franklin Medal (1972) [2-4]. In 1982, his documents were prepared for the Nobel Peace Prize [9]. The famous American chemist and physicist (this famous native from the Ukraine), who achieved significant results in the development of physical chemistry, in the theory and practice of chemical EM, in the development and creation of the first nuclear weapons and in the struggle for world peace, died on December 7, 1982 [2-4, 9].

Conclusions. American physicist and chemist George Bogdan Kistiakowsky (1900-1982) of Ukrainian origin left behind a notable scientific «trace» not only in the field of physical chemistry in the development of new chemical explosives, but also in the field of ultra-high-pressure physics and nuclear physics in the development and creation in the war period 1942-1945 in the USA within the framework of the «Manhattan»US Atomic Project Manhattan» of the first atomic bombs of the implosive type based on the isotope of plutonium $_{94}^{239}$Pu.

REFERENCES

1. George Bogdan Kistyakovsky and the project «Manhattan». *Newspaper «Zerkalo nedeli»*, 2015, no.28-29. (Rus).

2. Available at: http://gazeta.zn.ua/personalities/dzhordzh-bogdan-kistyakovskiy-i-proekt-manhetten (accessed 10 April 2014). (Rus).

3. Available at: https://en.wikipedia.org/wiki/George_Kistiakowsky (accessed 10 May 2012).

4. Available at: http://www.pseudology.org/science/KistyakovskyGB.htm (accessed 23 March 2013). (Rus).

5. Baranov M.I. *Antologiia vydaiushchikhsia dostizhenii v nauke i tekhnike: Monografiia v 2-kh tomakh. Tom 1.* [An anthology of outstanding achievements in science and technology: Monographs in 2 vols. Vol.1]. Kharkov, NTMT Publ., 2011. 311 p. (Rus).

6. Available at: http://ruatom.ru/milit/fm_at_tinian.jpg (accessed 03 October 2013). (Rus).

7. Available at: www.infozoom.ru/pervaya-atomnaya-bomba.html (accessed 11 May 2013). (Rus).
8. Ruze M. *Robert Oppengeymer i atomnaya bomba* [Robert Oppenheimer and the atomic bomb]. Moscow, Atomizdat Publ., 1965, 150 p. (Rus).
9. Available at: http://fraza.ua/analitics/26.09.15/230879/manhettenskij_proekt_ukrainskij_sled_chast_1_.html (accessed 12 June 2013). (Rus).
10. Kuz'michev V.E. *Zakony i formuly fiziki* [Laws and formulas of physics]. Kiev, Naukova Dumka Publ., 1989. 864 p. (Rus).
11. Available at: https://en.wikipedia.org/wiki/Nuclear_weapon (accessed 13 October 2010).
12. Khramov Yu.A. *Istoriia fiziki* [History of Physics]. Kiev, Feniks Publ., 2006. 1176 p. (Rus).
13. *Bol'shoj illjustrirovannyj slovar' inostrannyh slov* [Large illustrated dictionary of foreign words]. Moscow, Russkie slovari Publ., 2004. 957 p. (Rus).
14. Available at: http://www.2000.ua/v-nomere/aspekty/persona_aspekty/smog-vzorvat-atomnuju-bombu.htm (accessed 31 May 2013). (Rus).
15. Baranov M.I. *Izbrannye voprosy elektrofiziki: Monografija v 2-h tomah. Tom 2, Kn. 1: Teorija elektrofizicheskih effektov i zadach* [Selected topics of Electrophysics: Monograph in 2 vols. Vol. 2, book. 1: Theory of electrophysics effects and tasks]. Kharkov, NTU «KhPI» Publ., 2009. 384 p. (Rus).
16. Available at: www.dominating.ru/atombomb/teory/history.htm (accessed 23 October 2014). (Rus).
17. Jung R. *Yarche tysyachi zvezd* [Brighter thousands stars]. Moscow, Gosatomizdat Publ., 1961. 224 p. (Rus).
18. Available at: https://en.wikipedia.org/wiki/Atomic_bombings_of_Hiroshima_and_Nagasaki (accessed 14 June 2009).
19. Khariton Ju.B., Smirnov Ju.N. *Mify i real'nost' sovetskogo atomnogo proekta* [Myths and reality of the soviet atomic project]. Arzamas-16, USRIEP Publ., 1994. 72 p. (Rus).
20. Mikhailov V.N. *Sozdanye pervoy sovetskoy yadernoy bomby* [Creation of the first soviet nuclear bomb]. Moscow, Energoatomisdat Publ., 1995. 448 p. (Rus).
21. *The USSR Atomic Project. Documents and materials: In 3 Vol.* Ed. L.D. Ryabev. Vol. 1, 1938-1945: in 2 parts. Part 1. Min. of the RF for Atomic Energy; Ans. comp. L.I. Kudinova. Moscow, Science Publ., Fizmatlit Publ., 1998, 432 p.; Part 2: Moscow, Publishing House of MPhTI, 2002, 800 p.; Vol. 2 in 7 Books. Atomic bomb. 1945-1954: Book 1, 1999, 719 p.; Book 2, 2000, 640 p.; Book 3, 2003, 896 p.; Book 4, 2003, 816 p.; Book 5, 2005, 976 p.; Book 6, 2006, 896 p.; Book 7, 2007, 696 p. Russian Federal Atomic Energy Agency; Ans. comp. G.A. Goncharov. Sarov, RFNC-USRIEP, Moscow, Fizmatlit Publ. (Rus).

Received 29.06.2016

M.I. Baranov, Doctor of Technical Science, Chief Researcher,
Scientific-&-Research Planning-&-Design Institute «Molniya»
National Technical University «Kharkiv Polytechnic Institute»,
47, Shevchenko Str., Kharkiv, 61013, Ukraine,
phone +380 57 7076841,
e-mail: baranovmi@kpi.kharkov.ua

How to cite this article:
Baranov M.I. An anthology of the distinguished achievements in science and technique. Part 40: The scientific opening of the method of explosive implosion for the obtaining above critical mass of nuclear charge and Ukrainian «track» in the «Manhattan» American atomic project. *Electrical engineering & electromechanics*, 2017, no.5, pp. 3-13. **doi: 10.20998/2074-272X.2017.5.01.**

UDC 621.313:536.2.24:539.2 **doi: 10.20998/2074-272X.2017.5.02**

V.F. Bolyukh, I.S. Schukin

INVESTIGATION OF THERMAL PROCESSES IN A LINEAR PULSE-INDUCTION ELECTROMECHANICAL CONVERTER OF CYCLIC ACTION

Purpose. *Investigation of the influence of the intensity of cooling of active elements and the period of succession of power pulses on the thermal processes of linear pulse-induction electromechanical converter (LPIEC) operating in a cyclic mode.* ***Methodology.*** *The electromechanical and energy processes of LPIEC, which arise during the direct course of the working cycle, are investigated. It is shown that by the end of the operating cycle, a significant part of the energy is stored in the capacitive energy storage device, and is also converted into thermal energy of the armature and inductor. With a significant number of operating cycles, an unacceptably high temperature rise of LPIEC active elements occurs. To solve this problem, intensive cooling of the winding of the inductor, the movable armature or both of them, as well as an increase in the pulse repetition period are used. It has been experimentally established that when the LPIEC is operating in a cyclic mode, the inductor winding with a steel frame blown with air is heated more slowly than the winding with an insulating frame. The experimental dependences with an accuracy of 6 % coincide with the calculated results. A constructive scheme of the LPIEC of cyclic action with intensive cooling of the stationary winding of the inductor has been developed.* ***Results.*** *A mathematical model of the LPIEC of cyclic action is developed, taking into account a complex of interrelated electromechanical and thermal processes. The solutions of its equations are represented in a recurrent form. The electromechanical and energy processes of LPIEC, which arise during the direct course of the working cycle, are investigated. It is shown that for a considerable number of operating cycles, unacceptably high temperature excesses of active elements of the LPIEC are observed. It is shown that intensive cooling of the winding of the inductor, the movable armature or both of them, and also the increase in the pulse repetition period ensure the temperature stabilization of the LPIEC. Measurements of the temperature on the surface of the winding of the inductor LPIEC during cyclic operation are carried out. A constructive scheme of the LPIEC of cyclic action with intensive cooling of the stationary winding of the inductor has been developed.* ***Originality.*** *A mathematical model of the LPIEC of cyclic action is developed, taking into account a complex of interrelated electromechanical and thermal processes. The solutions of its equations are represented in a recurrent form. It is shown that by the end of the working cycle a significant part of the energy is converted into thermal energy of the armature and inductor. It is determined that for a significant number of operating cycles, unacceptably high temperature excesses of active elements of the LPIEC are observed. It is shown that intense cooling of active elements, as well as an increase in the pulse repetition period, ensure the temperature stabilization of the LPIEC. A design scheme of the LPIEC with intensive cooling of the stationary winding of the inductor has been developed.* ***Practical value.*** *It is shown that by thermal cooling of at least one of the active elements and by increasing the pulse repetition period, the temperature stabilization of the LPIEC is ensured. A constructive scheme of the LPIEC of cyclic action with intensive cooling of the stationary winding of the inductor has been developed.* References 13, tables 1, figures 12.

Key words: **linear pulse-induction electromechanical converter, cyclic action, thermal state, mathematical model, electromechanical and energy processes, intensive cooling, experimental studies, constructive scheme.**

Разработана математическая модель линейного импульсно-индукционного электромеханического преобразователя (ЛИИЭП) циклического действия, система уравнений которой учитывает комплекс взаимосвязанных электромагнитных, электромеханических и тепловых процессов. Решения этих уравнений представлены в рекуррентном виде. Исследованы процессы ЛИИЭП, протекающие при прямом ходе рабочего цикла. Показано, что к концу рабочего цикла значительная часть энергии сохраняется в емкостном накопителе энергии, а также преобразуется в тепловую энергию якоря и индуктора. При значительном числе рабочих циклов происходит недопустимый нагрев активных элементов ЛИИЭП. Для решения этой проблемы используется интенсивное охлаждение обмотки индуктора, подвижного якоря или их обоих, а также увеличение периода следования импульсов. Установлено, что при работе ЛИИЭП в циклическом режиме экспериментальные зависимости температуры нагрева обмотки индуктора с точностью до 6 % совпадают с расчетными результатами. Разработана конструктивная схема ЛИИЭП циклического действия с интенсивным водяным охлаждением обмотки индуктора. Библ. 13, табл. 1, рис. 12.

Ключевые слова: **линейный импульсно-индукционный электромеханический преобразователь, циклическое действие, тепловое состояние, математическая модель, электромеханические и энергетические процессы, интенсивное охлаждение, экспериментальные исследования, конструктивная схема.**

Introduction. Linear pulse-induction electromechanical converters (LPIEC) are used in many branches of science, engineering and technology. They are used for cleaning technological equipment and bunkers from the remains of bulk cargo, testing critical products and devices for impact, processing and forming of metal structures. Such converters are used in the mining industry and geological exploration, in mechanical engineering with magnetic pulse welding, stamping, perforation, in various measuring instruments, electromechanical accelerators, etc. [1-4].

In many technical systems, the LPIEC must provide a continuous sequence of power pulses with a specified period of travel. In such a converter, a short period of the load (active mode of operation) is realized in each working cycle, at which intense current pulses are excited in the active elements (inductor and armature), and the armature moves straight with the actuator, and a prolonged pause (passive mode work). During the passive mode, the armature moves backward with actuator under the action, for example, of a return spring, and the

ensuing resting mode of the armature, at which the capacitive energy storage (CES) device is charged. Although this regime resembles repeatedly with a short turn-on time for traditional electric machines, it has significant features [5, 6]. This is due to the fact that the impulse load is so short that the temperature rise in the active elements of the LPIEC occurs practically in adiabatic conditions.

In the cyclical mode of operation, they are subject to investigation:

- permissible excess temperatures of active elements for a given number of operating cycles;
- the power pulse repetition period, in the passive mode of which the active elements of the LPIEC are cooled to a given thermal state;
- allowable number of cycles for a given pulse repetition period and cooling intensity.

In LPIEC, in a forward motion, a stationary inductor driven from a CES, by means of a pulsed magnetic field, induces currents in an electrically conductive armature, which, under the action of electrodynamic forces, provides a rapid movement of actuator in a forward motion, which exerts, for example, impact force on the object. In the reverse course, the armature with the actuator returns to its original position in the zone of maximum magnetic coupling with the inductor, followed by a pause, during which the charge of the CES is performed for the subsequent operating cycle. Thus, in the considered converters with the return-post motion of the armature with actuator, complex spatio-temporal, dependent from each other impulse electrical, magnetic, mechanical and thermal processes [7].

Since pulsed current loads in LPIEC repeatedly exceed similar indicators of electromechanical devices of continuous action, in a cyclic mode of operation a special role is assumed by thermal processes that to a large extent determine the conditions and operating time of the converter. In turn, the thermal state of the LPIEC essentially depends on [6]:

- parameters and constructive performance of the inductor, armature and CES;
- the shape of the winding current of the inductor, determined by the electronic excitation circuit;
- the pulse repetition rate (period);
- the nature of the movement of the armature;
- intensity of cooling of active elements.

However, up to now, these thermal processes have not been practically studied, which can be explained by the complex and interrelated nature of processes of different physical nature, which, moreover, depend on the constructive performance, purpose and conditions of the LPIEC operation. Particularly topical is the question of the effect of the cooling intensity of the active elements of the transducer and the duration of the pulse repetition period on their thermal state.

The goal of the paper is investigations of the influence of the intensity of cooling of active elements and the period of the succession of power pulses on the thermal state of the LPIEC in a cyclic mode of operation.

Design of LPIEC. As the object of research, the LPIEC of cyclic action is chosen, the actuator of which contains a spring-loaded punch making power pulses along the test plate installed below (Fig. 1) [7].

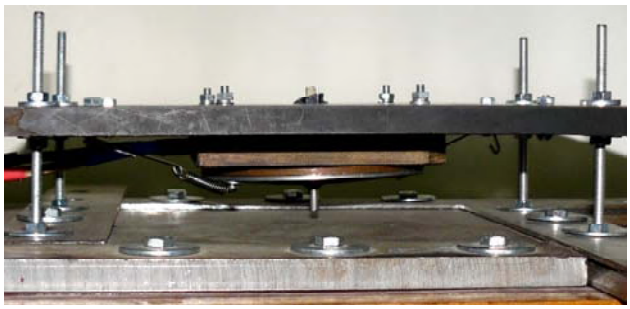

Fig. 1. General view of the LPIEC of cyclic action

The LPIEC operates in an environment with natural cooling. The electronic circuit of excitation of the inductor provides a series of unipolar current pulses, which allows to save some of the energy in the CES by the end of the working cycle [5].

The LPIEC of the coaxial configuration contains a fixed inductor with a two-layer winding of the disk shape, which is wound with a rectangular copper busbar, is epoxy resin and is laid either in a thick-walled insulating (fiberglass) or in a thin-walled (1 mm) steel frame [8] (Fig. 2). The feature of the steel frame is that through it, it is possible to provide intensive air or water cooling of the winding of the inductor.

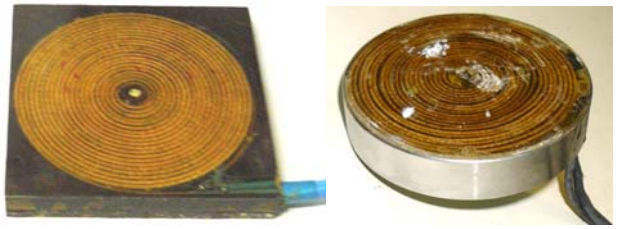

a *b*

Fig. 2. LPIEC inductors with glass-textolite (*a*) and steel (*b*) frames

Coaxially with the inductor there is a copper disk armature, which is connected to the power disk, which ensures the movement of the striker towards the target object. Thus, the actuator consists of a power disk and striker, which are made of stainless non-magnetic steel.

To the power disk, return springs are connected, ensuring a tight clamping of the armature to the inductor before and after the force pulse. The main parameters of the LPIEC are presented in Table 1.

Mathematical model of LPIEC. The mathematical model of the LPIEC of cyclic action should promptly calculate the complex of interrelated electromagnetic, electromechanical and thermal processes in each operational cycle, take into account the variable magnetic coupling between the armature and the inductor winding during a forward stroke, the change in the resistance of the winding of the inductor and the armature due to heating by impulse currents, acting on the armature, the cooling conditions and the thermal interaction of the active elements. It should be taken into account that there are insignificant temperature gradients along the cross-section of active elements [6]. Field methods of

calculation are expedient for applying to the investigation of LPIEC processes under a single operating regime [9, 10].

Table 1

LPIEC parameters

Designation	Symbol	Value
Outer diameter of inductor winding, mm	D_{ex1}	100
Inner diameter of inductor winding, mm	D_{in1}	10
Height of inductor winding, mm	h_1	10
Outer diameter of armature, mm	D_{ex2}	100
Inner diameter of armature, mm	D_{in2}	10
Height of armature, mm	h_2	2.5
Insulation thickness between inductor winding and armature, mm	ΔZ_0	0.5
Number of turns of inductor winding	w_1	42
Turn section of the inductor winding, mm^2	$a \times b$	1.8×4.8
Coefficient of elasticity of return spring, kN/m	K_p	25.0
Actuator mass, kg	m_a	0.35
CES capacitance, μF	C	3000
CES charging voltage, V	U_0	310

In the cyclic mode of operation, it is advisable to use the LPIEC chain model with lumped parameters [11], and solve the equations in a recurrent form assuming all the parameters on the interval $\Delta t = t_{k+1} - t_k$ are unchanged [12].

Electromagnetic processes arising in the LPIEC at the connection to the CES can be described by the following system of equations:

$$\left[R_1(T_1)+R_0\right]\cdot i_1 + L_1\frac{di_1}{dt} + \frac{1}{C}\int_0^t i_1 dt + M_{12}(z)\frac{di_2}{dt} + \\ + v(t) i_2 \frac{dM_{12}}{dz} = 0, \quad \frac{1}{C}\int_0^t i_1 dt = U_0, \tag{1}$$

$$R_2(T_2)\cdot i_2 + L_2\frac{di_2}{dt} + M_{21}(z)\frac{di_1}{dt} + i_1 v(t)\frac{dM_{12}}{dz} = 0, \tag{2}$$

where n = 1, 2 are the indexes of the inductor and the armature, respectively; R_n, L_n, T_n, i_n are the active resistance, inductance, temperature and current of the n-th element, respectively; C is the capacitance of the CES charged to the voltage U_0; $M_{12}(z) = M_{21}(z)$ is the mutual inductance between the inductor and the armature moved along the axis z with velocity v.

We indicate

$$R_1 = R_1(T_1) + R_0;\ R_2 = R_2(T_2);\ M = M_{12}(z) = M_{21}(z).$$

The system of equations (1) - (2) after a series of transformations is reduced to the equation:

$$a_3\frac{d^3 i_1}{dt^3} + a_2\frac{d^2 i_1}{dt^2} + a_1\frac{di_1}{dt} + a_0 i_1 = 0, \tag{3}$$

where

$$a_3 = \upsilon;\ a_2 = \chi - 2Mv\frac{dM}{dz};\ a_1 = R_1R_2 + \frac{L_2}{C} - v^2\left(\frac{dM}{dz}\right)^2;$$

$$a_0 = \frac{R_2}{C};\ \upsilon = L_1L_2 - M^2;\ \chi = R_1L_2 + L_1R_2.$$

If the discriminant of its characteristic equation is less than zero, then all the roots are real and the solution for the currents after a series of transformations is represented in a recurrent form [5]

$$i_n(t_{k+1}) = \delta^{-1}\left[1 - \frac{v^2}{R_1R_2}\left(\frac{dM}{dz}\right)^2\right]^{-1}\left\{\left[i_n(t_k) - \frac{i_m(t_k)v^2}{R_1R_2}\left(\frac{dM}{dz}\right)^2\right]\times\right. \\ \times\left(\alpha_1x_2x_3 + \alpha_2x_1x_3 + \alpha_3x_1x_2\right) + \left(\Omega_n - \frac{v\Omega_m}{R_n}\frac{dM}{dz}\right)\left[\alpha_1(x_2+x_3) + \right. \\ \left. + \alpha_2(x_1+x_3) + \alpha_3(x_1+x_2)\right] + \left(\Lambda_n - \frac{v\Lambda_m}{R_n}\frac{dM}{dz}\right)(\alpha_1+\alpha_2+\alpha_3)\Big\}, \tag{4}$$

where m = 2, 1 at n = 1, 2;

$$\delta = x_1x_2(x_2-x_1) + x_1x_3(x_1-x_3) + x_2x_3(x_3-x_2);$$

$$\alpha_1 = (x_3-x_2)\exp(x_1\Delta t);\ \alpha_2 = (x_1-x_3)\exp(x_2\Delta t);$$

$$\alpha_3 = (x_2-x_1)\exp(x_3\Delta t);$$

$$x_p = \left\{2\left(a_2^2 - 3a_1a_3\right)^{0.5}\cos\left[2\pi(p-1)/3 + \varsigma\right] - a_2\right\}/3a_3;$$

$$p = 1, 2, 3;$$

$$\varsigma = \arccos\left[\left(a_2^2 - 3a_1a_3\right)^{-1.5}\left(4{,}5a_1a_2a_3 - a_2^3 - 13.5a_0a_3^2\right)\right];$$

$$\Omega_n = B_n + \frac{B_mv}{R_n}\frac{dM}{dz};\ \Lambda_n = E_n + \frac{E_mv}{R_n}\frac{dM}{dz};$$

$$\gamma_1 = L_2;\ \gamma_2 = -M;$$

$$B_n = \upsilon^{-1}\left[i_n(t_k)\left(Mv\frac{dM}{dz} - R_nL_m\right) + i_m(t_k)\times\right. \\ \left.\times\left(R_mM - L_mv\frac{dM}{dz}\right) - \gamma_k u_c(t_k)\right];$$

$$E_1 = \upsilon^{-2}\Big\{i_1(t_k)\left[R_1\left(R_2M^2 + R_1L_2^2 - C^{-1}L_2\upsilon\right) - vM\times\right. \\ \times\frac{dM}{dz}\left(\chi + 2R_1L_2\right) + v^2\left(L_1L_2 + M^2\right)\left(\frac{dM}{dz}\right)^2\Big] + \\ + i_2(t_k)\left[v\left(L_2\chi + 2R_2M^2\right)\frac{dM}{dz} - MR_2\chi - v^2ML_2\times\right. \\ \left.\times\left(\frac{dM}{dz}\right)^2\right] + u_c(t_k)\left(R_2M^2 + L_2^2R_1 - 2L_2vM\frac{dM}{dz}\right)\Big\};$$

$$E_2 = \upsilon^{-2}\Big\{i_1(t_k)\left[M\left(C^{-1}\upsilon - R_1\chi\right) + v\left(2R_1M^2 + L_1\chi\right)\times\right. \\ \times\frac{dM}{dz} - 2v^2L_1M\left(\frac{dM}{dz}\right)^2\Big] + i_2(t_k)\left[R_2\left(R_1M^2 + R_2L_1^2\right) - \right. \\ \left.\left[-Mv\left(2L_1R_2 + \chi\right)\frac{dM}{dz} + \left(L_1L_2 + M^2\right)v^2\left(\frac{dM}{dz}\right)^2\right] + \right. \\ \left. + u_c(t_k)\left[v\left(L_1L_2 + M^2\right)\frac{dM}{dz} - M\chi\right]\Big\};$$

u_c is the CES voltage.

If the discriminant of the characteristic equation for equation (3) is greater than zero, then one of its roots is real $x_1 = d$, and the other two are complex conjugate $x_{2,3} = f \pm jg$, and the solution for the currents takes the form:

$$i_n(t_{k+1}) = \left(\xi_n - \frac{\xi_m v}{R_n} \frac{dM}{dz} \right) \Bigg/ \left[1 - \frac{v^2}{R_1 R_2} \left(\frac{dM}{dz} \right)^2 \right], \quad (5)$$

where

$$\xi_n = g^{-1}\left[g^2 + (f-d)^2\right]^{-1} \Big\langle g \cdot \exp(d\Delta t)\left[\left(g^2 + f^2\right)\Theta_n - 2f\Omega_n + \Lambda_n\right] +$$
$$+ \exp(f\Delta t)\Big\{\sin(g\Delta t)\left[d\left(f^2 - g^2 - fd\right)\Theta_n + \left(g^2 + d^2 - f^2\right)\Omega_n + (f-d)\Lambda_n\right] +$$
$$+ g \cdot \cos(g\Delta t)\left[d(d-2f)\Theta_n + 2f\Omega_n - \Lambda_n\right]\Big\rangle;$$

$$\Theta_n = i_n(t_k) + \frac{v \cdot i_m(t_k)}{R_n} \frac{dM}{dz}.$$

Mechanical processes in the LPIEC in the general case can be described by the following equation:

$$i_1(t) i_2(t) \frac{dM}{dz}(z) = \left(m_a + m_2\right)\frac{dv}{dt} + K_P \Delta z(t) + K_T v(t) + \quad (6)$$
$$+ 0.125\pi\gamma_a \beta_a D_{2m}^2 v^2(t),$$

where m_2, m_a are the masses of the armature and the actuator, respectively; K_P is the coefficient of elasticity of the return spring; $\Delta z(t)$ is the value of the displacement of the armature with the actuator; K_T is the coefficient of the dynamic friction; γ_a is the density of the medium of the displacement; β_a is the coefficient of the aerodynamic resistance; D_{2m} is the outer diameter of the actuator.

On the basis of equation (6), the value of the displacement of the armature with actuator can be represented in the form of a recurrence relation [5]:

$$\Delta z(t_{k+1}) = \Delta z(t_k) + v(t_k)\Delta t + \vartheta \cdot \Delta t^2 / \left(m_a + m_2\right), \quad (7)$$

where $v(t_{k+1}) = v(t_k) + \vartheta \cdot \Delta t / \left(m_a + m_2\right)$ is the velocity of the armature with actuator;

$$\vartheta = i_1(t_k) i_2(t_k) \frac{dM}{dz}(z) - K_P \Delta z(t_k) - K_T v(t_k) -$$
$$- 0.125\pi\gamma_a \beta_a D_{2m}^2 v^2(t_k).$$

Thermal processes are largely determined by the period of operation of the LPIEC during the working cycle. So, in the absence of armature movement which occurs either before the start of the direct stroke or after the return stroke, there is thermal contact between the active elements through the insulating liner. The temperatures of the n-th active elements of the LPIEC can be described here by the recurrence relation [6]:

$$T_n(t_{k+1}) = T_n(t_k)\xi + (1-\xi)\Big[\pi^{-1} i_n(t_k) R_n(T_n)\left(D_{en}^2 - D_{in}^2\right)^{-1} +$$
$$+ 0.25\pi T_0 D_{en} H_n \alpha_{Tn} + T_m(t_k)\lambda_a(T) d_a^{-1}\Big]\{0.25\pi\alpha_{Tn} D_{en} H_n + \quad (8)$$
$$+ \lambda_a(T) d_a^{-1}\}^{-1},$$

where $\xi = \exp\left\{ -\frac{\Delta t}{c_n(T_n)\gamma_n}\left(0{,}25 D_{en}\alpha_{Tn} + \frac{\lambda_a(T)}{d_a H_n} \right) \right\}$;

$\lambda_a(T)$ is the heat transfer coefficient of the insulating gasket; d_a is the gasket thickness; D_{en}, D_{in} is the outer and inner diameters of the active elements, respectively; α_{Tn} is the heat exchange coefficient of the n-th active element; c_n is the specific heat of the n-th active element.

The temperatures of the n-th active elements when moving the armature and the absence of thermal contact between the armature and the inductor can be described by the recurrence relation:

$$T_n(t_{k+1}) = T_n(t_k)\chi + (1-\chi)\Big[T_0 + 4\pi^{-2} i_n(t_k) R_n(T_n)\alpha_{Tn}^{-1} \times$$
$$\times D_{en}^{-1} H_n^{-1}\left(D_{en}^2 - D_{in}^2\right)^{-1}\Big], \quad (9)$$

where $\chi = \exp\left\{ -0.25\Delta t D_{en}\alpha_{Tn} c_n^{-1}(T_n)\gamma_n^{-1} \right\}$.

Initial conditions of the system of equations (1) – (9):

$T_n(0) = T_0$ – the temperature of the n-th active element;

$i_n(0) = 0$ – the current of the n-th active element;

$\Delta z(0) = \Delta z_0$ – the initial axial distance between the armature and the inductor winding;

$u_c(0) = U_0$ – the CES voltage;

$v(0) = 0$ – the armature velocity.

Functioning of LPIEC at natural cooling. Electromechanical processes of LPIEC in the direct course of a working cycle with natural cooling (α_{Tn}=20 W·m^{-2}·K^{-1}) are shown in Fig. 3. The current density in the winding of the inductor j_1 is in the form of a polar pulse with a longer fade front compared to the rise front. The maximum value of the induced current density of the armature j_2 of opposite polarity is more than 2 times greater than the current density of the inductor winding. Since the induced current of the armature decays faster, then after 0.8 ms it changes its polarity, increasing until the current in the coil of the inductor stops. After that, the armature current gradually decays. Due to this pattern of current pulses, the electrodynamic force initially has the character of repulsion, and after 0.8 ms, the character of the slight attraction between the armature and the inductor. After the specified time, the resultant force f_z, acting on the armature, becomes inhibitory. The subsequent change in the braking force is due to the elastic deformation of the return spring. Under the action of these forces, the armature with the actuator accomplishes the displacement Δz with a velocity v, which after 0.8 ms decreases under the action of the resultant braking force f_z.

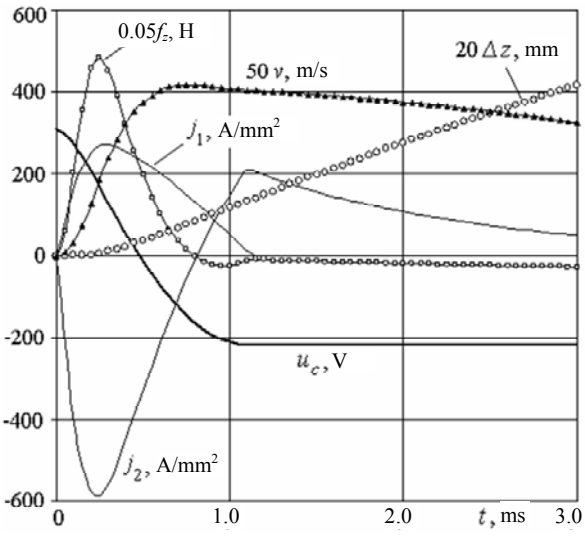

Fig. 3. LPIEC electromechanical characteristics

Let's consider power processes at a direct course of a working cycle of LPIEC. The following energy components take place:

$W_{p1} = \int i_1^2(t) R_1(T_1) dt$ – losses in the inductor;

$W_{p2} = \int i_2^2(t) R_2(T_2) dt$ – losses in the armature;

$W_{mag} = 0{,}5 \sum_{n=1}^{2} L_n i_n^2(t) + M(z) \cdot i_1(t) \cdot i_2(t)$ – magnetic energy;

$W_{kin} = 0{,}5(m_2 + m_a) v^2(t)$ – kinetic energy;

$W_c = 0{,}5 \cdot C \cdot u_c^2(t)$ – CES energy;

$W_{pr} = 0{,}5 \cdot K_P \Delta z^2(t)$ –compressed spring energy.

LPIEC efficiency is estimated by the expression [5]

$$\eta = 100 \frac{(m_a + m_e) v^2 + K_P \Delta z^2}{C\left(U_0^2 - u_c^2\right)} \% \qquad (10)$$

at the end of the direct stroke of the working cycle.

Fig. 4 shows the relative values (marked *) of the energy components during the direct stroke of the LPIEC work cycle.

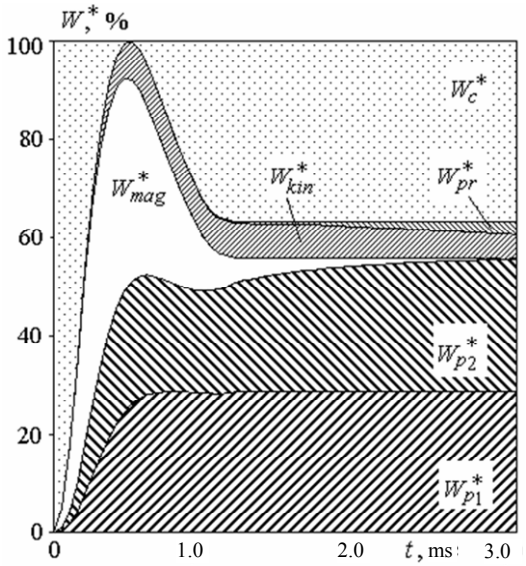

Fig. 4. Relative values of the energetic components at the direct stroke of the LPIEC work cycle

As follows from the presented results, by the end of the working cycle, a significant part of the energy is converted into the thermal energy of the armature (W^*_{p2}=26.8 %) and the inductor (W^*_{p1}=28.7 %). This explains the low efficiency of the LPIEC, which at the end of the direct stroke is η=19.5 %. Note that a significant part of the energy is stored in the CES (W^*_c=36.7 %).

Thermal energy leads to an increase in the temperature rise of the inductor θ_1 and the armature θ_2. In this case, it should be taken into account that in the active mode with the forward motion of the armature with actuator there is no thermal connection between the armature and the inductor. And in the passive mode, after the anchor, under the action of the return spring, takes its initial position, thermal interaction occurs between the active elements of the LPIEC. This thermal interaction is particularly manifested in the cyclic operation of the LPIEC.

Fig. 5 shows the temperature rise of the inductor winding θ_1 and the armature θ_2 during operation of the LPIEC with natural cooling in the cyclic operation mode. The first four operating cycles with the pulse repetition period T_{imp}=1 s are considered. This figure shows the short (5 ms) active mode of the LPIEC operation, in which the armature moves in a straight line, and a long (995 ms) passive mode of operation, in which the armature is mainly in thermal contact with the winding of the inductor.

In the active mode of the LPIEC operation, the temperature rise of the inductor θ_1 and the armature θ_2 is increasing. In this case, the temperature rise of the inductor θ_1 is less than that of the armature θ_2 in the initial operating cycles. In the passive mode, due to thermal contact, there is an increase in the temperature rise of the winding of the inductor and a decrease in the temperature rise of the armature. And with the increase in the number of working cycles, this regularity manifests itself more strongly because of the increasing difference between the temperatures of the armature and the winding of the inductor.

With a significant number of operating cycles, unacceptably high temperature excesses occur at which the epoxy resin of the winding of the inductor is softened: after 400 cycles, the excess of the temperature of the winding of the inductor is θ_1=110 °C, and after 800 cycles – θ_1=170 ° C. In this case, the excess temperatures of the winding of the inductor and the armature are practically equalized.

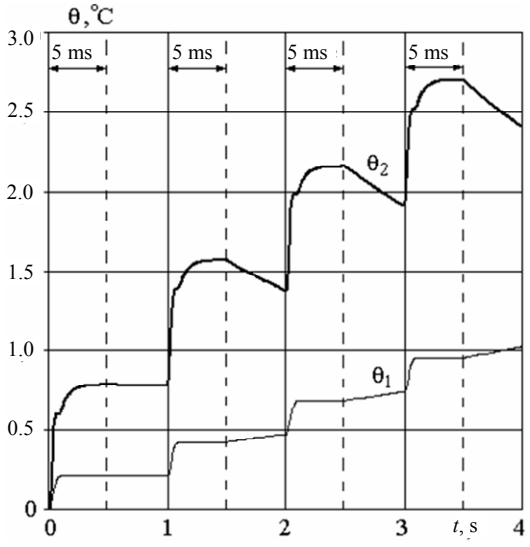

Fig. 5. The excess of the temperatures of the inductor winding θ_1 and the armature θ_2 during cyclic operation (T_{imp}=1 s)

Ways to reduce the heating of LPIEC. One of the ways to solve the problem of unacceptably high heating, which is especially important for the epoxy-coiled inductor winding, is the intensive cooling of it or the anchor.

Consider the effect on the thermal state of the LPIEC of intense water (α_{Th}=2 kW·m^{-2}·K^{-1}) cooling of one or both active elements. Fig. 6 shows the dynamics of temperature rise in the winding of the inductor and the armature during intensive cooling of the inductor (cooling mode I), the armature (cooling mode II) and their co-cooling (cooling mode III) for the first 4 cycles with the pulse repetition period T_{imp}=1 s.

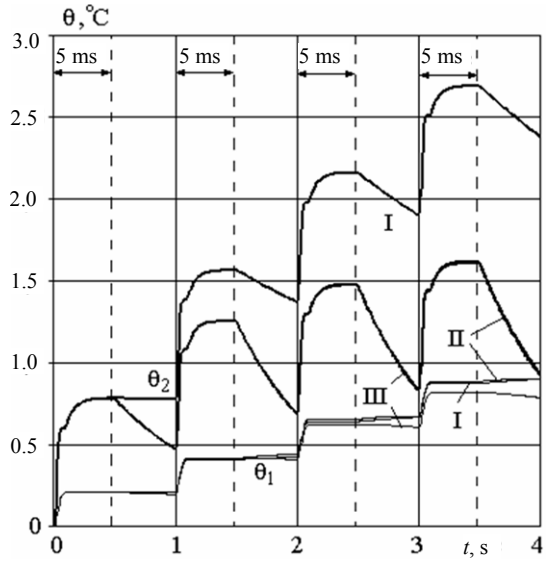

Fig. 6. The excess of the temperatures of the inductor winding θ_1 and the armature θ_2 during cyclic operation (T_{imp}=1 s) in cooling modes I, II and III

When cooling mode I is used, the excess of the temperature of the inductor winding θ_1 decreases by 12 % in the first 4 cycles, while the temperature of the armature θ_2 does not practically change. In the cooling mode II, the armature temperature is reduced by 61 %, while the inductor winding is only 12 % lower. In cooling mode III, the smallest excess occurs both in the winding of the inductor (23 %) and in the armature (62 %). In this case, in the passive mode, the temperature rise of the armature θ_2 decreases substantially, and θ_1 of the winding of the inductor practically does not change. The heating of the active elements changes markedly during the long operation of the LPIEC. Fig. 7 shows the dynamics of temperature excesses of active elements of the LPIEC during operation for 100 s (T_{imp}=1 s).

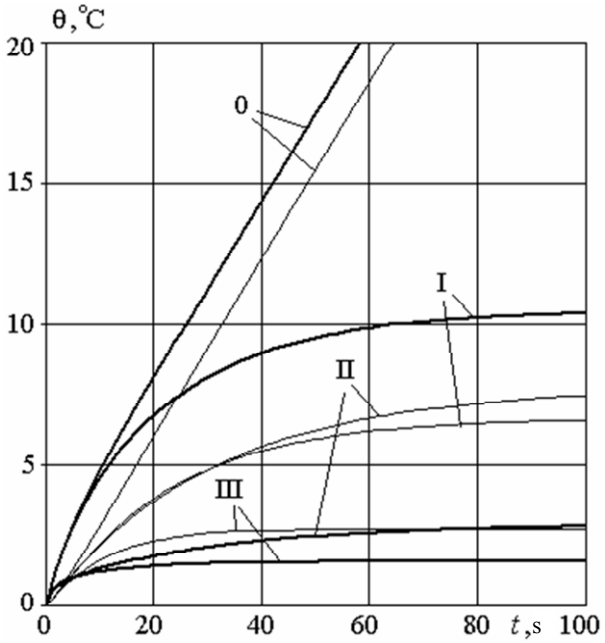

Fig. 7. The excess of the temperatures of the inductor winding θ_1 (thin lines) and the armature θ_2 (thick lines) during cyclic operation (T_{imp}=1 s) in cooling modes I, II and III

As follows from the presented dependencies, intensive cooling of at least one of the active elements practically prevents inadmissible heating of both elements. Excess of the temperatures of the active elements reach certain values, after which they practically do not change. Thus, intensive cooling of one of the active elements of the LPIEC reduces the heating temperature of the other element. So for 100 working cycles, when cooling mode I is used, the temperature rise of the armature is θ_2 = 10.4 ºC, and in the cooling mode II – the temperature of the inductor winding θ_1 = 7.5 ºC is exceeded.

Another way to reduce the heating of active elements of the LPIEC is to increase the pulse repetition period, at which the passive period increases, and hence the interaction time of the inductor and armature.

Fig. 8 shows the dynamics of temperature excesses of active elements of the LPIEC for four initial operating cycles with a follow-up period of T_{imp}=5 s. With an increase in the pulse repetition period, there is a noticeable decrease in the excess of the temperatures of the active elements.

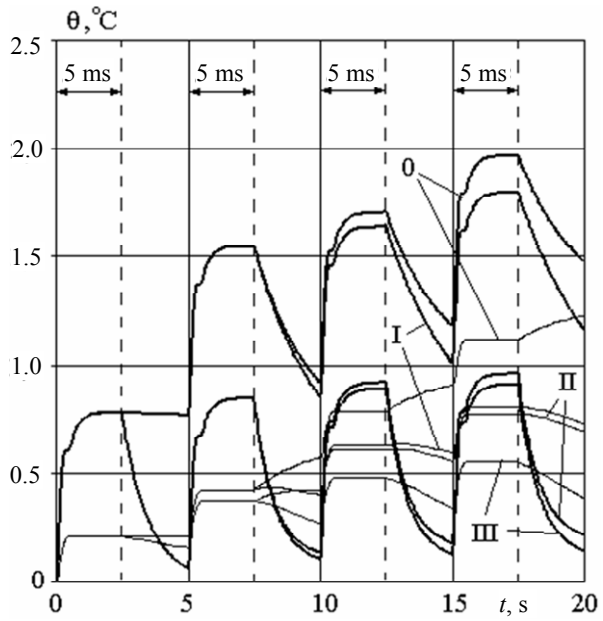

Fig. 8. The excess of the temperatures of the inductor winding θ_1 (thin lines) and the armature θ_2 (thick lines) during cyclic operation (T_{imp}=5 s) with natural cooling (0) and in cooling modes I, II and III

At the pulse repetition period T_{imp}=5 s there is a significant decrease in the temperature rise of the armature θ_2 in the passive mode of the LPIEC operation, including with natural cooling (0). The excess of the temperature of the inductor winding θ_1 in the passive mode of operation of the LPIEC occurs only with natural cooling (0). In cooling modes I, II and III, the temperature rise of the inductor winding θ_2 also decreases.

Fig. 9 shows the dynamics of the relative excess of the temperatures of the inductor θ_1^* and the armature θ_2^* with the natural and intensive cooling of the inductor, the armature and both of them, depending on the value of T_{imp}

per 100 pulses. The values of the excess temperatures are normalized by the corresponding values at T_{imp}=1 s. As follows from the presented values, an increase in the pulse repetition period T_{imp} leads to a decrease in the temperature excesses of both the inductor θ_1 and the armature θ_2 under any cooling method. However, when working with natural cooling of the temperature rise of the winding of the inductor and the armature, the impulses decrease practically linearly and insignificantly with an increase in the pulse repetition period. So, at T_{imp}=5 s in comparison with T_{imp}=1 s the temperature rise of inductor θ_1 decreases by 23 %, and θ_2 of armature – by 28 %.

With intensive cooling of at least one of the active elements of the LPIEC, with a similar increase in the pulse repetition period, the excess of the temperatures of the active elements decreases by 80-90 %. It should be noted that the strongest decrease (by 67-77 %) of temperature elevations occurs with an increase in T_{imp} from 1 s to 2 s. With a further increase in the pulse repetition period, the decrease in temperature excesses occurs much more slowly.

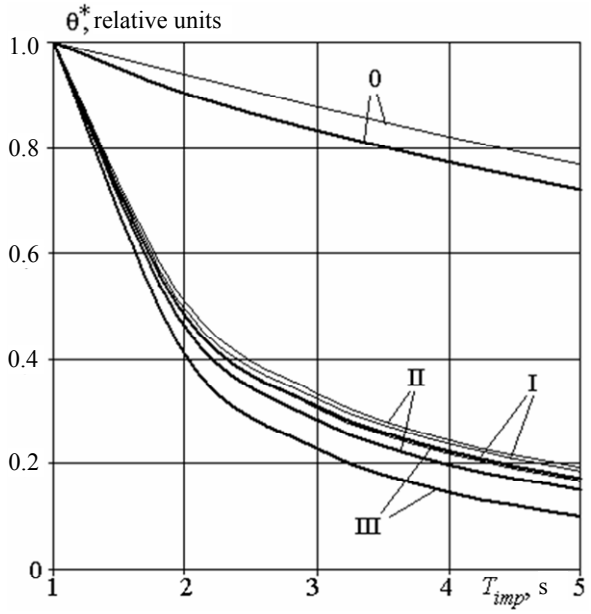

Fig. 9. The dynamics of the relative excesses of the temperatures of the winding of the inductor θ_1^* (thin lines) and the armature θ_2^* (thick lines) with natural cooling (0) and in cooling modes I, II and III per 100 pulses depending on T_{imp}

Thus, intensive cooling of one of the active elements of the LPIEC allows to significantly reduce the temperature excess of both active elements.

Experimental research. To test the main theoretical results, an experimental setup was made, shown in Fig. 10,*a*.

The experimental sample of LPIEC contains a stationary inductor with a two-layer winding of disk shape, which is wound with a rectangular copper busbar, is encased in epoxy resin and is laid either in a thick-walled glass-fiber-reinforced frame or in a thin-walled steel frame with the possibility of intensive cooling (Fig. 2).

Intensive cooling was created by a directional flow of cold air onto the steel frame. Temperature measurements were made on the surface of the winding of the inductor LPIEC during cyclic operation with the pulse repetition period T_{imp}=1 s. The winding temperature was measured with a thermocouple of the M 890G. During measurements, the sensor with the thermocouple was installed in the most heat-stretched area - in the middle of the open side of the winding.

a *b*

Fig. 10. Experimental installation for LPIEC research with a thin-walled steel framework (*a*) and temperature measurement process (*b*)

It was found that the winding of the inductor with the steel frame blown by air, is heated weaker than the winding with the insulating frame (Fig. 11). We note that during 270 s the temperature of the winding with the insulating frame increased so that its epoxy resin softened. It was found that the experimental dependences with an accuracy of 6 % coincide with the calculated results.

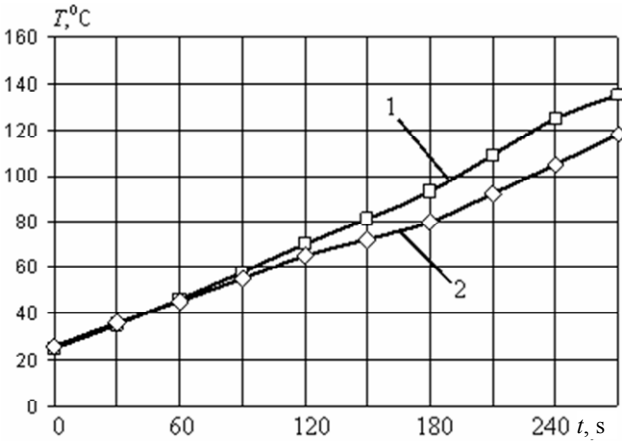

Fig. 11. Experimental temperature dependences on the surface of the inductor winding with the insulating (1) and steel (2) LPIEC frames while working at T_{imp} = 1 s

Constructive scheme of LPIEC with intensive water cooling of the inductor winding. Since the use of intensive water cooling for a movable armature is associated with a number of design difficulties, this cooling is advisable to apply only to the stationary winding of the inductor. Proceeding from this, a constructive scheme of the LPIEC of cyclic action was developed which is shown in Fig. 12 [13].

In the LPIEC of cyclic action upon excitation of the winding 1 of the inductor from the CES, the magnetic

field induces currents in the electrically conducting armature 2, eddy currents. The electrodynamic force that arises between them moves the armature 2 together with the impact disc 3 and the striker 4. The guide part of the striker is connected to a flat piston 5 located inside the cooling chamber 6 with water. Arranged on a flat piston 5 one-way valves 7 with a straight armature stroke freely pass water. In this case, the return spring 8 and the resilient waterproofing bellows 9 surrounding it are stretched. The cooling chamber 6 is located in the insulating housing 10.

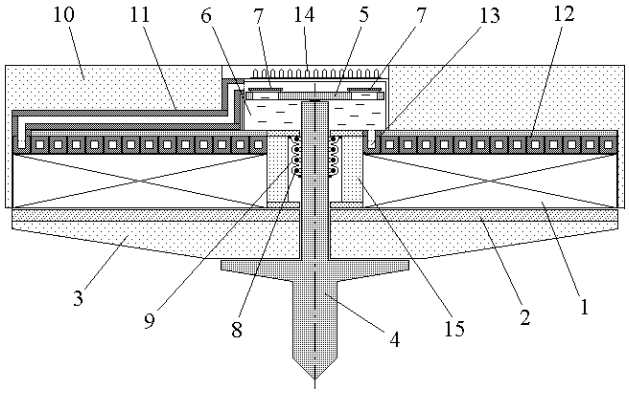

Fig. 12. Constructive scheme of LPIEC of cyclic actions with intensive water cooling of the inductor winding

After the direct stroke under the action of the spring 8, the armature 2 with the striker 4 is reversed, and the one-way valves 7 are closed. The piston 5 pushes water which is squeezed out of the chamber 6. It enters the inlet end 11 of the tube wound in the form of a disk 12, passes through its inner channel and through the outlet end 13 enters the chamber 6. The water circulating in the tube 12 removes heat energy separated in the winding 1, preventing heating of both active elements, since a thermal interaction takes place between them in the passive mode of operation of the LPIEC. The heat of the heated water is drawn from the cooling chamber 6 to the surrounding space through the radiators 14 mounted on its outer side. The guide sleeve 15 serves as a technological framework for the winding 1 of the inductor and protects the waterproofing bellows 9 from mechanical influences. Since the piston 5 is subjected to the action of a resistance force caused mainly by the hydraulic resistance of the water in the internal channel 13 of the multi-turn tube 12, the smooth movement of the striker 4 towards the winding 1 of the inductor occurs. Thus, an unstressed contact of the armature 2 with the winding 1 of the inductor is effected.

Conclusions.

1. A mathematical model of the LPIEC of cyclic action is developed taking into account a complex of interrelated electromagnetic, electromechanical and thermal processes.

2. Electromagnetic, electromechanical and energy processes of LPIEC are investigated which arise during the direct course of the working cycle. It is shown that by the end of the working cycle a significant part of the energy is converted into thermal energy of the armature (26.8 %) and the inductor (28.7 %).

3. At a significant number of working cycles with pulse repetition period of T_{imp}=1 s, unacceptably high temperature excesses of active elements of the LPIEC are observed.

4. One of the ways to solve the problem of heating the winding of the inductor is to intensively cool it, the movable armature or both of them. In this case, the excess of the temperatures of the active elements reach certain values, after which they practically do not change.

5. The increase in the pulse repetition period leads to decrease in the temperature excesses of the active elements of the LPIEC. With an increase in this period, with natural cooling, the excess of the temperatures of the active elements decrease practically linearly and insignificantly. With intensive cooling of at least one of the active elements, the excess of the temperatures of the active elements is reduced by 80-90 %.

6. Temperature measurements were made on the surface of the winding of the inductor LPIEC during cyclic operation with pulse repetition period T_{imp}=1 s. It is established that the winding of the inductor with the steel frame, blown by air, heats up more slowly than the winding with the insulating frame. The experimental dependences with an accuracy of 6 % coincide with the calculated results.

7. The constructive scheme of the LPIEC of cyclic action with intensive water cooling of the inductor winding was developed.

REFERENCES

1. Bissal A. *Licentiate thesis on the design of ultra-fast electro-mechanical*. Stockholm, Sweden. 2013. 120 p.

2. Chemerys V.T., Bolyukh V.F. Prospectives of new coilgun design development. *Artillery and small arms*, 2008, no.3, pp. 44-52.

3. Bolyukh V.F., Vinnichenko A.I. Concept of an induction-dynamic catapult for a ballistic laser gravimeter. *Measurement Techniques*, 2014, vol.56, iss.10, pp. 1098-1104. **doi: 10.1007/s11018-014-0337-z.**

4. Naumov I.V, Bolyukh V.F., Breslavskiy D.V. Deformation and fracture of the plates during loading cylindrical drummer. *Mechanics and engineer*, 2010, no.1, pp. 207-216. (Rus).

5. Bolyukh V.F., Shchukin I.S. *Lineinye induktsionno-dinamicheskie preobrazovateli* [Linear induction-dynamic converters]. Saarbrucken, Germany, LAP Lambert Academic Publ., 2014. 496 p. (Rus).

6. Bolyukh V.F., Shchukin I.S. The thermal state of an electromechanical induction converter with impact action in the cyclic operation mode. *Russian electrical engineering*, 2012, vol.83, no.10, pp. 571-576. **doi: 10.3103/s1068371212100045**.

7. Bolyukh V.F., Luchuk V.F., Rassokha M.A., Shchukin I.S. High-efficiency impact electromechanical converter. *Russian electrical engineering*, 2011, vol.82, no.2, pp. 104-110. **doi: 10.3103/s1068371211020027**.

8. Bolyukh V.F., Oleksenko S.V. The influence of the parameters of a ferromagnetic shield on the efficiency of a linear induction-dynamic converter. *Russian Electrical Engineering*, 2015, vol.86, no.7, pp. 425-431. **doi: 10.3103/s1068371215070044**.

9. D.-K. Lim, D.-K. Woo, I.-W. Kim, D.-K. Shin, J.-S. Ro, T.-K. Chung, H.-K. Jung. Characteristic Analysis and Design of a Thomson Coil Actuator Using an Analytic Method and a Numerical Method. *IEEE Transactions on Magnetics*, 2013, vol.49, no.12, pp. 5749-5755. **doi: 10.1109/tmag.2013.2272561**.

10. Podoltsev A.D., Kucheriava I.N. *Mul'tifizicheskoe modelirovanie v elektrotekhnike* [Multiphysical modeling in electrical engineering]. Kyiv: Institute of Electrodynamics of NAS of Ukraine, 2015. 305 p. (Rus).

11. L. Shoubao, R. Jiangjun, P. Ying, Z. Yujiao, Z. Yadong. Improvement of Current Filament Method and Its Application in Performance Analysis of Induction Coil Gun. *IEEE Transactions on Plasma Science*, 2011, vol.39, no.1, pp. 382-389. **doi: 10.1109/tps.2010.2047276.**

12. Bolyukh V.F., Lysenko L.I., Bolyukh E.G. Parameters of high-efficiency pulsed inductive electromechanical converters. *Russian Electrical Engineering*, 2004, vol.75, no.12, pp. 1-11.

13. Bolyukh V.F., Luchuk V.F., Shchukin I.S. *Induktsionno-dinamicheskii elektrodvigatel' tsiklicheskogo deistviia* [Induction-dynamic electric motor of cyclic action]. Patent Russian Federation, no. 2467455, 2012. (Rus).

Received 28.06.2017

V.F. Bolyukh[1]*, Doctor of Technical Science, Professor,*
I.S. Schukin[2]*, Candidate of Technical Science, Associate Professor,*
[1] National Technical University «Kharkiv Polytechnic Institute»,
2, Kyrpychova Str., Kharkiv, 61002, Ukraine,
phone +380 57 7076427, e-mail: vfbolyukh@gmail.com
[2] Firm Tetra, LTD,
2, Kyrpychova Str., Kharkiv, 61002, Ukraine,
phone +380 57 7076427, e-mail: tech@tetra.kharkiv.com.ua

How to cite this article:
Bolyukh V.F., Schukin I.S. Investigation of thermal processes in a linear pulse-induction electromechanical converter of cyclic action. *Electrical engineering & electromechanics*, 2017, no.5, pp. 14-22. **doi: 10.20998/2074-272X.2017.5.02.**

UDC 621.314 **doi: 10.20998/2074-272X.2017.5.03**

E.V. Yagup

AN ACTIVE POWER FILTER AT OPERATION ON THE UNBALANCED AND NONLINEAR LOADS WITH CONTROL BY OPTIMIZATION ALGORITHM

Purpose is to develop a method for controlling a power active filter based on search optimization using software of Mathlab package and applying this method for balancing and compensating for all components of reactive power in a three-phase system feeding unbalanced linear and nonlinear loads simultaneously. Methodology consists in the development of a visual model of the power supply system that supplies unbalanced and non-linear loads, to the connection points of which a power active filter on IGBT transistors is connected according to a parallel type scheme. We propose an algorithm for calculating the chosen optimization criterion using a visual model, linking the visual model with an optimizing program, and performing a search engine optimization process using an embedded program that implements the deformable polyhedron algorithm. Results lead to an optimal mode, which is characterized by the amplitudes of the control signals of the power active filter control system determined by the search, as well as the initial value of the voltage on the filter energy exchange capacitor. Originality lies in the fact that the proposed method of controlling the operation of the power filter makes it possible to dispense with the construction of a relatively complex filter control system based on Clark's mathematical transformations. Practical value lies in the fact that finding a quasi-steady-state optimal mode of the power supply system with a power active filter is performed automatically in the process of search optimization with a simplified control system. The above principles can be implemented in the microprocessor control system for power active filters. References 9, figures 4.

Key words: **search optimization, visual model, three-phase power supply system, reactive power, power active filter.**

Статья посвящена исследованию трехфазной четырехпроводной системы электроснабжения, питающей несимметричную трехфазную и однофазную нелинейную нагрузки. Силовой активный фильтр представляет собой четырехплечевой мостовой инвертор на IGBT транзисторах. Инвертор питается от энергообменного конденсатора и инжектирует корректирующие токи через буферные реакторы. В отличие от классической системы управления, основанной на преобразованиях Кларк для напряжений и токов, в рассматриваемом варианте предложено управление источниками эталонных сигналов, априори имеющими синусоидальную форму и совпадающими с фазами питающих источников электрической энергии. Определение необходимых амплитуд эталонных сигналов составляет сущность задачи поисковой оптимизации. Оптимизация осуществляется методом деформируемого многогранника с использованием визуальной модели системы электроснабжения с силовым активным фильтром. По завершении оптимизации система приходит к оптимальному режиму, характеризующемуся полной компенсацией всех составляющих реактивной мощности. Библ. 9, рис. 4.

Ключевые слова: **поисковая оптимизация, визуальная модель, трехфазная система электроснабжения, реактивная мощность, силовой активный фильтр.**

Introduction. Unbalanced and nonlinear loads in three-phase power supply systems give rise to a number of problems associated, ultimately, with reactive power. Circulation of reactive power in the system in turn leads to an increase in the currents in the power lines, an increase in irreversible heat losses in the wires, overheating and premature failure of the insulation of electrical devices [1]. In this regard, the issues of balancing and compensation of reactive power in power supply systems represent a great and unflagging interest in recent decades. A number of works in this area are related to research on the physical nature of reactive power and mathematical interpretations of its behavior, depending on the causes of its appearance [2]. In this respect, a departure from the traditional ideas that emerged in the 20-50th of the last century and the identification of the weaknesses of these theories [3, 4] is characteristic. The need to apply new theories based, in particular, on the use of the concept of instantaneous power, is dictated by the development of control systems for power active filters [4-8], which can fundamentally solve the problems associated with asymmetry and nonsinusoidality of voltages and currents in three-phase power supply systems. Power circuits of active filters are built on the basis of three-phase inverters on IGBT transistors with an energy-exchange capacitor charged through shunt back diodes. The generated corrective currents through the buffer reactors are injected into the power supply system at the load connection points for the case of a parallel active filter. The responsible element of the power active filter is the transistor control system which is an intelligent device containing rather complex computational blocks realized with the help of microcontrollers. The tradition of designing control systems based on the use of Clark transformations and the theory of instantaneous power has already been established [5-7]. At the same time, there are still attempts to apply other approaches for controlling power active filters, in particular, based on the application of search engine optimization algorithms [9]. These algorithms presuppose finding a quasi-steady-state mode of the power supply system with an active filter using software optimization tools, thereby making it possible to eliminate these traditional transformations and obtain optimal solutions for the desired mode.

The goal of the work is to apply search optimization methods to find a quasi-steady-state mode of the three-phase power supply system with a power active filter of parallel type while simultaneously feeding a three-phase asymmetrical active-inductive load and a nonlinear valve load.

The main material of investigations. *A visual model* of the power supply system under investigation is shown in Fig. 1.

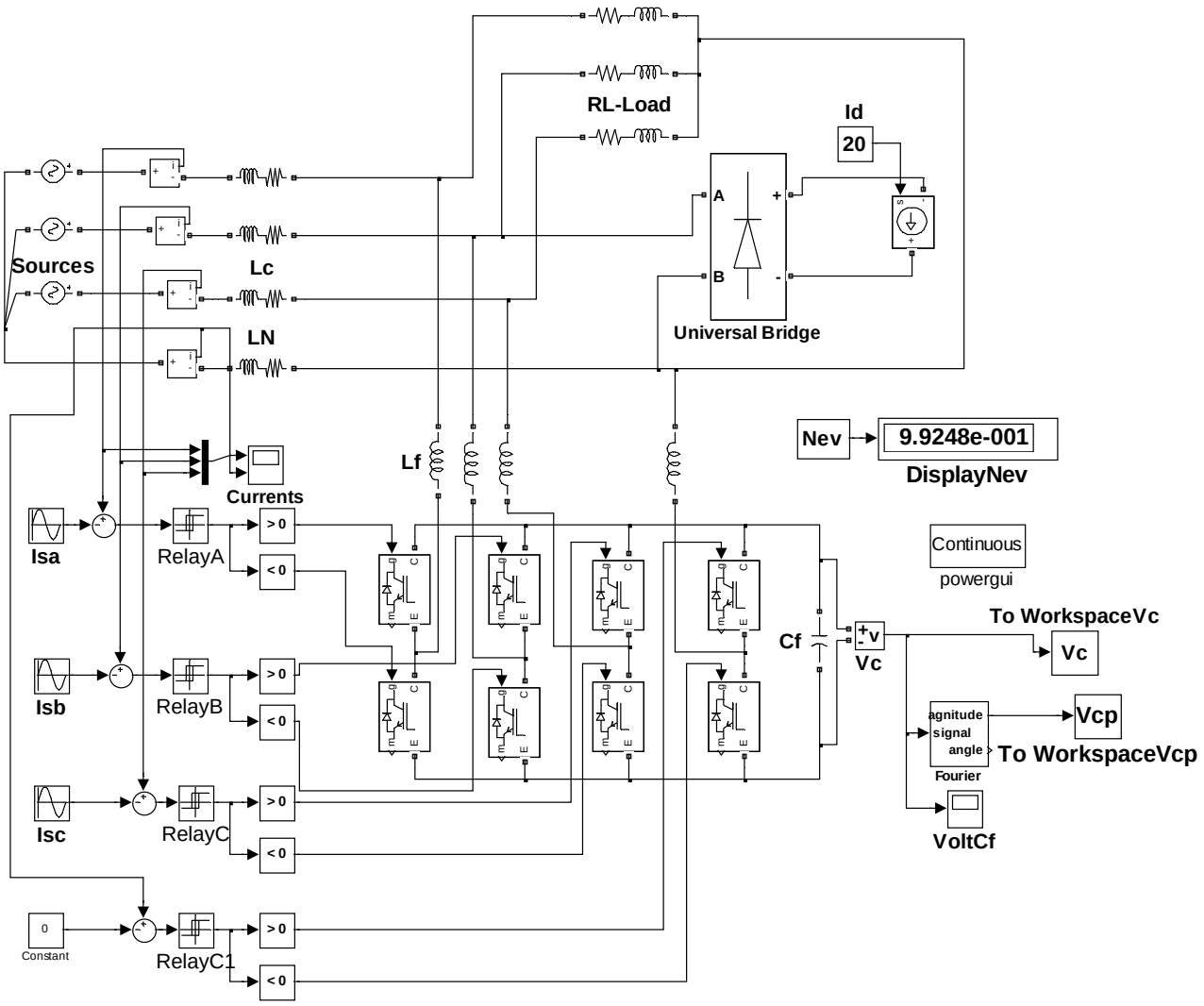

Fig. 1. A visual model of the system under investigation

Here, the supplying three-phase symmetric network of infinite power is represented by voltage sources Sources having a normalized amplitude of 100 V and a frequency of 50 Hz. Power transmission lines, unlike [2], are not included in the load, but are considered separately and, therefore, are not covered by a power active filter. They are represented by active-inductive elements L_c, resistor resistances of which are assumed to be equal to 0.1 Ω, and inductance 0.001 H. The resistance and inductance of the neutral wire L_N are three times higher than the corresponding values of the transmission line parameters. The three-phase unbalanced linear load RL-Load according to the star circuit connected to the neutral wire has the following phase parameters: R_a=1.5 Ω, L_a=0.025 H, R_b=1.0 Ω, L_b=0.01 H, R_c=2.0 Ω, L_c=0.04 H. The non-linear load is represented by a single-phase bridge rectifier Universal Bridge. It is connected to phase B at the point of connection of the linear load and to the neutral wire, so the rectifier is fed by phase voltage. The load of the rectifier is controlled by a constant current source of fixed value I_d=20 A. The power block of the active filter is represented as an inverter by four shoulders of IGBT transistors, each of which is shunted by a reverse diode. Through the reverse diodes, the energy-exchange capacitor C_f is charged, which actually feeds the active filter, for which it is necessary to ensure the charge of this capacitor to a voltage exceeding the amplitude of the line voltage of the network at the connection points of the loads. To these points, correcting currents taken from the diagonals of the inverter bridges are fed through the buffer reactors L_r. These currents should provide sinusoidal currents in the transmission lines that coincide in phase with the phase voltages of the respective power supplies.

The *control system* of the active filter is built according to the relay principle. It is implemented with the help of four relay elements Relay, with the outputs of which the signals are divided into two channels using the elements of comparison with zero. The resulting pairs of impulse signals are fed to the transistors of the upper and lower arms of the corresponding phase. In this way, pulse-width modulation is implemented, thanks to which the correcting currents of the active filter are formed. To generate signals using the relay principle, currents in power lines and neutral conductors are taken with current meters. Further, from the received signals, reference signals are subtracted, the shape of which must be repeated as a result of the action of the correcting filter currents in the load lines and in the neutral wire. Therefore, the reference signals I_{sa}, I_{sb}, I_{sc} for the phases

A, B, C are respectively given in the form of a three-phase symmetric system of sinusoids similar to sinusoids of supply voltages of the power supply system. Since the neutral wire must be completely unloaded, the reference signal for it is given by a zero-constant source. Under such conditions, only the amplitude of the reference signals, which ensures this regime, remains unknown for reaching the quasi-steady state.

Unbalanced mode with the power filter off is characterized by non-sinusoidality and non-linearity of currents and voltages in the system and overloading of the neutral current wire. In Fig. 2 three currents in the transmission lines (upper diagrams) and current in the neutral wire are shown. It is seen that the current in phase B, which is loaded with a rectifier, reaches an amplitude of 40 A, and the current in the neutral wire is 25 A, which is twice the amplitudes of the linear currents of phases A and C. All currents have pronounced non-sinusoidal shape which means the presence in the system of currents of higher harmonics and reactive power distortions.

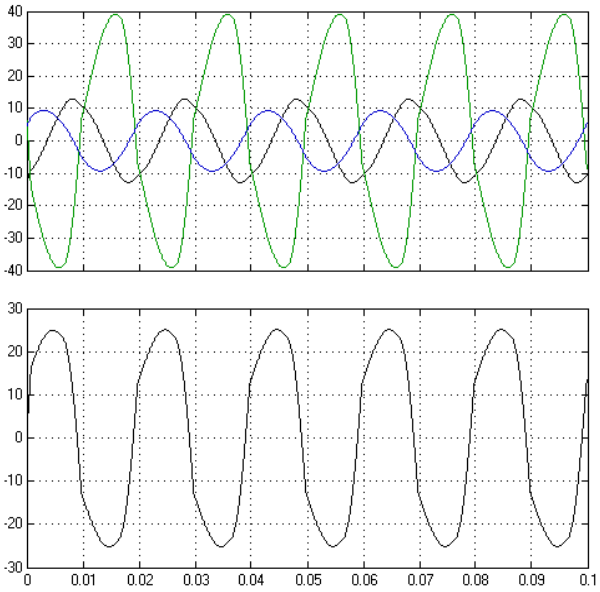

Fig. 2. Currents at the unbalanced mode

Optimization of the mode is carried out when the power filter is connected by Mathlab software using the presented visual model. The optimization is based on the requirement of specifying such a single value of the amplitudes of the reference signals for the phases at which a quasi-steady-state regime takes place in the system. It is characterized by the establishment of periodic currents and voltages on all elements of the system. In particular, the voltage on the energy-exchange capacitor must represent the sum of the constant and the variable components. The constant component of the voltage across the capacitor, as indicated above, must exceed the amplitude of the line voltage. The voltage pulsations on the capacitor, representing the alternating component, depend on the load and capacitance of the energy-exchange capacitor. From the point of view of the efficiency of the filter, we can assume that this capacitance is infinite, and in this case plays the role of a voltage source. In this case, ripple will be absent. However, in practice the capacity of the energy-exchange capacitor is finite (in the model its value is assumed equal to 600 μF). With a finite value of capacitance of the capacitor, the voltage on it reflects the difference between the amplitude of the reference signal and the optimum value. When this value is exceeded, excess energy enters the system and the voltage on the energy-exchange capacitor tends to increase, reaching in the asymptotics a certain very large value corresponding to the balance of active powers. If the amplitude of the reference signal is insufficient, the voltage on the energy-exchange capacitor tends to decrease due to the lack of energy entering the system, reaching zero in the asymptotics which does not at all correspond to the normal operating conditions of the power active filter. Thus, the voltage on the energy-exchange capacitor of the filter, provided that its capacity is finite, is an indicator of the achievement of the optimal compensated regime in the system.

The optimization software is taken from the standard Matlab library, where there are such non-linear optimization programs as fminsearch() that implements the deformable polyhedron algorithm, and fminunc() using the conjugate gradient method. Both programs are easily interchangeable with changing the name by which they are called, the arguments for both functions can be the same. As the optimization variables, the amplitude of the reference signal of the control system and the initial voltage on the energy-exchange capacitor are used. The objective function is formed from discrete voltage values on the energy-exchange capacitor. These values are output at the run interval of the visual model for five periods of the supply voltage with a sampling interval equal to the period of the supply voltage. To form the objective function, the differences of adjacent discrete values are compiled, from which the spherical metric is formed. In addition, the condition for achieving discrete values of a given level (it was assumed to be 400 V) was also introduced. Thus, when the model is run, discrete values are transferred to the working area of Matlab, where they are picked up by an additional function that executes the visual model and then calculates the value of the objective function, which is then passed to the parent program that calls the optimization function. Fig. 1 shows the state of the model after reaching the minimum, where you can see the value of the objective function in the form of the global constant N_{ev}=0.99248, which sufficiently accurately determines the compensated mode in the system. The amplitudes of the reference signals in this case were I_{sm}=12.369 A. From this value, 4.243 A are incident on the supply of an asymmetric linear load, as shown in [10], and the remaining fraction of 8.126 A is due to the supply of a nonlinear load to the rectifier. The fairness of this distribution is illustrated by a simple estimate of the fraction of active power consumed by the rectifier. Fig. 3 shows the current diagrams in the lines of the neutral wire in the compensated mode (similar to the diagrams in Fig. 2). It is seen that the amplitudes of the linear currents are equalized, and their phases coincide with the phases of the supply voltages. The current in the neutral wire is almost gone. This indicates a complete balancing and balancing of the mode in the power supply system.

Fig. 4 shows the voltage diagram on the energy-exchange capacitor. It starts with the voltage at the zero moment V_{co}=401.562 V found during the search optimization and forms a vector of discrete quantities V_c=[400.099,399.878,399.885,399.356,399.179] that testify to the provision of a given stable voltage on the energy-exchange capacitor within the specified error.

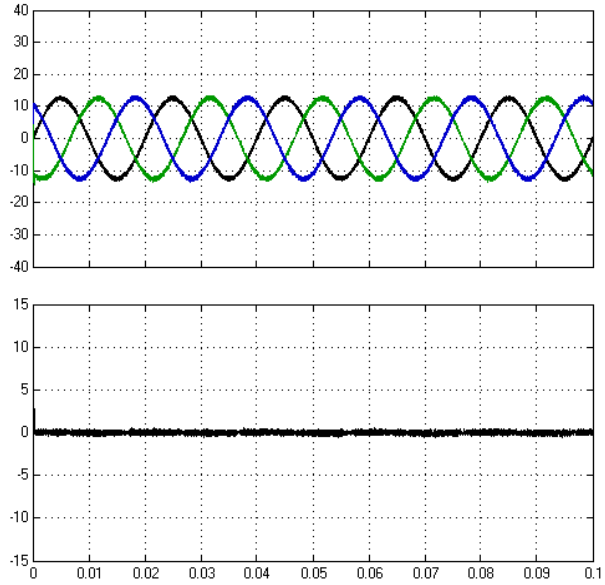

Fig. 3. Current at the balanced mode

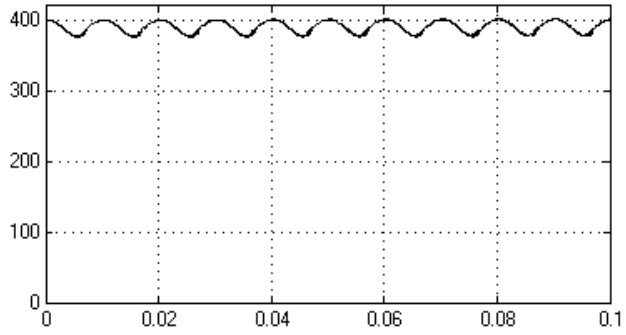

Fig. 4. Voltage on the capacitor

Conclusions. The research carried out shows that the proposed algorithm for active filter control based on the application of search optimization in conjunction with the visual model of the power supply system makes it possible to determine the quasi-steady state of the system and to reach the optimal mode of full compensation of all components of reactive power when feeding asymmetrical linear and nonlinear loads. It is possible to form the target function from the discrete voltage values on the energy-exchange capacitor, and use the amplitude of the reference sinusoidal signal for the proposed control system and the initial value of the voltage on the energy-exchange condenser as optimization variables. An introduction to the expression for the objective function of the voltage stabilization parameter on the energy-exchange capacitor also allows to set the proper level of the voltage over the capacitor above the amplitude of the line voltage of the network, thus providing the necessary direction of the energy flow from the filter to the network.

REFERENCES

1. Acha E., Agelidis V.G., Anaya-Lara O., Miller T.J.E. *Power Electronic Control in Electrical Systems*. Bodmin, MPG Books Ltd, Cornwall, 2002. 443 p. ISBN 0 7506 5126 1.

2. Zhemerov G.G., Tugay D.V. Components of total electric energy losses power in PQR spatial coordinates. *Electrical engineering & electromechanics*, 2016, no.2, pp. 11-20. (Rus). **doi: 10.20998/2074-272X.2016.2.02.**

3. Czarnecki L.S. What is wrong with the Budeanu concept of reactive and distortion power and why it should be abandoned. *IEEE Transactions on Instrumentation and Measurement*, 1987, vol.IM-36, no.3, pp. 834-837. **doi: 10.1109/TIM.1987.6312797**.

4. Nabae A., Tanaka T. A new definition of instantaneous active-reactive current and power based on instantaneous space vectors on polar coordinates in three-phase circuits. *IEEE Transactions on Power Delivery*, 1996, vol.11, no.3, pp. 1238-1243. **doi: 10.1109/61.517477.**

5. Akagi H., Watanabe E. H. and Aredes M. *Instantaneous Power Theory and Applications to Power Conditioning*. Wiley-IEEE Press, April 2007. 379 p. ISBN: 978-0-470-10761-4.

6. Akagi H., Kanazawa Y., Nabae A. Generalized theory of the instantaneous power in three phase circuits. *Int. Power Electronics Conf.*, Tokyo, Japan, 1983, pp. 1375-1386.

7. Akagi H., Kanazawa Y., Nabae A. Instantaneous reactive power compensators comprising switching devices without energy storage components. *IEEE Transactions on Industry Applications*, 1984, vol.IA-20, no.3, pp. 625-630. **doi: 10.1109/TIA.1984.4504460**.

8. Peng F.Z., Ott G.W., Adams D.J. Harmonic and reactive power compensation based on the generalized instantaneous reactive power theory for three-phase four-wire systems. *IEEE Transactions on Power Electronics*, 1998, vol.13, no.6, pp. 1174-1181. **doi: 10.1109/63.728344**.

9. Yagup E.V. Optimization of the mode of asymmetric three-phase system using an active filter and a modified control algorithm. *Bulletin of the National Technical University «KhPI» Series: New solutions in modern technologies*, 2016, no.42(1214), pp. 124-128. (Rus). **doi: 10.20998/2413-4295.2016.42.20.**

Received 27.08.2017

E.V. Yagup, Candidate of Technical Science, Associate Professor,
O.M. Beketov National University of Urban Economy in Kharkiv,
17, Marshal Bazhanov Str., Kharkiv, 61002, Ukraine,
phone +380 57 7073114,
e-mail: kata3140@gmail.com

How to cite this article:
Yagup E.V. An active power filter at operation on the unbalanced and nonlinear loads with control by optimization algorithm. *Electrical engineering & electromechanics*, 2017, no.5, pp. 23-26. **doi: 10.20998/2074-272X.2017.5.03.**

UDC 621.317.332.1:621.79.03:617-7 **doi: 10.20998/2074-272X.2017.5.04**

I.V. Krivtsun, I.V. Pentegov, V.M. Sydorets, S.V. Rymar

A TECHNIQUE FOR EXPERIMENTAL DATA PROCESSING AT MODELING THE DISPERSION OF THE BIOLOGICAL TISSUE IMPEDANCE USING THE FRICKE EQUIVALENT CIRCUIT

Purpose. ***Modeling the dispersion of the biological tissue impedance of vegetable and animal origin using the Fricke equivalent circuit; development of a technique for experimental data processing to determine the approximation coefficients of the dispersion of the biological tissue impedance for this equivalent circuit; study of the features of the equivalent circuit at modeling the dispersion of the impedance, resistance, and reactance; the definition of the frequency domain in which using of the equivalent circuit is correct; revealing and generalization of the main regularities of dissipation of biological tissue impedance of vegetable and animal origin.*** ***Methodology.*** ***The technique is based on the scientific provisions of theoretical electrical engineering – the theory of the electromagnetic field in nonlinear media in modeling the dispersion of the biological tissue impedance.*** ***Results.*** ***The electric circuit of the Fricke equivalent circuit allows modeling the dependences of the impedance module of biological tissues, active and reactive components of impedance with acceptable accuracy for practical purposes in the frequency domain from 10^3 to 10^6 Hz. The equation of impedance of the Fricke equivalent circuit for biological tissues makes it possible to approximate the frequency dependences of the impedance modulus, active and reactive parts of the total resistance only by using the approximation coefficients corresponding to each part. The developed method for determining the values of the approximation coefficients of the impedance equation for the Fricke equivalent circuit for biological tissues allows to determine these values with high accuracy for various biological tissues. It is shown that the frequency dependences of the active component of the total resistance for tissues of vegetable and animal origin are similar.*** ***Originality.*** ***The developed technique operates with the normalized values of the impedance modulus of the Fricke equivalent circuit, the active and reactive components of the impedance as a function of frequency, which allows a comparative analysis of the dependencies of these parameters of various biological tissues of plant and animal origin.*** ***Practical value.*** ***The approximate dependences of the absolute impedance modulus, active and reactive components of the impedance allow modeling processes occurring in biological tissues with the passage of a current of different frequency. Dependence of the impedance of biological tissue can be applied to the design of diagnostic and control equipment to determine the properties of tissues of animal and vegetable origin, including developing more effective medical equipment.*** References 15, tables 3, figures 16.

Key words: **biological tissue, electrical properties, simulation, impedance dispersion, Fricke substitution scheme, technique, approximation coefficients.**

Разработана методика обработки экспериментальных данных для определения коэффициентов аппроксимации импеданса биологических тканей растительного и животного происхождения при моделировании дисперсии импеданса с помощью схемы замещения Фрике. Проведен анализ свойств схемы замещения Фрике, ее возможностей и особенностей при моделировании дисперсии импеданса, резистанса и реактанса. Показано, что при нормировании дисперсии активные составляющие импеданса для тканей растительного и животного происхождения подобны. Библ. 15, табл. 3, рис. 16.

Ключевые слова: **биологическая ткань, электрические свойства, моделирование, дисперсия импеданса, схема замещения Фрике, методика, коэффициенты аппроксимации.**

Introduction. The dispersion, that is, the frequency dependence, of the impedance (total or complex resistance) and its components - resistance (active resistance) and reactance (reactive resistance) of biological tissues is important in the study of the effect of electric current on them. This applies to electrical safety, diagnosis and treatment of humans and animals, monitoring the quality of agricultural products. Now this issue has become very relevant in connection with the creation of special surgical equipment for welding live tissues by currents of high frequency [1].

The goal of the paper is simulation of dispersion of the impedance of biological tissues of plant and animal origin using the Fricke substitution scheme [2, 3]; creation of a technique for processing experimental data to determine the coefficients of approximation of the dispersion of the impedance of biological tissues for the Fricke substitution scheme; the study of the features of this substitution circuit in modeling the variance of impedance, resistances, and reactance; the determination of the frequency range in which the use of the replacement circuit is correct; identification and generalization of the main regularities of dispersion of the impedance of biological tissues of plant and animal origin.

The studies are based on experimental data from different authors. The examples of data processing presented in the article are presented in a form that is intended for use in the MathCAD package [4].

The results of solving this problem are **relevant** for specialists who create diagnostic and control instrumentation for determining the properties of tissues of animal and plant origin. Also they will be in demand when creating medical equipment for welding live tissues.

Structure of biological tissue. Biological tissue consists of cells and intercellular substance. The cells themselves are complex formations, consisting of many

elements found in a protein substance bounded by cellular membranes (see Fig. 1).

From the point of view of electrical engineering, we will be interested in the change in the impedance of biological tissue from the frequency while passing through it an alternating electric current (AC) which is supplied to the tissue by electrodes with area *S* spaced from each other at a distance *l*.

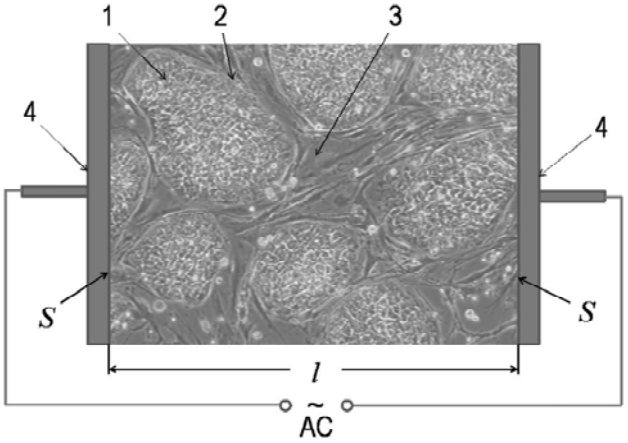

Fig. 1. The structure of a biological tissue consisting of cells 1 bounded by the cell membranes 2 and the intercellular substance 3 (when measuring the impedance, it is placed between the two electrodes 4)

The electromagnetic properties of biological tissues are determined by the characteristics of the organic material filled with electrolyte. In biological tissues, the electrolyte is an intercellular substance and cellular contents [5, 6]. Due to the presence of membranes and films that have capacitance, cell resistance is mainly capacitive in nature.

When measuring the electrical parameters of biological tissues at the boundary between the measuring electrodes and the tissue (electrolyte) when an electric current passes, a double electric layer appears, also having a capacitive character. The double electric layer is approximately described by Stern adsorption theory [7]. The effect of the double electric layer is particularly pronounced with constant current and low frequencies. It is here that the greatest error is introduced into the measurement of the electrical parameters of biological tissues. With increasing frequency, the effect of the double electrical layer decreases.

To reduce the influence of the double electrical layer, when measuring the electrical parameters of biological tissues, as a rule, two pairs of electrodes are used. One pair is supplied with an electric current, and the measurements are made by another pair of electrodes [8].

Dielectric permeability of biological tissue. The permittivity $\underline{\varepsilon}$ [9, 10] (here and below the underlining indicates the complex value) of the biological tissue contains the real ε' and the imaginary part ε", both of which depend on the frequency *f*: $\underline{\varepsilon}(f) = \varepsilon'(f) - j\cdot\varepsilon''(f)$, where $j = \sqrt{-1}$ is the imaginary unit. Fig. 2 shows a typical dependence of the dielectric permeability modulus $|\underline{\varepsilon}|$ of the biologic tissue (in this case, muscle [3, 5, 6]) of the frequency in the frequency range from 10^1 до 10^{12} Hz. Dependence has three characteristic areas α, β, γ.

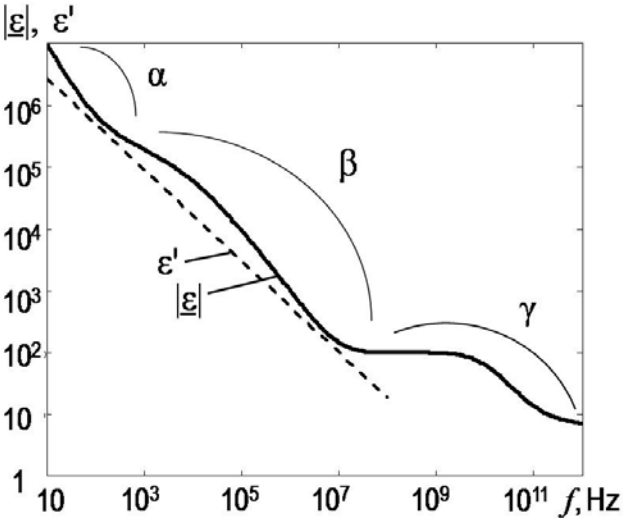

Fig. 2. Dependence of the dielectric permeability module $|\underline{\varepsilon}|$ of biological tissue [3, 5, 6] and the largest calculated values of its real part ε" on the frequency *f*

The presence of ranges of sites is due to [5, 6]:

• α: ($f < 10^3$ Hz) - the flow of current through the intercellular substance, when the resistance of cells for low-frequency current is still high and the dielectric constant is determined by the polarization of intracellular compartments and the inertia of the motion of molecules with a large molecular mass at resonance phenomena, and phenomena in a double electric layer;

• β: (10^3 Гц $< f < 10^8$ Hz) - current flow through the intercellular substance, cellular membranes and cellular contents and reflects the relaxation polarization of polar macromolecules, and is determined by their effective radii and viscosity of the medium, as well as the dielectric losses in the cell membranes - tangent the dielectric loss angle $\mathrm{tg}\delta = \varepsilon''/\varepsilon'$ serving as a quantitative measure of the relative contribution of the electrically conductive and dielectric properties of the medium when the electromagnetic field interacts with it [5, 10]. Note that the values of tgδ, ε' и ε" only partially simulate the reaction of the tissue to the passage of the electromagnetic field through it and do not reflect all the physical processes taking place in the tissue;

• γ: ($f > 10^8$ Hz) - phenomena of resonance of water molecules of intercellular substance and cellular contents, and orientational polarization of water molecules.

The boundaries of the ranges α, β, γ and the values $|\underline{\varepsilon}|$ can differ from those shown in Fig. 2, depending on the type of biological tissue.

One of the methods of modeling in electrical engineering is the creation of electrical circuits of substitution [11]. In modeling the electrical processes in biological tissue, we will adhere to this method.

Fricke electrical circuit for the replacement of biological tissues. When modeling the dispersion of the impedance of biological tissues, the substitution scheme [2] (Fig. 3) proposed in the early 20s of the 20th century

by the Danish-American physicist Hugo Fricke (1892-1972) is often used. The circuit simulates electrical processes in biological tissue at frequencies from 10^1 до 10^6 Hz, that is, in sections α (with the exception of very low frequencies) and β.

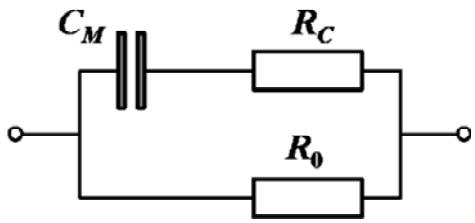

Fig. 3. Fricke electrical circuit for the replacement of biological tissue

The replacement circuit contains: C_M – the frequency-dependent equivalent electrical capacitance of cell membranes; frequency independent equivalent active resistances (resistances) of cell contents R_C and of intercellular substance R_0.

If we consider the resistivities and capacitances with dimensionality, respectively, [Ω·m] and [F/m], then the elements of the substitution circuit in Fig. 3 should be considered as specific.

In the simplest case shown in Fig. 1, the relationship between the specific total electrical resistance and the total electrical resistance (impedances) has the form:

$$\underline{Z}_s(f) = \underline{Z}(f)\cdot S/l;$$

the relationship between the active resistivities and the active electrical resistances:

$$R_{s.C}(f) = R_C\cdot S/l;\ R_{s.0}(f) = R_0\cdot S/l;$$

the equivalent specific electrical capacitance of cell membranes $C_{s.M}$ is determined from the expression:

$$C_{s.M}(f) = C_M(f)\cdot l/S.$$

The specific electric capacitances directly proportional to the product of the dielectric constant $\varepsilon_0 = 8.854\cdot10^{-12}$ F/m and the real part ε' of the complex relative dielectric permeability $\underline{\varepsilon}$:

$$C_{s.M}(f) = C_M(f)\cdot l/S = \varepsilon_0\cdot\varepsilon'(f).$$

The total electrical resistance of the Fricke substitution scheme as a function of frequency is:

$$\underline{Z}(f) = \frac{1}{\dfrac{1}{R_0} + \dfrac{1}{R_C + \dfrac{1}{j\cdot 2\cdot\pi\cdot f\cdot C_M(f)}}}. \qquad (1)$$

Dividing the right and left parts of formula (1) by the resistance R_0, we obtain the expression for the impedance $\underline{Z}_*(f) = \underline{Z}(f)/R_0$ of the substitution scheme in dimensionless form (the values denoted by the asterisk "*" are dimensionless) when normalized to unity [12] in the low-frequency range:

$$\underline{Z}_*(f) = \frac{1}{1 + \dfrac{1}{\dfrac{R_c}{R_0} + \dfrac{1}{j\cdot 2\cdot\pi\cdot f\cdot C_M(f)\cdot R_0}}}. \qquad (2)$$

We introduce dimensionless coefficients a_1, a_2 and a_3 and a power function:

$$R_0/R_C = a_1; \qquad (3)$$

$$2\cdot\pi\cdot f\cdot C_M(f)\cdot R_0 = \frac{R_0}{X(f)} = \left(\frac{f}{f_0}\right)^{a_2}\cdot a_3. \qquad (4)$$

Here X is the reactive resistance (reactance):

$$X(f) = \left[2\cdot\pi\cdot f\cdot C_M(f)\right]^{-1}; \qquad (5)$$

f_0 is the base frequency, which can be assumed equal to 1 Hz. It is introduced because the exponentiation of a dimensional quantity f in the irrational power of a_2 is not correct. We denote the ratio f / f_0 by the dimensionless quantity f_*.

As a result, we write the expression for the Fricke substitution circuit (1) normalized per unit impedance in the form of an approximation function:

$$\underline{Z}_*(f_*, a_1, a_2, a_3) = \frac{1}{1 + \dfrac{1}{\dfrac{1}{a_1} + \dfrac{1}{j\cdot f_*^{a_2}\cdot a_3}}}. \qquad (6)$$

With this form of writing, we obtain $\underline{Z}_*(0,a_1,a_2,a_3) = 1$; $\underline{Z}_*(\infty,a_1,a_2,a_3) = 1/(1 + a_1)$ at any values of a_i, where i is the index number at the coefficient a, $i = 1, 2, 3$.

Approximate dimensionless coefficients a_1, a_2 and a_3 will be found from experimental data.

We have considered the case when in expressions (1) - (4) resistances have the dimension [Ω], and the capacitances - [F]. If the experimental data are obtained for specific resistances and capacitances with dimension of [Ω·m] and [F/m], then the elements of the substitution circuit in Fig. 3 will be specific.

In the analysis, the values can be applied either in [Ω] and [F], or in [Ω·m] and [F/m], since using the specific values in expression (2) instead of absolute values, l and S are shortened, and the result remains the former.

When passing from dimensionless to dimension in expression (6), it is necessary to multiply $\underline{Z}_*(f,a_1,a_2,a_3)$ by R_0 when calculating absolute resistances in [Ω], or by $R_{s.0}$ when calculating resistivities in [Ω·m]. The values of R_0 and $R_{s.0}$ for obtaining the minimum error must be determined at frequency of up to 50 Hz.

We explain the choice of the power function in expression (4) in determining the ratio of the quantities $R_0/X(f)$.

Since the complex dielectric permeability $\underline{\varepsilon}$ contains also the imaginary part ε", its modulus is determined from the expression: $|\underline{\varepsilon}| = \sqrt{(\varepsilon')^2 + (\varepsilon'')^2}$ from which it follows that the condition $\varepsilon' \le |\underline{\varepsilon}|$ is always satisfied. In this connection, the values of ε'(f) which can be determined by the power function $(f/f_0)^{a_2}\cdot a_3$ (in the logarithmic scale, it is the straight line ε' in Fig. 2), should lie below the values of the curve $|\underline{\varepsilon}|$. In this case, the expression (4) corresponds to a given power function.

Frequency dependences of the impedance of biological tissues. The publications [6, 13] contain information on the frequency dependences of the

impedance module $|\underline{Z}_s|$ the active and reactive component of the impedance - the specific resistivity R_s and the specific reactance X_s of plant tissues - apple, carrot and potato in the frequency range from 25 Hz to 1 MHz. Frequency dependences of the active resistance R of biological tissues of animal origin (rat) - liver, heart, kidney, breast and thyroid gland in the frequency range from 0.5...1.5 kHz to 1.0...1.5 MHz are given in [14].

Fig. 4 by points shows the experimental values of the electrical resistances of apple, carrot and potato on the frequency [6, 13], the lines show the approximations obtained with the lspline and interp functions of the MathCAD package, and Fig. 5 - experimental values of active electrical resistances on the frequency [14]: liver, heart (along the fibers), kidney, breast, thyroid gland.

Minimizing the root-mean-square deviations to find the values of the impedance approximation coefficients for the Fricke replacement circuit. To find the coefficients a_i, the approximation function of the impedance of the Fricke substitution circuit (6), we use the genfit function of the MathCAD package implementing the numerical Levenberg-Marquardt method [15]. For this function, a vector $V(f,a_1,a_2,a_3)$ is formed from equation (6) and the equations of its partial derivatives with respect to the required coefficients a_i.

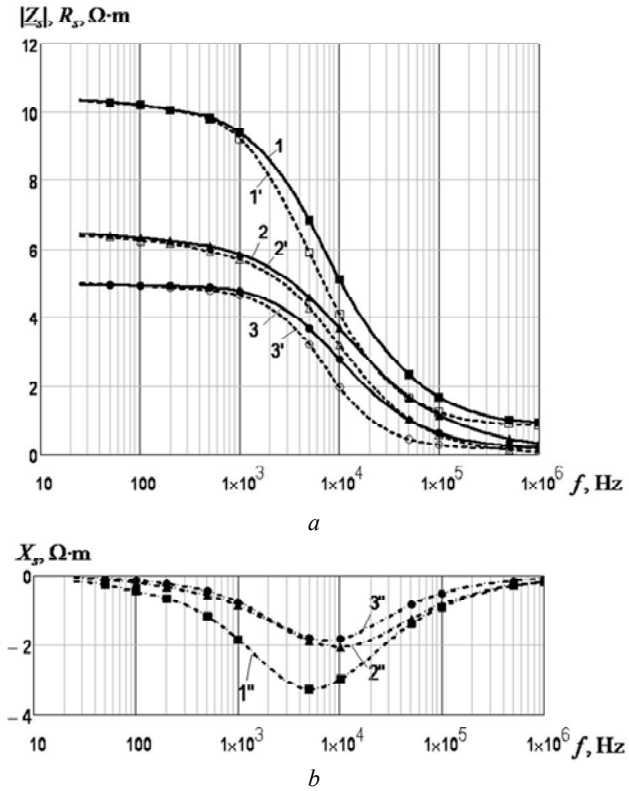

Fig. 4. Frequency dependences of experimental values of electrical resistances of biological tissues of plant origin [6, 13]: (*a*) - modulus of total resistivity $|\underline{Z}_s(f)|$ (digits without a stroke), active $R_s(f)$ (digits with a stroke) and (*b*) - reactive $X_s(f)$ (digits with two strokes) - impedance components, respectively, for tissues: 1, 1', 1" - *apple*, 2, 2', 2" - *carrots* and 3, 3', 3" – *potatoes*

With the known experimental dependences of the resistances: $|\underline{Z}_*| = |\underline{Z}_s|/R_{s.0}$ or $|\underline{Z}_*| = |\underline{Z}|/R_0$; $R_* = R_s/R_{s.0}$ or $R_* = R/R_0$; $X_* = X_s/R_{s.0}$ or $X_* = X/R_0$ on the frequency f for a biological tissue, for example for apple, carrot or potato (Fig. 4), it is possible to compose the vectors V_Z, V_R, or V_X, respectively, for the impedance modulus, active and reactive components of impedance, see Annex.

We define an arbitrary vector of values of the frequencies for valuation by unity

$$f_{*n} = 10^n, \qquad (7)$$

where n is the index at the frequency f_* which determines the ordinal number of the number in the vector f_{*n}, for example, $n = 1...6$ (note that the more terms in n, the more accurate the approximation dependence).

At given some initial values to the coefficients a_i, minimization using the function genfit, written as:

$$a_{Z,i} = \text{genfit}(f_*,|\underline{Z}_*|,a_1,a_2,a_3,V_Z);$$
$$a_{R,i} = \text{genfit}(f_*,R_*,a_1,a_2,a_3,V_R);$$
$$a_{X,i} = \text{genfit}(f_*,X_*,a_1,a_2,a_3,V_X),$$

occurs when determining the values of the coefficients $a_{Z,i}$, $a_{R,i}$ и $a_{X,i}$ which in the best way approximate the approximation curves

$$|\underline{Z}_*(f_*)| = |\underline{Z}_*(f_*,a_{Z,1},a_{Z,2},a_{Z,3})|;$$
$$R_*(f_*) = \text{Re}[\underline{Z}_*(f_*,a_{R,1},a_{R,2},a_{R,3})];$$
$$X_*(f_*) = \text{Im}[\underline{Z}_*(f_*,a_{X,1},a_{X,2},a_{X,3})]$$

(using formula (6)) to the corresponding experimental values normalized to unity.

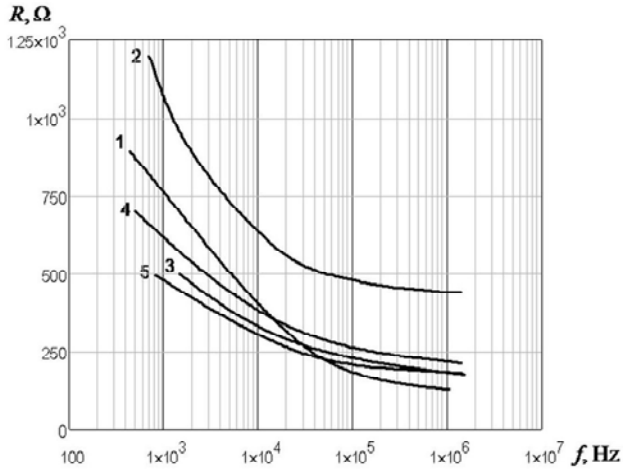

Fig. 5. Frequency dependences of experimental values of active electrical resistances $R(f)$ of biological tissues of animal origin (rat) [14]: 1 - liver; 2 - hearts (along the fibers); 3 - kidney; 4 - the breast; 5 - thyroid gland

For biological tissues of plant origin - apples, carrots and potatoes [6, 13] in Fig. 6, 8, and 10, the experimental and calculated values of the frequency dependences of the impedance modulus $|\underline{Z}_*(f_*)|$ of the Fricke replacement circuit, the active $R_*(f_*)$ and the reactive $X_*(f_*)$ impedance components are presented. For biological tissues of animal origin - liver, heart, kidney, breast and thyroid gland [14] in Fig. 12 the frequency dependences of the values of the active components $R_*(f_*)$ of the impedance of the Fricke substitution scheme are plotted for tissues: 1 - liver; 2 - heart (along the fibers); 3 - the kidney; 4 - breast; 5 - thyroid gland.

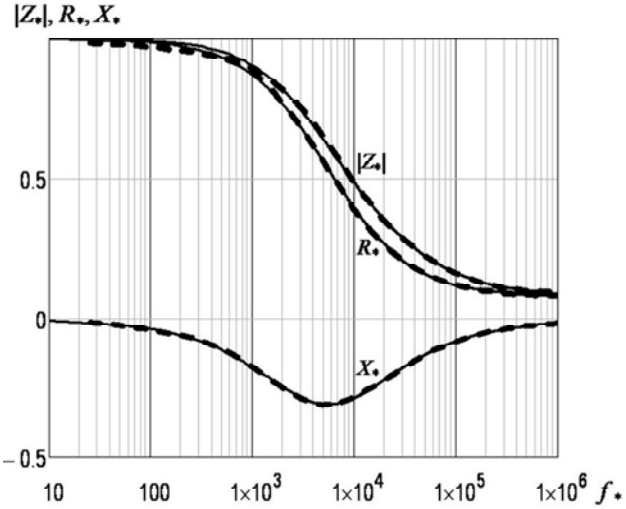

Fig. 6. The frequency dependences of the impedance modulus $|\underline{Z}_*(f_*)|$ of the Fricke substitution scheme, the active $R_*(f_*)$ and the reactive $X_*(f_*)$ impedance components for the *apple* tissue. Thickened dashed curves - experimental values [6, 13], thin solid curves - calculated values

From the consideration of the graphs it can be seen that the calculated curves along their entire length coincide with the experimental values.

In Fig. 7, 9 and 11 graphs are presented of the frequency dependences of the relative deviations Δ_Z, Δ_R and Δ_X [%] of the calculated values of the quantities $\underline{Z}_*(f_*)|$, $R_*(f_*)$ and $X_*(f_*)$, respectively, on their experimental values for tissues of plant origin, and in Fig. 13 graphs of frequency dependences of relative deviations Δ_R [%] of calculated values of $R_*(f_*)$ from their experimental values for tissues of animal origin.

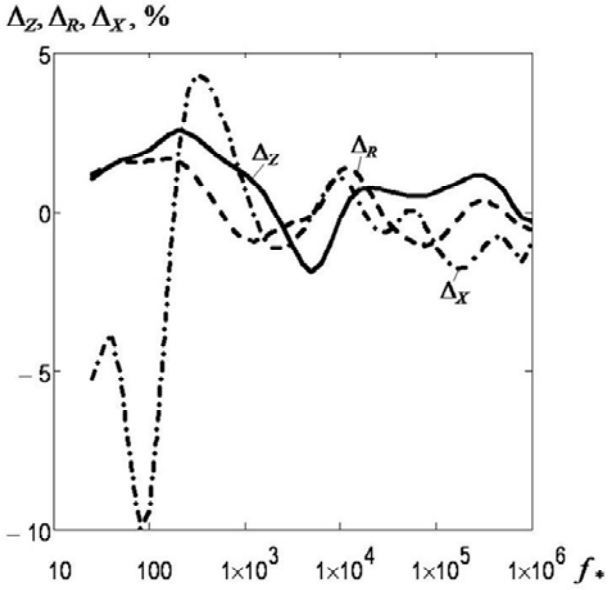

Fig. 7. Frequency dependences of relative deviations Δ_Z, Δ_R and Δ_X of the calculated values of the quantities, respectively, $|\underline{Z}_*(f_*)|$, $R_*(f_*)$ and $X_*(f_*)$ from their experimental values for the *apple* tissue

In the frequency range widely used in the analysis of the impedance of biological tissues [3] in the range $f = 10^3 \ldots 10^6$ Hz for apple, the deviations $|\Delta|$ do not exceed 1.9%, for carrots 2.3%, for potatoes -2.5%, for the liver 3.0%, for the heart 1.8%, for the kidney -2.0%, for the breast 1.0 %, for thyroid gland 1.5%. This is an acceptable for practical purposes coincidence of calculated values with experimental data in the specified frequency range.

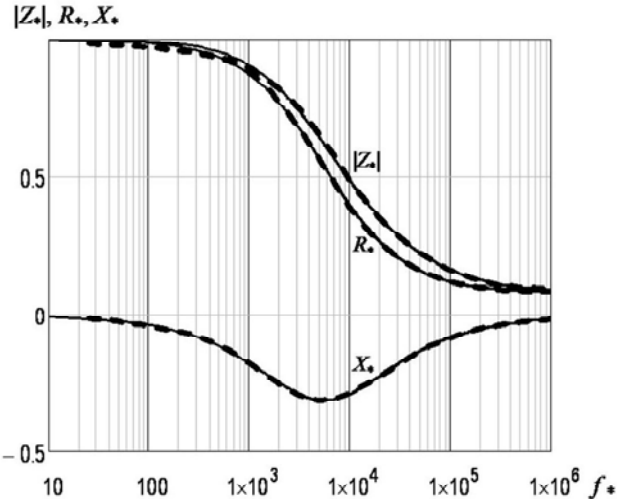

Fig. 8. *Carrot* tissue (the designations correspond to Fig. 6)

Table 1 shows the values of the coefficients a_i and the largest deviation $|\Delta|$ of the calculated values of $|\underline{Z}_*|$, R_* and X_* from their experimental values in the frequency range $f_* = 10^3 \ldots 10^6$ for biological tissues of plant origin: apple, carrot and potato, and Table 2 presents the values of the coefficients a_i and the largest deviation $|\Delta|$ of the calculated values of R_* from their experimental values for biological tissues of animal origin: liver, heart (along the fibers), kidney, breast and thyroid gland. Table 3 shows the *calculated* values of $R_{s.0}$ and R_0 for various biological tissues of plant and animal origin.

For tissues of plant origin, the estimated values of $R_{s.0}$were roughly determined from the graphs in Fig. 4,*a* by interpolating the experimental $R_s(f)$ curves from 25 Hz to small frequency values.

With the $R_{s.0}$ values obtained, the approximation curves $|\underline{Z}_*(f_*)|$, $R_*(f_*)$ and $X_*(f_*)$ have a small deviation from the experimental curves. Although it should be understood here that the $R_{s.0}$ values obtained for tissues of plant origin may deviate somewhat from the real values of $R_{s.0}$ at a low frequency because of the effect of the double electrical layer in the near-electrode regions. It is also possible to change the resistance of cell membranes with a close arrangement of cells and the difficult passage of current through the intercellular substance because of the presence of small conductors of small bridges between the cell membranes that touch each other. This issue requires further research.

When choosing the calculated values of R_0 of biological tissues of animal origin, difficulties arose because the experimental values of the curves in Fig. 5 were presented with minimum frequencies of 0.5...1.5 kHz, and it was not possible to correctly interpolate the dependences of $R(f)$ on the ordinate axis to determine R

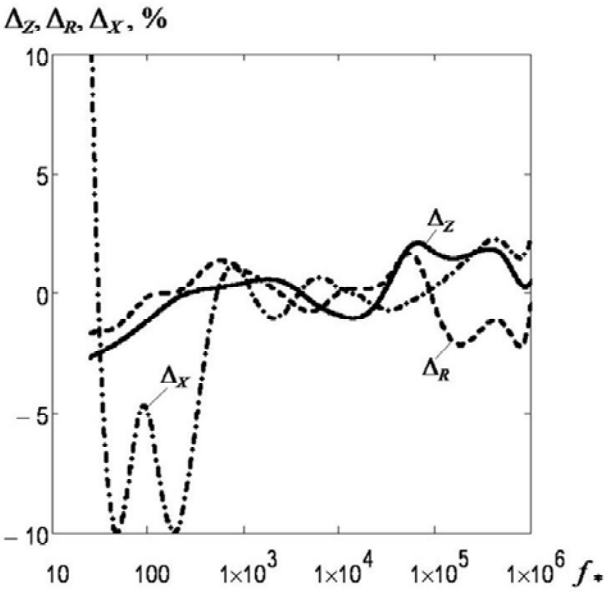

Fig. 9. *Carrot* tissue (the designations correspond to Fig. 7)

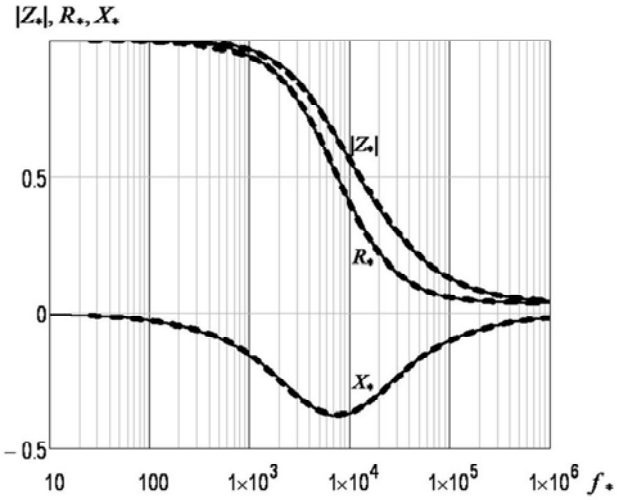

Fig. 10. *Potato* tissue (the designations correspond to Fig. 6)

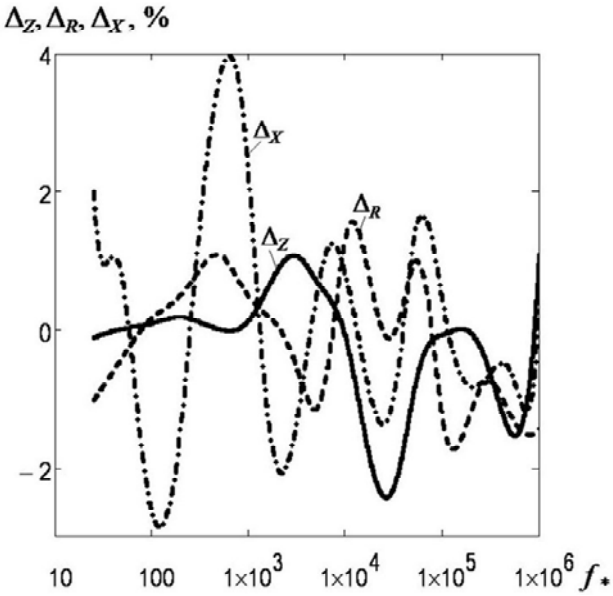

Fig. 11. *Potato* tissue (the designations correspond to Fig. 7)

values at low frequencies. Therefore, the calculated values of R_0 are taken very approximately and such that the approximation curves $R_*(f)$ coincide with the experimental curves in the entire range of available experimental data. Thus, the calculated values of R_0 of tissues of animal origin in Table 3 may differ from the actual values. But in determining the values of $R(f)$ in the frequency range $10^3 \ldots 10^6$ Hz from the approximate dependences $R_*(f)$ obtained, taking into account the values of R_0, the result obtained coincides with the data in Fig. 4, which is proved by the obtained dependences of Δ_R in Fig. 13.

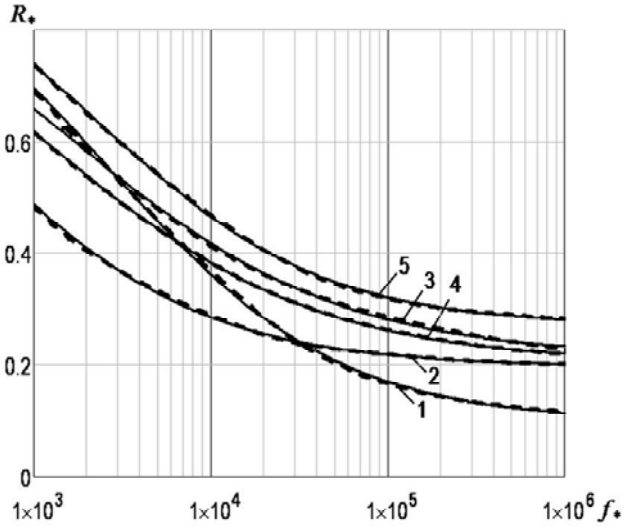

Fig. 12. Frequency dependences of the active components $R_*(f_*)$ values of impedance $\underline{Z}_*(f_*)$ of the Fricke substitution scheme for tissues: 1 - *liver*; 2 - *heart* (along the fibers); 3 - *kidney*; 4 - *breast*; 5 - *thyroid gland*. Thickened dashed curves - experimental values [14], thin solid curves - calculated values

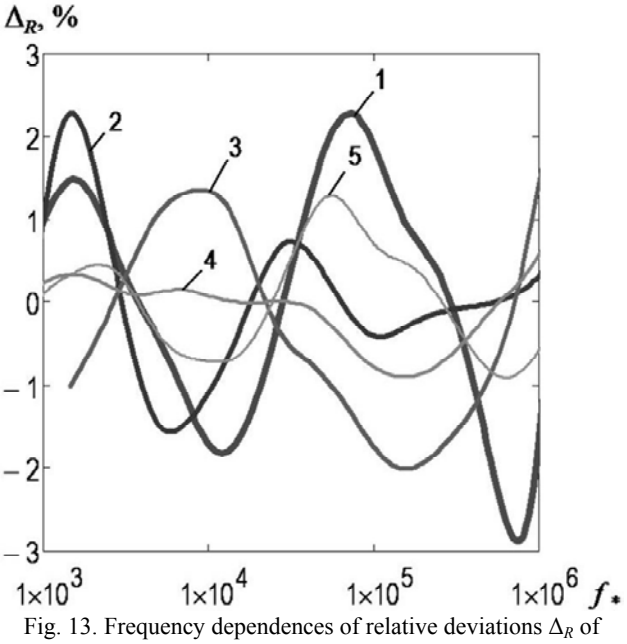

Fig. 13. Frequency dependences of relative deviations Δ_R of calculated values of $R_*(f_*)$ values from their experimental values for tissues: 1 - *liver*; 2 - *heart* (along the fibers); 3 - *kidney*; 4 - *breast*; 5 - *thyroid gland*

Table 1

The coefficients a_i and the largest deviation $|\Delta|$ of the calculated values of $|\underline{Z}_*|$, R_* and X_* from their experimental values in the frequency range $f_* = 10^3 \ldots 10^6$ for various biological tissues of plant origin

Coefficients for $\lvert\underline{Z}_*\rvert$				
Tissue	$a_{Z,1}$	$a_{Z,2}$	$a_{Z,3}$	$\lvert\Delta\rvert$, %
Apple	11.2	0.588	$7.413\cdot10^{-3}$	1.9
Carrot	444.0	0.570	$7.395\cdot10^{-3}$	2.1
Potato	26.2	0.740	$1.556\cdot10^{-3}$	2.5
Coefficients for R_*				
Tissue	$a_{R,1}$	$a_{R,2}$	$a_{R,3}$	$\lvert\Delta\rvert$, %
Apple	11.7	0.536	$9.131\cdot10^{-3}$	1.4
Carrot	443.3	0.506	$9.369\cdot10^{-3}$	2.2
Potato	28.1	0.710	$1.775\cdot10^{-3}$	1.7
Coefficients for X_*				
Tissue	$a_{X,1}$	$a_{X,2}$	$a_{X,3}$	$\lvert\Delta\rvert$, %
Apple	1.646	0.681	$1.748\cdot10^{-3}$	1.6
Carrot	1.911	0.665	$1.476\cdot10^{-3}$	2.3
Potato	3.200	0.760	$8.684\cdot10^{-3}$	2.2

Table 2

The coefficients a_i and the largest deviation Δ of the calculated values of R_* from their experimental values in the frequency range R_* for various biological tissues of animal origin

Coefficients for R_*				
Tissue	$a_{R,1}$	$a_{R,2}$	$a_{R,3}$	$\lvert\Delta\rvert$, %
Liver	9.265	0.339	0.062	3.0
Heart	4.084	0.330	0.109	1.8
Kidney	3.679	0.286	0.095	2.0
Breast	3.899	0.285	0.107	1.0
Thyroid gland	2.701	0.344	0.051	1.5

Table 3

The calculated values of R_0 and $R_{s.0}$ for various biological tissues of plant and animal origin

Tissue	
$R_{s.0}$, Ω·m	
Apple	10.50
Carrot	6.30
Potato	4.95
R_0, Ω	
Liver	1100
Heart	2200
Kidney	800
Breast	1000
Thyroid gland	650

After finding the unknown variables a_i, $a_{R,i}$ da $a_{X,i}$ it is possible to determine the values of the total resistivity of the Fricke replacement circuit, the active and reactive components of the total resistivity in absolute values as a function of frequency:

$$|\underline{Z}_s(f)| = R_{s.0}\cdot|\underline{Z}_*(f_*,a_{Z,1},a_{Z,2},a_{Z,3})|;$$

$$R_s(f) = R_{s.0}\cdot\mathrm{Re}[\underline{Z}_*(f_*,a_{R,1},a_{R,2},a_{R,3})];$$

$$X_s(f) = R_{s.0}\cdot\mathrm{Im}[\underline{Z}_*(f_*,a_{X,1},a_{X,2},a_{X,3})],$$

and for tissues of animal origin - the active component of the impedance:

$$R(f) = R_0\cdot\mathrm{Re}[\underline{Z}_*(f_*,a_{R,1},a_{R,2},a_{R,3})].$$

Having pairs of dependences of the quantities $|\underline{Z}_*(f_*)|$, $R_*(f_*)$ or $X_*(f_*$ we can determine the third value by the formulas:

$$|\underline{Z}_*(f_*)| = \left\{\left[R_*\left(f_*,a_{R,1},a_{R,2},a_{R,3}\right)\right]^2 + \left[X_*\left(f_*,a_{X,1},a_{X,2},a_{X,3}\right)\right]^2\right\}^{\frac{1}{2}}; \quad (8)$$

$$R_*(f_*) = \left\{\left|\underline{Z}_*\left(f_*,a_{Z,1},a_{Z,2},a_{Z,3}\right)\right|^2 - \left[X_*\left(f_*,a_{X,1},a_{X,2},a_{X,3}\right)\right]^2\right\}^{\frac{1}{2}}; \quad (9)$$

$$X_*(f_*) = \left\{\left|\underline{Z}_*\left(f_*,a_{Z,1},a_{Z,2},a_{Z,3}\right)\right|^2 - \left[R_*\left(f_*,a_{X,1},a_{X,2},a_{X,3}\right)\right]^2\right\}^{\frac{1}{2}}. \quad (10)$$

In Fig. 14, the approximation dependences of the active components R_* of the total impedances of the Fricke substitution scheme for biological tissues [6, 13] of plant and the animal [14] origin on the frequency f_* are jointly presented at unitized values. It can be seen that *the behavior of the curves for tissues of plant and animal origin is similar*.

Using the approximation coefficients $a_{Z,i}$, $a_{R,i}$ or $a_{X,i}$ in the impedance expression for the Fricke replacement circuit for all the dependences $|\underline{Z}_*(f_*)|$, $R_*(f_*)$ and $X_*(f_*)$. We show that using the approximation coefficients $a_{Z,i}$ to construct the curves $R_*(f_*)$ и $X_*(f_*)$, as well as the coefficients $a_{R,i}$ for constructing the curves $|\underline{Z}_*(f_*)|$ and $X_*(f_*)$, and the coefficients $a_{X,i}$ for the construction of the curves $|\underline{Z}_*(f_*)|$ and $R_*(f_*)$ does not lead to coincidence of calculated and experimental data. We show this by the example of the approximation coefficients $a_{Z,i}$, $a_{R,i}$ and $a_{X,i}$ for apple.

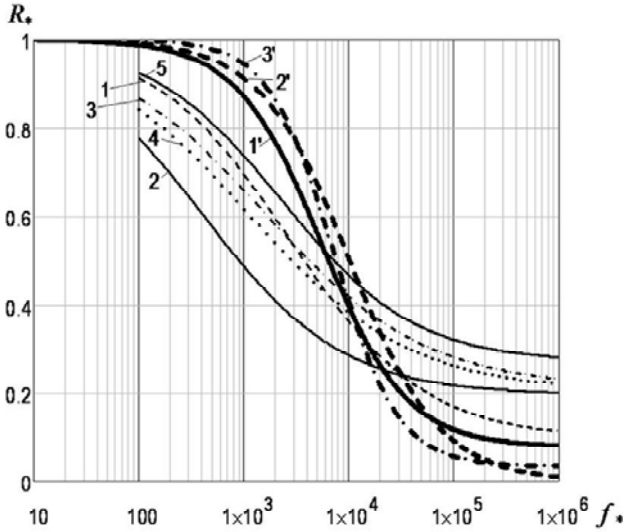

Fig. 14. The normalized per unit approximated frequency dependences of the values of the active components $R_*(f_*)$ of the impedance of the Fricke substitution scheme for biological tissues of plant [6, 13] and the animal [14] origin: 1 - *liver*; 2 - *heart* (along the fibers); 3 - *kidney*; 4 - *breast*; 5 - *thyroid gland*; 1' - *apple*; 2'- *carrots*; 3' - *potatoes*

We use the formula (6). We take the values of $a_{Z,i}$ from Table 1 for the apple. In Fig. 15 by thin solid lines we build dependencies

$$|\underline{Z}_{Z*}(f_*)| = |\underline{Z}_*(f_*,a_{Z,1},a_{Z,2},a_{Z,3})|;$$
$$R_{Z*}(f_*) = \mathrm{Re}[\underline{Z}_*(f_*,a_{Z,1},a_{Z,2},a_{Z,3})];$$
$$X_{Z*}(f_*) = \mathrm{Im}[\underline{Z}_*(f_*,a_{Z,1},a_{Z,2},a_{Z,3})],$$

and by thickened dashed lines - their experimental values $|\underline{Z}_*(f_*)|$, $R_*(f_*)$ and $X_*(f_*)$. Let's see how the obtained curves are correlated with the experimental data.

It can be seen that the curves $|\underline{Z}_{Z*}(f_*)|$ and $|\underline{Z}_*(f_*)|$ practically coincided, since the approximation coefficients $a_{Z,i}$ were calculated precisely from the experimental values of this curve. The curves of the dependence $R_{Z*}(f_*)$ fall below the experimental values $R_*(f_*)$, as well as the curves of the dependencies $X_{Z*}(f_*)$ of the experimental values $X_*(f_*)$.

Now take the values of $a_{R,i}$ for the apple and also substitute them in the formula (6). In Fig. 15 by thin dotted lines we construct the dependencies:

$$|\underline{Z}_{R*}(f_*)| = |\underline{Z}_*(f_*,a_{R,1},a_{R,2},a_{R,3})|;$$
$$R_{R*}(f_*) = \mathrm{Re}[\underline{Z}_*(f_*,a_{R,1},a_{R,2},a_{R,3})];$$
$$X_{R*}(f_*) = \mathrm{Im}[\underline{Z}_*(f_*,a_{R,1},a_{R,2},a_{R,3})].$$

In this case, the curve $R_{R*}(f_*)$ coincided with the curve $R_*(f_*)$, the curve $|\underline{Z}_{R*}(f_*)|$ passed above the curve with the experimental values of $|\underline{Z}_*(f_*)|$, and the curve $X_{R*}(f_*)$ passed below the curve with the experimental values of $X_*(f_*)$.

If we take the values of $a_{X,i}$ for the apple, then in Fig. 15 by thin dot-dash lines we can build dependencies

$$|\underline{Z}_{X*}(f_*)| = |\underline{Z}_*(f_*,a_{X,1},a_{X,2},a_{X,3})|;$$
$$R_{X*}(f_*) = \mathrm{Re}[\underline{Z}_*(f_*,a_{X,1},a_{X,2},a_{X,3})];$$
$$X_{X*}(f_*) = \mathrm{Im}[\underline{Z}_*(f_*,a_{X,1},a_{X,2},a_{X,3})].$$

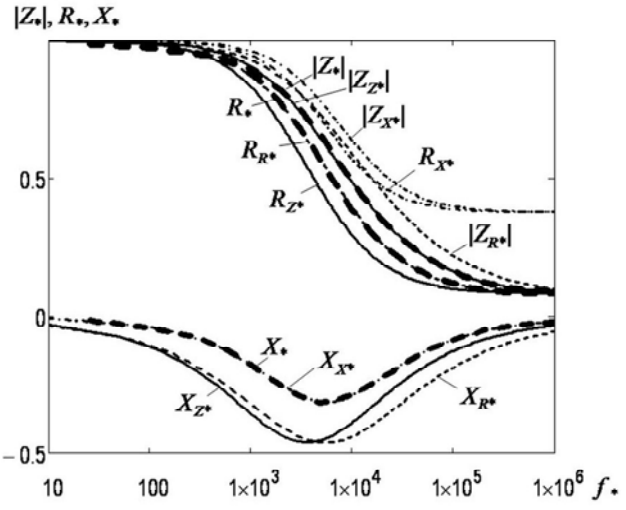

Fig. 15. The frequency dependences of the impedance modulus $|\underline{Z}_*|$ of the Fricke substitution scheme, the active R_* and the reactive X_* impedance components for the *apple* tissue. Thickened dashed curves are the experimental values of $|\underline{Z}_*|$, R_* and X_*; thin solid curves - calculated values for the coefficients $a_{R,i}$ - the curves $|\underline{Z}_{Z*}|$, R_{Z*} and X_{Z*}; fine dotted curves - calculated values for the coefficients $a_{R,i}$ - curves $|\underline{Z}_{R*}|$, R_{R*} and X_{R*}; thin dash-dotted curves - calculated values for the coefficients $a_{X,i}$ - the curves $|\underline{Z}_{X*}|$, R_{X*} and X_{X*}

The curve $X_{X*}(f_*)$ coincided with the curve $X_*(f_*)$, the curves $|\underline{Z}_{X*}(f_*)|$ and $R_{X*}(f_*)$, especially at high frequencies, have significantly exceeded the corresponding curves of the experimental values $|\underline{Z}_*(f_*)|$ and $R_*(f_*)$.

Thus, the coefficients $a_{Z,i}$, $a_{R,i}$ and $a_{X,i}$ can be used only to approximate the corresponding curves $|\underline{Z}_*(f_*)|$, $R_*(f_*)$ и $X_*(f_*)$ by the values of which they were obtained and for which the calculated curves coincide with the experimental curves.

Hence, having the values of the approximation coefficients $a_{R,i}$ in the impedance expression of the Fricke substitution circuit (6) for the experimental dependences

$$R_*(f_*) = \mathrm{Re}[\underline{Z}_*(f_*,a_{R,1},a_{R,2},a_{R,3})]$$

of tissues of animal nature [14], see Table 2, it is impossible to obtain dependencies

$$|\underline{Z}_*(f_*)| = |\underline{Z}_*(f_*,a_{R,1},a_{R,2},a_{R,3})|;$$
$$X_*(f_*) = \mathrm{Im}[\underline{Z}_*(f_*,a_{R,1},a_{R,2},a_{R,3})].$$

This is the main drawback of the Fricke substitution scheme.

Finding the common coefficients a_i in the impedance expression of the Fricke replacement circuit for all the dependences $|\underline{Z}_*(f_*)|$, $R_*(f_*)$ and $X_*(f_*)$. Let us verify the possibility of finding the coefficients ai in the expression for the total complex resistance (6) of the Fricke substitution circuit, which simultaneously satisfy all the dependences $|\underline{Z}_*(f_*)|$, $R_*(f_*)$ and $X_*(f_*)$ for each particular tissue. In this case, by one dependence $|\underline{Z}_*(f_*)| = |\underline{Z}_*(f_*,a_1,a_2,a_3)|$ it would be possible to obtain the dependences $R_*(f_*) = \mathrm{Re}[\underline{Z}_*(f_*,a_1,a_2,a_3)]$ and $X_*(f_*) = \mathrm{Im}[\underline{Z}_*(f_*,a_1,a_2,a_3)]$. To do this, we use the minimization of the root-mean-square deviations of the function $F(a_1,a_2,a_3)$ written as:

$$F(a_1,a_2,a_3) =$$
$$= \sum_n \left\{ \left|\underline{Z}_*(f_{*n},a_1,a_2,a_3)\right| - \left|\underline{Z}_*(f_{*n},a_{Z,1},a_{Z,2},a_{Z,3})\right| \right\}^2 +$$
$$+ \sum_n \left\{ \mathrm{Re}\left[\underline{Z}_*(f_{*n},a_1,a_2,a_3)\right] - \right.$$
$$\left. - \mathrm{Re}\left[\underline{Z}_*(f_{*n},a_{R,1},a_{R,2},a_{R,3})\right] \right\}^2 +$$
$$+ \sum_n \left\{ \mathrm{Im}\left[\underline{Z}_*(f_{*n},a_1,a_2,a_3)\right] - \right.$$
$$\left. - \mathrm{Im}\left[\underline{Z}_*(f_{*n},a_{X,1},a_{X,2},a_{X,3})\right] \right\}^2, \qquad (11)$$

here the values of the vector f_{*n} are given from the expression (7), and the values $a_{Z,i}$, $a_{R,i}$, $a_{X,i}$ - from Table 1.

Minimization of the function $F(a_i) \to \min$ can be performed by the numerical method of conjugate gradients [15] with respect to the variables a_i (in the MathCAD package is the Minimize function) for some initial values of the variables a_i.

As an example, let's take an apple. As a result of minimization, the following coefficients were obtained: $a_1 = 6.91$; $a_2 = 0.784$; $a_3 = 1.144 \cdot 10^{-3}$. Based on these coefficients in Fig. 16 we build by solid curves for the curves of the calculated dependences of the quantities

$$|\underline{Z}_*(f_*)| = |\underline{Z}_*(f_*,a_1,a_2,a_3)|;$$
$$R_*(f_*) = \mathrm{Re}[\underline{Z}_*(f_*,a_1,a_2,a_3)];$$
$$X_*(f_*) = \mathrm{Im}[\underline{Z}_*(f_*,a_1,a_2,a_3)].$$

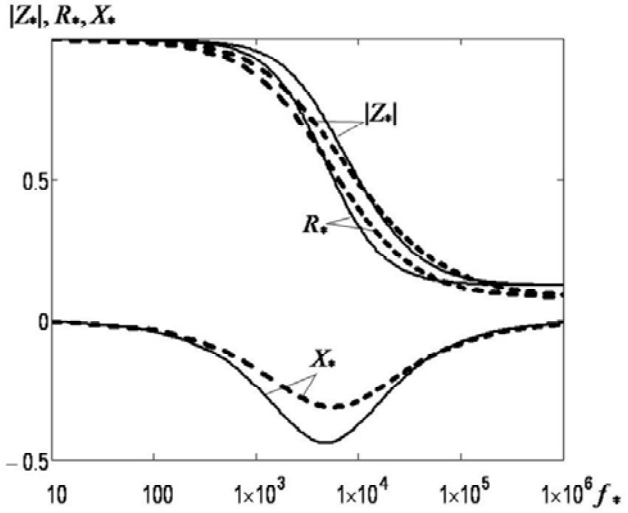

Fig. 16. The frequency dependences of the impedance modulus $|\underline{Z}_*|$ of the Fricke substitution scheme, the active R_* and the reactive X_* impedance components for the apple tissue. Dotted curves - experimental values, solid curves - calculated values

It can be seen that all these curves diverge from the corresponding experimental curves shown in the figure by dashed lines.

This shows that for the Fricke substitution scheme there are no common values of the approximation coefficients a_i that would simultaneously satisfy all the curves $|\underline{Z}_*(f_*)|$, $R_*(f_*) = \mathrm{Re}[\underline{Z}_*(f_*)]$ and $X_*(f_*) = \mathrm{Im}[\underline{Z}_*(f_*)]$ for each specific biological tissue.

Therefore, to approximate the curves $|\underline{Z}_*(f_*)|$, $\mathrm{Re}[\underline{Z}_*(f_*)]$ and $\mathrm{Im}[\underline{Z}_*(f_*)]$, only the corresponding coefficients $a_{Z,i}$, $a_{R,i}$ и $a_{X,i}$, at which the values of calculated and experimental data coincide, should be used. This is a consequence of the fact that the Fricke scheme does not reflect all the properties of biological tissues.

Therefore, the next stage of research should be devoted to the modernization of the Fricke substitution scheme with the introduction of elements in the scheme that take into account the effect of cell membranes and dielectric losses in cell membranes (the dielectric loss tangent tgδ) in order to obtain common values of the approximation coefficients a_i that would simultaneously satisfy all the curves $|\underline{Z}_*(f_*)|$, $R_*(f_*)$ and $X_*(f_*)$ for each specific biological tissue.

The developed technique allows modeling processes occurring in biological tissues when currents of different frequency pass through them, and also with greater efficiency to develop diagnostic and control equipment for determining the electrical properties of tissues of plant and living origin, including developing more efficient medical equipment. Dependencies of $R_*(f_*)$ can be applied in calculations of thermal processes occurring when welding live tissues of animal origin with special medical welding power sources.

Annex. The V_Z, V_R, and V_X vectors for the impedance, active and reactive impedance components are:

$$V_Z(f_*,a_1,a_2,a_3) = \left\| \left|\underline{Z}_*(f_*,a_1,a_2,a_3)\right|, \left|\frac{\partial \underline{Z}_*(f_*,a_1,a_2,a_3)}{\partial a_1}\right|, \left|\frac{\partial \underline{Z}_*(f_*,a_1,a_2,a_3)}{\partial a_2}\right|, \left|\frac{\partial \underline{Z}_*(f_*,a_1,a_2,a_3)}{\partial a_3}\right| \right\|^T;$$

$$V_R(f_*,a_1,a_2,a_3) = \left\| \mathrm{Re}\left[\underline{Z}_*(f_*,a_1,a_2,a_3)\right], \mathrm{Re}\left[\frac{\partial \underline{Z}_*(f_*,a_1,a_2,a_3)}{\partial a_1}\right], \mathrm{Re}\left[\frac{\partial \underline{Z}_*(f_*,a_1,a_2,a_3)}{\partial a_2}\right], \mathrm{Re}\left[\frac{\partial \underline{Z}_*(f_*,a_1,a_2,a_3)}{\partial a_3}\right] \right\|^T;$$

$$V_X(f_*,a_1,a_2,a_3) = \left\| \mathrm{Im}\left[\underline{Z}_*(f_*,a_1,a_2,a_3)\right], \mathrm{Im}\left[\frac{\partial \underline{Z}_*(f_*,a_1,a_2,a_3)}{\partial a_1}\right], \mathrm{Im}\left[\frac{\partial \underline{Z}_*(f_*,a_1,a_2,a_3)}{\partial a_2}\right], \mathrm{Im}\left[\frac{\partial \underline{Z}_*(f_*,a_1,a_2,a_3)}{\partial a_3}\right] \right\|^T,$$

here ∂ is the differential sign; T is the vector transpose symbol.

Transforming the right-hand sides of the vectors, taking into account formula (6), we obtain expressions for determining the coefficients a_i in terms of the vectors V_Z, V_R, and V_X written in explicit form:

$$V_Z(f_*,a_1,a_2,a_3) = \left\| \frac{\sqrt{\left[a_1^2+(1+a_1)\cdot\left(a_3\cdot f_*^{a_2}\right)^2\right]^2+\left(a_1^2\cdot a_3\cdot f_*^{a_2}\right)^2}}{F(f_*,a_1,a_2,a_3)}, \right.$$

$$-\frac{\left\{\begin{matrix}\left(1+3\cdot a_1+3\cdot a_1^2+a_1^3\right)\cdot\left(a_3\cdot f_*^{a_2}\right)^4- \\ -a_1^3\cdot\left[(1+a_1)\cdot\left(a_3\cdot f_*^{a_2}\right)^2-a_1\right]\end{matrix}\right\}\cdot\left(a_3\cdot f_*^{a_2}\right)^2}{F_1^2(f_*,a_1,a_2,a_3)\cdot\sqrt{F_2(f_*,a_1,a_2,a_3)}},$$

$$-\frac{(2+a_1)\cdot a_1^3\cdot\left(a_3\cdot f_*^{a_2}\right)^2\cdot\ln(f_*)}{F_1^2(f_*,a_1,a_2,a_3)\cdot\sqrt{F_2(f_*,a_1,a_2,a_3)}},$$

$$\left.-\frac{(2+a_1)\cdot a_1^3\cdot a_3\cdot f_*^{2\cdot a_2}}{F_1^2(f_*,a_1,a_2,a_3)}\right\|^T;$$

$$V_R(f_*,a_1,a_2,a_3) = \left\| \frac{a_1^2+(1+a_1)\cdot\left(a_3\cdot f_*^{a_2}\right)^2}{F_1(f_*,a_1,a_2,a_3)}, \right.$$

$$-\frac{\left\{\left[(1+a_1)\cdot a_3\cdot f_*^{a_2}\right]^2-a_1^2\right\}\cdot\left(a_3\cdot f_*^{a_2}\right)^2}{F_1^2(f_*,a_1,a_2,a_3)},$$

$$\left.-\frac{2\cdot(1+a_1)\cdot a_1^3\cdot\left(a_3\cdot f_*^{a_2}\right)^2\cdot\ln(f_*)}{F_1^2(f_*,a_1,a_2,a_3)}\right\|,$$

$$-\frac{2\cdot\left(1+a_1\right)\cdot a_1^3\cdot a_3\cdot f_*^{2\cdot a_2}}{F_1^2\left(f_*,a_1,a_2,a_3\right)}\Bigg\|^T;$$

$$V_X\left(f_*,a_1,a_2,a_3\right)=\Bigg\|-\frac{a_1^2\cdot a_3\cdot f_*^{a_2}}{F_1\left(f_*,a_1,a_2,a_3\right)},$$

$$-\frac{2\cdot a_1\cdot\left(1+a_1\right)\cdot\left(a_3\cdot f_*^{a_2}\right)^3}{F_1^2\left(f_*,a_1,a_2,a_3\right)},$$

$$-\frac{a_1^2\cdot a_3\cdot f_*^{a_2}\cdot\left\{a_1^2-\left[\left(1+a_1\right)\cdot a_3\cdot f_*^{a_2}\right]^2\right\}\cdot\ln\left(f_*\right)}{F_1^2\left(f_*,a_1,a_2,a_3\right)},$$

$$-\frac{a_1^2\cdot f_*^{a_2}\cdot\left\{a_1^2-\left[\left(1+a_1\right)\cdot a_3\cdot f_*^{a_2}\right]^2\right\}}{F_1^2\left(f_*,a_1,a_2,a_3\right)}\Bigg\|^T,$$

where functions

$$F_1\left(f_*,a_1,a_2,a_3\right)=a_1^2+\left[\left(1+a_1\right)\cdot a_3\cdot f_*^{a_2}\right]^2;$$

$$F_2\left(f_*,a_1,a_2,a_3\right)=\left[a_1^2+\left(1+a_1\right)\cdot\left(a_3\cdot f_*^{a_2}\right)^2\right]^2+$$

$$+\left(a_1^2\cdot a_3\cdot f_*^{a_2}\right)^2.$$

In some cases, expressions written in explicit form are more convenient to use.

Conclusions.

The electric substitution Fricke circuit makes it possible to model the dependences of the impedance module of biological tissues, the active and reactive components of the impedance with acceptable accuracy for practical purposes in the frequency range from 10^3 up to 10^6 Hz.

The expression of the impedance of the Fricke substitution scheme for biological tissues makes it possible to approximate the frequency dependences of the impedance modulus, the active and reactive components of the impedance only by using the approximation coefficients corresponding to each component.

The developed technique for processing experimental data in modeling the dispersion of the impedance of biological tissues using the Fricke substitution scheme for biological tissues allows these values to be determined with high accuracy.

The developed technique operates with normalized to unity values of the impedance modulus of the Fricke substitution circuit, the active and reactive components of the impedance depending on the frequency, which makes it possible to perform a comparative analysis of the parameters of various biological tissues of plant and animal origin.

It is shown that the frequency dependences of the active component of the total resistance for tissues of plant and animal origin are similar.

The approximation coefficients in the impedance equation can only be used to approximate the impedance, resistance and reactance curves corresponding to them by the values of which they were obtained which is the main drawback of the Fricke substitution scheme.

For the Fricke substitution scheme, there are no common values of the approximation coefficients which would correspond simultaneously to three dependences - the impedance module, the active and reactive component of the impedance. Therefore, the Fricke substitution scheme does not fully reflect all the characteristics of biological tissues and needs modernization.

Dependencies of the impedance of biological tissue can be used in the design of diagnostic, measuring and control equipment to determine the properties of tissues of animal and plant origin. Also they will be in demand when creating medical equipment for welding live tissues.

REFERENCES

1. Paton B.E., Krivtsun I.V., Marinsky G.S., Khudetsky I.Yu., Lankin Yu.N., Chernets A.V. Welding, cutting and heat treatment of live tissues. *The Paton welding journal*, 2013, no.10-11, pp. 142-153.

2. Fricke H. The electric resistance and capacity of blood for frequencies between 800 and 4½ million cycles. *The Journal of General Physiology*, 1925, vol.9, no.2, pp. 153-167. **doi: 10.1085/jgp.9.2.153.**

3. Kalakutskii L.I., Akulov S.A., Fedotov A.A. *Fundamentals of impulse impedance of biological tissues: an electronic textbook*. Minoboronauki Russia, Samara State Aerospace University named after S.P. Korolev (National Research University). Samara, 2011. 94 p. Available at: http://repo.ssau.ru/handle/Uchebnye-posobiya/ Osnovy-impulsnoi-impedansometrii-biologicheskih-tkanei-Elektronnyi-resurs-elektron-ucheb-posobie-54991. (Rus).

4. Kiryanov D.V. *MathCAD 14* [MathCAD 14]. St. Petersburg, BHV-Petersburg Publ., 2007. 704 p. (Rus).

5. Samoilov V.O. *Meditsinskaia biofizika: Uchebnik* [Medical Biophysics: Textbook]. St. Petersburg, SpetsLit Publ., 2004. 496 p. (Rus).

6. Golev I.M., Korotkov L.N. Dispersion of the electrical resistance of biological objects plant origin. *Bulletin of Voronezh State Technical University*, 2013, vol.9, no.4, pp. 26-29. (Rus).

7. Antropov E.I. *Teoreticheskaia elektrokhimiia. Uchebnik dlia khimiko-tekhnologicheskikh spetsial'nostei vuzov* [Theoretical electrochemistry. Textbook for high schools chemical technology specialties]. Moscow, Vysshaia shkola Publ., 1975. 560 p. (Rus).

8. Laufer S., Ivorra A., Reuter V.E., Rubinsky B., Solomon S.B. Electrical impedance characterization of normal and cancerous human hepatic tissue. *Physiological Measurement*, 2010, vol.31, iss.7, pp. 995-1009. – **doi: 10.1088/0967-3334/31/7/009**.

9. Neiman L.R., Demirchian K.S. *Teoreticheskie osnovy elektrotekhniki. V 2 T., T.2, Ch. 3, 4. Teoriia nelineinykh elektricheskikh i magnitnykh tsepei. Teoriia elektromagnitnogo polia* [Theoretical foundations of electrical engineering. In 2 vols. Vol. 2, part 3, 4. Theory of nonlinear electric and magnetic circuits. Theory of electromagnetic field]. Moscow-Leningrad, Energiia Publ., 1966. 407 p. (Rus).

10. Privalov E.E. *Elektrotekhnicheskoe materialovedenie: uchebnoe posobie* [Electrotechnical materials science: Tutorial]. Moscow-Berlin: Direkt-Media Publ., 2015. 234 p. (Rus).

11. Bessonov L.A. *Teoreticheskie osnovy elektrotekhniki* [Theoretical foundations of electrical engineering]. Moscow, Vysshaia shkola Publ., 1964. 750 p. (Rus).

12. Tolstov Iu.G. *Teoriia lineinykh elektricheskikh tsepei* [Theory of linear electric circuits]. Moscow, Vysshaia shkola Publ., 1978. 279 p. (Rus).

13. Golev I.M., Bobkina E.Iu. The temperature dependence of the electrical impedance of the parenchymal tissue of vegetables. *Teoreticheskie i prakticheskie aspekty estestvennykh i matematicheskikh nauk: Materialy mezhdunarodnoi zaochnoi nauchno-prakticheskoi konferentsii* [Theoretical and practical aspects of the natural and mathematical sciences: Proceedings of the International correspondence scientific-practical conference]. Novosibirsk, 24 December 2012, SibAK Publ., 2012, pp. 103-108. (Rus). Available at: http://sibac.info/conf/naturscience/i/30882. (Rus).

14. Belik D.V. *Impedansnaia elektrokhirurgiia* [Impedance electrosurgery]. Novosibirsk, Nauka Publ., 2000. 237 p. (Rus).

15. Gill Ph., Murray W., Wright M. *Prakticheskaia optimizatsiia* [Practical Optimization]. Moscow, Mir Publ., 1985. 509 p. (Rus).

Received 20.08.2017

I.V. Krivtsun[1]*, Academician of the National Academy of Science of Ukraine, Doctor of Technical Science, Professor,*
I.V. Pentegov[1]*, Doctor of Technical Science, Professor,*
V.M. Sydorets[1]*, Doctor of Technical Science, Professor,*
S.V. Rymar[1]*, Doctor of Technical Science, Senior Research Scientist,*
[1] Paton Electric Welding Institute of National Academy of Sciences of Ukraine,
11, Kazymyr Malevych Str., Kiev, 03680, Ukraine,
phone +380 44 2061388,
e-mail: elmag@paton.kiev.ua

How to cite this article:
Krivtsun I.V., Pentegov I.V., Sydorets V.M., Rymar S.V. A technique for experimental data processing at modeling the dispersion of the biological tissue impedance using the Fricke equivalent circuit. *Electrical engineering & electromechanics*, 2017, no.5, pp. 27-37. **doi: 10.20998/2074-272X.2017.5.04.**

UDC 621.3 **doi: 10.20998/2074-272X.2017.5.05**

V.M. Mikhailov, K.V. Chunikhin

ON ELECTROSTATIC ANALOGY OF MAGNETOSTATIC FIELD IN INHOMOGENEOUS MAGNETIZED MEDIUM

Purpose. ***The application in electrostatic analogy of magnetostatics for inhomogeneous magnetized media of two known magnetization models.*** ***Methodology.*** ***A comparison of basic equations and formulas of electrostatic and magnetostatic field in immoveable isotropic inhomogeneous polarized medium for dipole model and the magnetization model by molecular currents is made. The value-analogues for dipole model of magnetization are established.*** ***Results.*** ***We have shown that the using of dipole model of magnetization is correct. There is not even formal analogy with electrostatic field in the case of using the magnetization model by molecular currents. The relation between the magnetizations for various models is obtained. It allows us to justify the using magnetization by molecular currents in electrostatic analogy.*** ***Originality.*** ***The magnetization for dipole model is introduced and the possibility of using magnetization by molecular currents in the formulas for calculating potential magnetostatic field in magnetized medium is substantiated.*** ***Practical value.*** ***The results allow to obtain correct formulation and solution of the problem of magnetostatic field calculation in inhomogeneous magnetized medium.*** References 5, tables 1.

Key words: **magnetostatics, magnetized medium, electrostatic analogy, dipole model, magnetization by molecular currents.**

Сделан анализ применения электростатической аналогии в магнитостатике неоднородных намагничивающихся сред на основе дипольной модели и модели намагничивания молекулярными токами. Показано, что корректным является использование дипольной модели намагничивания. Получено соотношение между намагниченностями для различных моделей, поясняющее применение в электростатической аналогии намагниченности молекулярными токами. Библ. 5, табл. 1.

Ключевые слова: **магнитостатика, намагничивающаяся среда, электростатическая аналогия, дипольная модель, молекулярный ток намагничивания, намагниченность.**

Introduction. The use of fictitious magnetic charges for the calculation of magnetostatic fields in magnetized media is associated with the development of ideas about the nature of magnetic phenomena and is based on the electrostatic analogy of the polarization of dielectrics and magnets [1]. This analogy is based on the formation of magnetic dipoles, like electric dipoles, but consisting of two point fictitious magnetic charges (hereinafter – the dipole model of magnetization). The electrostatic analogy was used, in particular, by G.A. Greenberg [2] and K. Simonyi [3].

Subsequently it turned out that magnetization occurs due to the flow of molecular (microscopic) currents inside the magnets (such a model will be called the magnetization model by molecular currents), and the electrostatic analogy is far from the nature of magnetism [1, 4]. Despite the formal nature, the electrostatic analogy, when correctly used, is very effective [1-4].

To different models of magnetization we put in correspondence various magnetizations: $\vec{J}^e$ – magnetization by dipoles; $\vec{J}$ – magnetization by molecular currents. In some books and articles, the authors describe the magnetostatic field of magnetized bodies with the help of the scalar potential φ_m which corresponds to the dipole model, and the magnetization $\vec{J}$ is used in the formulas for determining φ_m. A possible reason for this is the analogy proposed in the textbook [1] between the polarization of the dielectric $\vec{P}$ and $\mu_0\vec{J}$ (μ_0 is the magnetic constant), but the latter requires a theoretical justification.

The relevance of this paper is that the application of the electrostatic analogy for the formulation and testing of numerical algorithms for solving magnetostatic problems of magnetized bodies leads to difficulties associated with a lack of clarity in well-known publications.

The goal of the work is analysis of the correctness of the application in the electrostatic analogy of magnetostatics of inhomogeneous magnetizing media of two known models of magnetization.

Basic equations and formulas of electrostatic analogy. We consider the electrostatic and magnetostatic field in a stationary isotropic inhomogeneous polarized medium. The basic equations of these fields and formulas are presented in Table 1 [1-4]. The analogues in the case of the dipole model of magnetization are: $\vec{E}$ and $\vec{H}$, $\vec{D}$ and $\vec{B}$ are the intensities, as well as the induction of the electric and magnetic fields; and; $\vec{P}$ and $\vec{J}^e$; ρ_e and ρ_m are the volume densities of the polarization electric and fictitious magnetic charges; ρ_e^{st} and ρ_m^{st} are the volume densities of external [2] electric and fictitious magnetic charges; ε_0 и μ_0, ε_0 is the electric constant; $\vec{p}$ and $\vec{p}_{me}$ are the moments of electric and magnetic dipoles; $\pm q$ and $\pm m$ are the point electric and fictitious magnetic charges located in the dipoles at distance l. In the formulas for determining $\vec{P}$ and $\vec{J}^e$ the quantity ΔV is a sufficiently small volume of the polarizable medium, over which the sums of the corresponding dipole moments are averaged. The field of magnetic dipoles is potential, its scalar potential φ_m is analogous to the potential of the electrostatic field φ. A consequence of the formality of the analogy in question is that magnetic flux density $\vec{B}$ becomes an auxiliary vector. In the formulas for calculating φ_m and φ, the following designations are accepted: in the case of dipoles distributed in a volume V, the quantity dV_M is the elementary volume centered at the point $M \in V$; in the case of surface fictitious magnetic charges distributed on the boundary surface S, the quantity dS_M is the elementary area centered at the point $M \in S$; r_{MQ} is the distance between the point with the current coordinates M and the observation point Q.

Table 1

Basic equations and formulas for analogous fields calculation

Electrostatic field	Magnetostatic field (dipole magnetization model)
$\operatorname{div}\vec{E}=\frac{\rho_e}{\varepsilon_0}+\frac{\rho_e^{st}}{\varepsilon_0}$	$\operatorname{div}\vec{H}=\frac{\rho_m}{\mu_0}+\frac{\rho_m^{st}}{\mu_0}$
$\operatorname{div}\vec{P}=-\rho_e$	$\operatorname{div}\vec{J}^e=-\rho_m$
$\vec{D}=\varepsilon_0\vec{E}+\vec{P}$	$\vec{B}=\mu_0\vec{H}+\vec{J}^e$
$\operatorname{div}\vec{D}=\rho_e^{st}$	$\operatorname{div}\vec{B}=\rho_m^{st}$
$\vec{P}=\frac{1}{\Delta V}\sum_{\Delta V}\vec{p}$	$\vec{J}^e=\frac{1}{\Delta V}\sum_{\Delta V}\vec{p}_{me}$
$\vec{p}=q\vec{l}$	$\vec{p}_{me}=m\vec{l}$
$\vec{E}=-\operatorname{grad}\varphi$	$\vec{H}=-\operatorname{grad}\varphi_m$
$\varphi(Q)=\frac{1}{4\pi\varepsilon_0}\int_V\left(\vec{P}(M),\operatorname{grad}_M\frac{1}{r_{MQ}}\right)dV_M$	$\varphi_m(Q)=\frac{1}{4\pi\mu_0}\int_V\left(\vec{J}^e(M),\operatorname{grad}_M\frac{1}{r_{MQ}}\right)dV_M$
$\varphi(Q)=\frac{1}{4\pi\varepsilon_0}\int_S\sigma(M)\frac{1}{r_{MQ}}dS_M$	$\varphi_m(Q)=\frac{1}{4\pi\mu_0}\int_S\sigma_m(M)\frac{1}{r_{MQ}}dS_M$

For the interface of two different homogeneous media 1 and 2 in the absence of external sources and assuming that the normal to the boundary is directed to the medium 1, from the equations of the first row of Table 1, 1 the boundary conditions [2] for the electrostatic field follow –

$$E_{1n}-E_{2n}=\frac{\sigma_e}{\varepsilon_0}, \tag{1}$$

and for the magnetostatic field –

$$H_{1n}-H_{2n}=\frac{\sigma_m}{\mu_0}, \tag{2}$$

where σ_e, σ_m are the surface densities of polarization electric and fictitious magnetic charges at the interface, and

$$\sigma_e=P_{2n}-P_{1n},\ \sigma_m=J^e_{2n}-J^e_{1n}. \tag{3}$$

In the boundary conditions (1) and (2), as well as in formulas (3), the indices $1n$ and $2n$ have normal projections of the corresponding vectors in media 1 and 2.

Analysis of the application of the model of magnetization by molecular currents. First, let us cite in the same sense order, as for the dipole model (see Table 1), the basic equations and magnetostatic formulas for magnetized media based on the model of magnetization by molecular currents [1, 4]:

$$\begin{gathered}\operatorname{rot}\vec{B}=\mu_0\left(\vec{j}_m+\vec{\delta}^{st}\right);\\ \operatorname{rot}\vec{J}=\vec{j}_m;\\ \vec{B}=\mu_0\left(\vec{H}+\vec{J}\right);\\ \operatorname{div}\vec{B}=0;\\ \vec{J}=\frac{1}{\Delta V}\sum_{\Delta V}\vec{p}_m;\\ \vec{p}_m=i_m s\vec{n};\end{gathered} \tag{4}$$

$$\vec{B}=\operatorname{rot}\vec{A};$$

$$\vec{A}(Q)=\frac{\mu_0}{4\pi}\int_V\vec{j}_m(M)\frac{1}{r_{MQ}}dV_M,$$

where $\vec{j}_m$ is the density of molecular magnetizing currents; $\vec{\delta}^{st}$ is the density of external conductive currents; $\vec{p}_m$ is the magnetic moment of the molecular magnetizing current i_m; s is the area of a microscopic circle bounded by the current i_m flow path; $\vec{n}$ is the normal to the microscopic circle in its center; $\vec{A}(Q)$ is the vector potential of the magnetic field created by the molecular magnetizing currents.

Comparison of the basic equations and formulas of the electrostatic field of the polarizable media (see Table 1) and the magnetostatic field of the magnetized media. This question is not limited only to the discrepancy between the relations between the vectors $\vec{D}$, $\vec{E}$, $\vec{P}$ and $\vec{B}$, $\vec{H}$, $\vec{J}$, and the difference between the sources of the fields, the sources of the electrostatic field, dipole-scalar sources, the magnetostatic sources are the currents (vector sources). The magnetic field of molecular currents, in contrast to the field of magnetic dipoles, is vortical, so its vectors and source densities are related to other equations.

Therefore, we can only talk about the use in electrostatic analogy based on the dipole model of magnetization.

On the relationship between magnetizations $\vec{J}^e$ and $\vec{J}$. As we already noted in the Introduction, K.M. Polivanov proposed an analogy of $\vec{P}$ and $\mu_0\vec{J}$ [1] using the transformation of formula (4) to form

$$\vec{B}=\mu_0\vec{H}+\mu_0\vec{J}.$$

In this case, to the term $\mu_0\vec{J}$ is not given a certain physical meaning, which can be guessed. To clarify the latter, we find the relationship between $\vec{J}^e$ and $\vec{J}$.

First, let us use the idea of replacing circuits with conduction currents by double magnetic layers [4, 5]. Applying this idea to the contour of the molecular magnetization current i_m, we arrive at a microscopic homogeneous double layer of fictitious magnetic charges, which is equivalent to a magnetic dipole.

Secondly, we use the condition of equivalence of the magnetic fields of the circuit with the conduction current at large distances from it and a magnetic dipole in a homogeneous medium with absolute magnetic permeability μ [5]. Applying this condition to the magnetization models under consideration with microscopic sources, we have

$$\vec{p}_{me} = \mu_0 \vec{p}_m . \qquad (5)$$

Averaging left and right sides of condition (5) over a sufficiently small volume of the magnetized medium ΔV, we find

$$\vec{J}^e = \mu_0 \vec{J} . \qquad (6)$$

The relation (6) makes it possible to use magnetization by molecular currents in the dipole model of magnetization and reveals the physical meaning of $\mu_0\vec{J}$ in the analogy under discussion.

Conclusions. The dipole magnetization model and the magnetization model by molecular currents have a different physical meaning which results in different definitions of magnetization and mathematical descriptions of the magnetostatic field in a magnetized medium. The field of the dipole model is potential and is described by a scalar potential, the field of molecular currents is vortex and is described by a vector potential. The application of the electrostatic analogy for the calculation of the magnetostatic field of inhomogeneous magnetizing media is correct on the basis of the dipole magnetization model, however in the calculated formulas of the potential field, it is possible to correctly use the magnetization by molecular currents.

REFERENCES

1. Polivanov K.M. *Teoreticheskie osnovy elektrotekhniki, ch. 3. Teoriia elektromagnitnogo polia* [Theoretical foundations of electrical engineering, Part 3. Theory of electromagnetic field]. Moscow, Energija Publ., 1969. 352 p. (Rus).

2. Grinberg G.A. *Izbrannye voprosy matematicheskoi teorii elektricheskikh i magnitnykh iavlenii* [Selected questions of mathematical theory of electric and magnetic phenomena]. Moscow-Leningrad, Acad. of Sci. USSR Publ., 1948. 730 p. (Rus).

3. Simonyi K. *Teoreticheskaya elektrotekhnika* [Theoretical Electrical Engineering]. Moscow, Mir Publ., 1964. 775 p. (Rus).

4. Tamm I.E. *Osnovy teorii elektrichestva* [Fundamentals of electricity theory]. Moscow, Nauka Publ., 1954. 620 p. (Rus).

5. Brunov B.Ia., Gol'denberg L.M., Kliatskin I.G., Tseitlin L.A., *Teoriia elektromagnitnogo polia* [Theory of electromagnetic field]. Moscow-Leningrad, Gosenergoizdat Publ., 1962. 512 p. (Rus).

Received 28.08.2017

V.M. Mikhailov[1]*, Doctor of Technical Science, Professor,*
K.V. Chunikhin[2]*, Postgraduate Student,*
[1] National Technical University «Kharkiv Polytechnic Institute»,
2, Kyrpychova Str., Kharkiv, 61002, Ukraine,
phone +380 57 7076052,
e-mail: valery.m.mikhailov@gmail.com
[2] State Institution «Institute of Technical Problems
of Magnetism of the NAS of Ukraine»,
19, Industrialna Str., Kharkiv, 61106, Ukraine,
phone +380 57 2992162,
e-mail: kvchunikhin@gmail.com

How to cite this article:
Mikhailov V.M., Chunikhin K.V. On electrostatic analogy of magnetostatic field in inhomogeneous magnetized medium. *Electrical engineering & electromechanics*, 2017, no.5, pp. 38-40. **doi: 10.20998/2074-272X.2017.5.05.**

UDC 621.3.013 **doi: 10.20998/2074-272X.2017.5.06**

V.Yu. Rozov, V.S. Grinchenko, O.O. Tkachenko

CALCULATION OF MAGNETIC FIELD OF THREE-PHASE CABLE LINES WITH TWO-POINT BONDED CABLE SHIELDS COVERED BY FERROMAGNETIC CORES

In this paper we obtain compact expressions for the magnetic field shielding factor of a high-voltage three-phase cable line consisting of single-core cables with two-point bonded cable shields and ferromagnetic cores installed. To obtain these expressions we develop the analytical model of the cable line. Following assumptions are made to develop the model: the current distribution in each cable shield is uniform, cylindrical ferromagnetic cores covering the cables are not magnetized to saturation and their magnetic permeability is constant, each of the ferromagnetic cores is magnetized only by the core current and the shield current of the cable that it covers, the magnetic field inside ferromagnetic cores is axisymmetric, the magnetic field is plane-parallel over the entire cable line. We consider common cases of flat and trefoil cable lines. The proposed expressions for the magnetic field shielding factor are verified experimentally. The physical model is made of three cables of the type NA2XSF(L)2Y-110 1×240/70. It is shown that the difference between numerical simulation results and experimental data lays within 15 %. References 11, figures 3.

Key words: **cable line, shield of cable, magnetic field, bonded shields, ferromagnetic core.**

Получены компактные соотношения для расчета эффективности экранирования магнитного поля высоковольтной трехфазной кабельной линии, состоящей из одножильных кабелей, которые охвачены ферромагнитными сердечниками, при двустороннем замыкании собственных экранов. Рассмотрены кабельные линии с укладкой кабелей треугольником и в плоскости. Предложенные соотношения для расчета эффективности экранирования магнитного поля верифицированы экспериментально. Библ. 11, рис. 3.

Ключевые слова: **кабельная линия, экран кабеля, магнитное поле, двустороннее заземление, ферромагнитный сердечник.**

Introduction. Compliance with the maximum permissible levels of magnetic induction is mandatory when laying high-voltage cable lines (CL). In Ukraine, the maximum permissible level of magnetic induction inside living quarters located near the CL is 0.5 μT [1, p. 277]. As the distance between single-core cables with cross-linked polyethylene insulation increases, the value of the magnetic induction of the CL can significantly exceed the permissible level [1, p. 285].

Electromagnetic, magnetostatic and contoured shields are used to reduce the magnetic field (MF) of CLs [2-4]. Another approach to reducing the MF of the CL which does not require the installation of additional screens, is the two-way closure of the CL cable shields by two-way grounding at both ends of the shielding zone [5-7]. In this case, the MF shielding efficiency is 1.5 ÷ 2.5 [5], which is not always sufficient for the normalization of the MF of the CL. A further increase in MF shielding efficiency can be achieved by strengthening the magnetic coupling between the cores and shields of the CL cables [8]. To do this, each of the cables (Fig. 1) is covered by a ferromagnetic core (FC) made of laminated electrical steel.

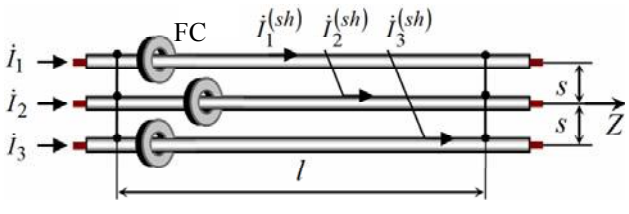

Fig. 1. A three-phase CL with installed FC

In [8], the dependence of the shielding efficiency of the MF on the number of PSs installed on each of the cables was experimentally investigated. The measurements made on the physical model of the CL confirmed the possibility of 2 to 4 times increase in shielding efficiency in comparison with the traditional two-sided closure of cable screens. However, the relations proposed in [8] for calculating the shielding efficiency of a magnetic field with a ferromagnetic core need to be refined.

The goal of the work is obtaining theoretically grounded relationships for calculating the shielding efficiency of the magnetic field of a three-phase cable line with two-sided closed shields and ferromagnetic cores installed on the cables.

The effectiveness of shielding the MF of the CL when laying cables in a triangle. The effectiveness of shielding MF is defined as the ratio of the effective value of magnetic induction to two-sided closure of the cable shields to the effective value of the magnetic induction after closing the cable shields [9]:

$$SF = |\dot{\bar{B}}_0| / |\dot{\bar{B}}| \quad (1)$$

We assume that the cables are straight (or the radius of their curvature can be neglected) and are parallel to each other. In the case when the cable shields are open, the MF of the CL is determined only by the currents in the veins. If the X axis is parallel to the ground level and perpendicular to the cable axes, and the Y axis is directed upwards, the complex amplitude of the magnetic flux density at the point with the (x, y) coordinates is [9]:

$$\dot{\vec{B}}_0 = \frac{\mu_0}{2\pi}\cdot\sum_{k=1}^{3}\dot{I}_k\cdot\left(-\frac{y-y_k}{(x-x_k)^2+(y-y_k)^2}\cdot\vec{e}_x + \right.$$
$$\left. + \frac{x-x_k}{(x-x_k)^2+(y-y_k)^2}\cdot\vec{e}_y\right), \quad (2)$$

where $k=\overline{1,3}$ is the cable number; $\dot{I}_k$ is the complex current amplitude in the core of the *k*-th cable; $\vec{e}_x$, $\vec{e}_y$ are the orts of the Cartesian coordinate system; (x_k, y_k) are the axes coordinates of the *k*-th cable; $\mu_0=4\pi\cdot10^{-7}$ H/m is the magnetic constant.

For two-sided closure of shields, the complex amplitude of the magnetic flux density is [9]:

$$\dot{\vec{B}} = \frac{\mu_0}{2\pi}\cdot\sum_{k=1}^{3}\left(\dot{I}_k+\dot{I}_k^{(sh)}\right)\times$$
$$\times\left(-\frac{y-y_k}{(x-x_k)^2+(y-y_k)^2}\cdot\vec{e}_x + \right. \quad (3)$$
$$\left. + \frac{x-x_k}{(x-x_k)^2+(y-y_k)^2}\cdot\vec{e}_y\right),$$

where $\dot{I}_k^{(sh)}$ is the complex current amplitude in the shield of the *k*-th cable.

As can be seen from (1)-(3), in order to calculate the shielding efficiency, it is necessary to determine the currents in the cable shields in the presence of ferromagnetic cores.

Consider a three-phase CL with a triangular laying of cables covered by cylindrical ferromagnetic cores (see Fig. 1).

Since the cable screens are closed at both ends of the CL, the first Kirchhoff law of is satisfied for the currents induced in them:

$$\dot{I}_1^{(sh)}+\dot{I}_2^{(sh)}+\dot{I}_3^{(sh)}=0. \quad (4)$$

We consider the contour formed by shields of the 1st and the 2nd cables, and a circuit formed by shields of the 2nd and the 3rd cables. EMFs induced in circuits are determined by magnetic fluxes that permeate them [10, p. 59]. Based on the Ohm law in complex form and the law of electromagnetic induction, we write the following relationships for each of the circuits:

$$\left(\dot{I}_1^{(sh)}-\dot{I}_2^{(sh)}\right)\cdot R^* = -j\,\omega\cdot\left(\dot{\Psi}_1^{(1,2)}-\dot{\Psi}_2^{(1,2)}\right),$$
$$\left(\dot{I}_2^{(sh)}-\dot{I}_3^{(sh)}\right)\cdot R^* = -j\,\omega\cdot\left(\dot{\Psi}_2^{(2,3)}-\dot{\Psi}_3^{(2,3)}\right), \quad (5)$$

where *j* is the imaginary unit; $\omega = 2\pi\cdot50$ s^{-1} is the angular frequency of current; R^* is the active resistance of the unit of the cable shield length, Ω/m; $\dot{\Psi}_k^{(m,n)}\equiv\dot{\Psi}_k^{(n,m)}$ is the complex amplitude of the total flux of the magnetic field which is created by the currents of the core and shield of the *k*-th cable and penetrates the circuit formed by the shields of cables with numbers *m* and *n*.

For the triangle CL because of axial symmetry $\dot{\Psi}_k^{(m,n)}=0$, when $k\neq m$ and $k\neq n$.

For the calculation of $\dot{\Psi}_k^{(k,n)}$ we take the following assumptions:

– the distribution of the induced current in the screen of each cable is uniform;

– cylindrical FCs covering cables are not magnetized to saturation, and their magnetic permeability is constant and equal to μ;

– each of the FC is magnetized by the currents of the vein and shield of only the cable that it covers, and the MF inside the FC is axisymmetric;

– over the entire length of the CL, the MF is plane-parallel.

Then the complex amplitude of the magnetic induction of the field created by the currents of the core and the screen of the *k*-th cable has only an angular component with respect to the axis of the *k*-th cable and is equal $\mu\mu_0\left(\dot{I}_k^{(sh)}+\dot{I}_k\right)/2\pi r$ inside the FC and $\mu_0\left(\dot{I}_k^{(sh)}+\dot{I}_k\right)/2\pi r$ outside the FC. By dividing the currents in cable shields with numbers *k* and *n* into elementary tubes of an infinitesimally small cross section [11, 8], and integrating over all possible contours formed by these tubes, we find:

$$\dot{\Psi}_k^{(k,n)} = \frac{\mu_0\left(\dot{I}_k^{(sh)}+\dot{I}_k\right)}{2\pi}\cdot\ln\frac{s}{r} + $$
$$+\frac{l_{core}}{l}\cdot\frac{(\mu-1)\mu_0\left(\dot{I}_k^{(sh)}+\dot{I}_k\right)}{2\pi}\cdot\ln\frac{r_1}{r_2}, \quad (6)$$

where *s* is the distance between cable axes, m; *r* is the shield radius, m; *l* is the length of the CL shielded part, m; l_{core} is the total length of the FC installed on each of cables, m; r_1 and r_2 are the external and internal FC radius, respectively, m;

Expressions (4)-(5) form a system of three equations with respect to $\dot{I}_1^{(sh)}$, $\dot{I}_2^{(sh)}$ and $\dot{I}_3^{(sh)}$. Substituting (6) we find its solution:

$$\dot{I}_k^{(sh)} = -\dot{I}_k\,\frac{j\,\omega M^*}{R^*+j\,\omega M^*} = \alpha\cdot\dot{I}_k,\ \alpha=\frac{-j\,\omega M^*}{R^*+j\,\omega M^*}, \quad (7)$$

where $M^* = \frac{\mu_0}{2\pi}\cdot\ln\frac{s}{r}+\frac{l_{core}}{l}\cdot\frac{(\mu-1)\mu_0}{2\pi}\cdot\ln\frac{r_1}{r_2}$ is the specific equivalent inductance of the shield covered by the core, H/m.

Substituting (7) in (1)-(3) we obtain the final relation for the shielding efficiency in case of triangular cable laying:

$$SF_{trefoil} = \frac{1}{|1+\alpha|} = \left|\begin{array}{l} 1+j\cdot\frac{\mu_0\omega}{2\pi R^*}\cdot\ln\frac{s}{r}+ \\ +\,j\cdot\frac{l_{core}}{l}\cdot\frac{(\mu-1)\,\mu_0\,\omega}{2\pi R^*}\cdot\ln\frac{r_1}{r_2}\end{array}\right|. \quad (8)$$

The effectiveness of the shielding of the MF of the CL when laying cables in the plane. In [9], the authors showed that for the analysis of the MF of the CL with a

plane cable laying, it is sufficient to consider the dipole component of the field, and a simplified relation for calculating the shielding efficiency when laying cables in the plane can be obtained by substituting $s \rightarrow 2 \cdot s$ into the ratio for shielding efficiency for laying cables in a triangle. Therefore, when laying cables in the plane

$$SF_{flat} = \left| \begin{array}{l} 1 + j \cdot \dfrac{\mu_0 \omega}{2\pi R^*} \cdot \ln \dfrac{2s}{r} + \\ + j \cdot \dfrac{l_{core}}{l} \cdot \dfrac{(\mu - 1)\mu_0 \omega}{2\pi R^*} \cdot \ln \dfrac{r_1}{r_2} \end{array} \right|. \quad (9)$$

To verify (9), we use the results of experimental studies performed by the authors of [8]. The research was carried out on the physical model of the CL. The model is made of NA2XSF(L)2Y-110 1×240/70 cables of length l=10 m (Fig. 2). The active resistance of the cable screen length unit is $R^*=0.29\times10^{-3}$ Ω/m. The distance between the axes of the cables is 0.2 m. The current value in the conductors of the cables is 95 A.

Fig. 2. Physical layout of the CL

As FC, stator cores of asynchronous electric motors were used, which are made of electrically bonded steel. The magnetic permeability of cores μ=3000 was determined experimentally. The outer radius of the core r_1=65 mm, the inner radius r_2 = 50 mm. The length of one core is 100 mm.

The number of FCs installed on each cable ranged from 0 to 3. Accordingly, the total length of the FC cores installed on each of the cables during the experimental studies was 0, 100 mm, 200 mm and 300 mm.

Measurement of magnetic induction was performed using a three-component EMF-828 magnetometer.

Fig. 3 shows: the curve of the shielding efficiency versus the total length of the FC installed on each of the cables constructed according to (9) and the points corresponding to the results of measuring the shielding efficiency in the FC layout. As can be seen from the figure, in the absence of FC the results of calculation and measurements coincide. When the FC is used, the deviation of the experimental data from the calculation results does not exceed 15 %.

The ratio (8) in comparison with (9) was obtained under milder assumptions. Therefore, it can be argued that the error of application (8) also does not exceed 15 %.

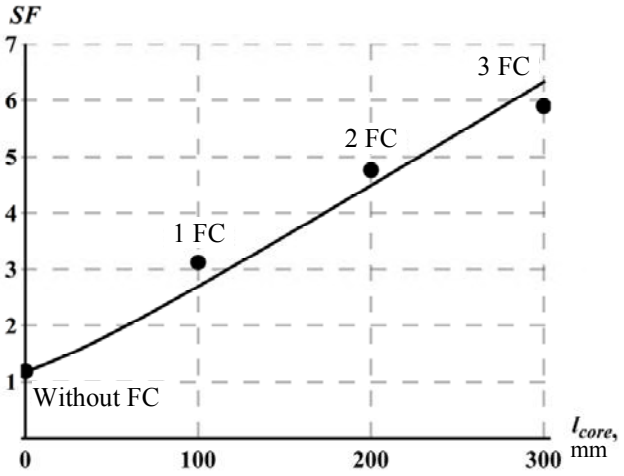

Fig. 3. Dependence of the shielding efficiency of the MF of the CL on the total FC

Conclusions.

1. Theoretically grounded relationships for the engineering calculation of the shielding efficiency of the magnetic field of the cable line for cases of laying cables in the plane and a triangle for two-sided closure of the cable shields covered by ferromagnetic cores were obtained for the first time.

2. Experimental investigations carried out on the physical layout of the cable line confirmed the correctness of the obtained calculated relationships, the error of which does not exceed 15% if the distance between the cables is three times larger than the outer radius of the ferromagnetic cores.

REFERENCES

1. *Pravila ulashtuvannya electroustanovok* [Electrical installation regulations]. 5th ed. Kharkiv, Minenergovugillya of Ukraine, 2014. 793 p. (Ukr).

2. Rezinkina M.M., Grinchenko V.S. Underground busbars magnetic field mitigation with the help of electro-magnetic shields, consisted of U-shaped elements. *Bulletin of NTU «KhPI»*, 2012, no.49, pp. 73-78. (Rus).

3. Canova A., Giaccone L. A novel technology for magnetic-field mitigation: High magnetic coupling passive loop. *IEEE Transactions on Power Delivery*, 2011, vol.26, no.3, pp. 1625-1633. **doi: 10.1109/tpwrd.2010.2099671.**

4. De Wulf M., Wouters P., Sergean P., Dupre´ L., Hoferlin E., Jacobs S., Harlet P. Electromagnetic shielding of high-voltage cables. *Journal of Magnetism and Magnetic Materials*, 2007, vol.316, no.2, pp. 908-911. **doi: 10.1016/j.jmmm.2007.03.137.**

5. Rozov V.Yu., Kvytsynskyi A.A., Dobrodeyev P.N., Grinchenko V.S., Erisov A.V. and Tkachenko O.O. Study of the magnetic field of three phase lines of single core power cables with two-end bonding of their shields. *Electrical engineering & electromechanics*, 2015, no.4, pp. 56-61. (Rus). **doi: 10.20998/2074-272X.2015.4.11.**

6. SOU-N MEV 40.1-37471933-49:2011.2. *Proektuvannia kabelnykh linii napruhoiu do 330 kV. Nastanova* [Design of cable lines with voltage up to 330 kV. Guidance]. Kyiv, Minenergovugillya of Ukraine Publ., 2017, 139 p. (Ukr).

7. SOU-N EE 20.179:2008. *Rozrakhunok elektrychnoho i mahnitnoho poliv linii elektroperedavannia. Metodyka* [Calculation of the electric and magnetic fields of power line. Method]. Kyiv, Minenergovugillya of Ukraine Publ., 2016, 34 p. (Ukr).
8. Rozov V.Yu., Dobrodeyev P.N., Erisov A.V., Tkachenko A.O. Increasing the efficiency of contour shielding of the magnetic field of high-voltage cable lines. *Tekhnichna Elektrodynamika*, 2016, no.4, pp. 5-7. (Rus).
9. Rozov V.Yu., Tkachenko O.O., Erisov A.V. and Grinchenko V.S. Analytical calculation of magnetic field of three-phase cable lines with two-point bonded shields. *Tekhnichna Elektrodynamika*, 2017, no.2, pp. 13-18 (Rus).
10. Demirchian K.S., Neiman L.R., Korovkin N.V., Chechurin V.L. *Teoreticheskie osnovy elektrotekhniki: V 3-kh t. Uchebnik dlia vuzov. Tom 1* [Theoretical bases of electrical engineering. In 3 vols. Vol.1]. St. Petersburg, Piter Publ, 2003. 463 p. (Rus).
11. Kalantarov P.L., Tseytlin L.A. *Raschet induktivnostey* [Inductance calculations]. Leningrad, Energoatomizdat Publ., 1986. 488 p. (Rus).

Received 07.08.2017

V.Yu. Rozov[1]*, Doctor of Technical Science, Corresponding member of NAS of Ukraine,*
V.S. Grinchenko[1]*, Candidate of Technical Science,*
O.O. Tkachenko[1]*, Postgraduate Student,*
[1] State Institution «Institute of Technical Problems of Magnetism of the NAS of Ukraine»,
19, Industrialna Str., Kharkiv, 61106, Ukraine,
phone +380 572 992162,
e-mail: vsgrinchenko@gmail.com

How to cite this article:
Rozov V.Yu., Grinchenko V.S., Tkachenko O.O. Calculation of magnetic field of three-phase cable lines with two-point bonded cable shields covered by ferromagnetic cores. *Electrical engineering & electromechanics*, 2017, no.5, pp. 41-44. **doi: 10.20998/2074-272X.2017.5.06.**

UDC 621.3.022: 621.319.53: 621.317.32 **doi: 10.20998/2074-272X.2017.5.07**

M.I. Baranov, V.V. Kniaziev, S.V. Rudakov

A COAXIAL DISK SHUNT FOR MEASUREMENT IN THE HIGH-CURRENT CIRCUIT OF HIGH-VOLTAGE GENERATOR OF STORM DISCHARGES OF PULSES OF CURRENT OF ARTIFICIAL LIGHTNING WITH THE INTEGRAL OF ACTION UP TO $15 \cdot 10^6$ J/OHM

Purpose. *Description of construction and basic technical descriptions developed and created in Research & Design Institute «Molniya» of the National Technical University «Kharkiv Polytechnic Institute» high-voltage high-current coaxial disk shunt of type of SC-300M2, allowing reliably to measure the peak-temporal parameters (PTP) of pulses of current of artificial lightning in wide peak and temporal ranges with the integral of their action to $15 \cdot 10^6$ J/Ohm.* ***Methodology.*** *Electrophysics bases of high-voltage impulsive technique, scientific and technical bases of development and creation of high-voltage high-current pulsive electrical equipment including the powerful generators of current of lightning (GCL), and also measuring methods in discharge circuit of the powerful high-voltage GCL AVP high pulse currents of micro- and millisecond temporal ranges.* ***Results.*** *Offered and described new construction of measuring high-voltage heavy-current shunt, containing a measuring round disk from stainless steel easily soiled 12X18H10T of thickness of 2 mm and external diameter 80 mm. Experimental a way pulse active resistance of $R_S \approx 0{,}08$ mOhm of the indicated measuring disk and on his basis a calculation coefficient transformation is found of S_S of coaxial disk shunt of type of SC-300M2, numeral equal in the concerted mode of operations of his coaxial cable line (CCL) $S_S \approx 2/R_S \approx 25 \cdot 10^3$ A/V. It is shown that it is expedient to use this value S_S for measuring in the heavy-current discharge circuit of the GCL ATP impulsive A- and repeated impulsive D- component of current of artificial lightning, and also ATP of aperiodic pulse of current of artificial lightning of temporal form 10 μc/350 μc. It is set that taking into account application in the end GCL of shunt of a co-ordinate divizor of voltage with two output coaxial sockets 1:1 (for $S_{SA} \approx 25 \cdot 10^3$ A/V) and 1:2 ($S_{SC} \approx 12.5 \cdot 10^3$ A/V) at measuring of ATP intermediate B-, protracted C- and shortened protracted C*- component of current of artificial lightning in GCL it is expedient to utillize a numeral value S_S for the examined shunt, equal $12.5 \cdot 10^3$ A/V. Practical approbation and verification of capacity of the improved measuring coaxial disk shunt of type of SC-300M2 is executed in the high-voltage heavy-current discharge circuit of the powerful GCL, forming on the actively-inductive loading of A- and C*- the components of current of artificial lightning with rationed ATP.* ***Originality.*** *Developed and created new high-voltage heavy-current measuring shunt of type of SC-300M2, allowing reliably to register rationed ATP of attenuation sinewave and aperiodic pulses of current of artificial lightning in the circuits of powerful GCL with amplitude to ±220 кА and integral them action to $13.5 \cdot 10^6$ J/Ohm. On the measuring coaxial disk shunt of type of SC-300M2 from Government Metrology Service of Ukraine the certificate of accordance of the set form is got.* ***Practical value.*** *Application of the created shunt of type of SC-300M2 in composition the high-voltage high-current discharge circuits of powerful GCL will allow in a certain measure to improve the metrology providing of tests of aviation and space-rocket technique, and also objects of electrical power engineering on stability to lightning.* References 11, figures 4.

Key words: **powerful high-voltage generator of current of lightning, measuring coaxial disk shunt, measuring disk of shunt from stainless steel, calculation estimation of parameters of shunt.**

Описана конструкция разработанного и созданного измерительного коаксиального дискового шунта типа ШК-300М2, позволяющего с помощью коаксиальной кабельной линии связи и цифровых запоминающих осциллографов одновременно измерять амплитудно-временные параметры (АВП) основных компонент тока искусственной молнии, генерируемых высоковольтным генератором грозовых разрядов в соответствии с требованиями нормативных документов США SAE ARP 5412: 2013 и SAE ARP 5416: 2013. Приведены основные технические характеристики измерительного коаксиального дискового шунта типа ШК-300М2. Показано, что данный шунт позволяет измерять и АВП апериодического импульса тока временной формы 10 мкс/350 мкс, нормированный интеграл действия которого согласно требований международного стандарта IEC 62305-1: 2010 может численно составлять до $13{,}5 \cdot 10^6$ Дж/Ом. Библ. 11, рис. 4.

Ключевые слова: **мощный высоковольтный генератор тока молнии, измерительный коаксиальный дисковый шунт, измерительный диск шунта из нержавеющей стали, расчетная оценка параметров шунта.**

Introduction. US normative documents SAE ARP 5412: 2013 [1] and SAE ARP 5416: 2013 [2] define the requirements for amplitude-time parameters (ATP) of artificial lightning current pulses generated by the corresponding high-voltage lightning generators, commonly referred to as high-voltage generators of current of lightning (GCL), on electrical loads of aerospace equipment, tested for lightning. One of these types of powerful GCL reproducing the necessary ATP pulses of the simulated lightning current according to the requirements [1, 2] on the active-inductive load, was developed and created in 2007 by the staff of the Departments No. 3 of high-voltage pulse technology and No. 4 of electromagnetic tests of the Research & Design Institute «Molniya» of the National Technical University «Kharkiv Polytechnic Institute» [3]. According to [1, 2], in these tests of aeronautical and space-rocket devices, pulsed *A*- (or repetitive pulsed *D*-), an intermediate *B*- and prolonged *C*- (or shortened long *C**-) current component of artificial lightning can be used. Moreover, combinations of these current components which follow

one after the other in time and differ greatly in their amplitudes (from hundreds of kA to tens of A) and flowing times (from hundreds of microseconds to one thousand milliseconds), can be different [1, 2]. Most often, in the practice of testing individual elements of such aircraft as civil and military aircraft for lightning, the following combinations of these lightning current components are used [1-4]: *A*-, *B*- and *C*- components, *A*-, *B*- and *C**- components and *D*-, *B*- and *C**- components.

For indicated lightning current components, such an important parameter for the electrothermal loading in the high-current discharge circuit of the powerful GCL of the test objects of aviation and rocket and space technology, in accordance with the requirements of [1, 2], as the integral of their action J_L, does not numerically exceed $2 \cdot 10^6$ J/Ω ± 20 %. We note that it is the value of this integral J_L that determines the value of the thermal energy released on the test element of an object. Therefore, the value of J_L often determines the electrothermal lightning capacity of such an object. In addition, when performing full-scale tests according to the requirements of the international standard IEC 62305-1: 2010 [5] of electric power facilities for the lightning strength of the value of the action integral JL of the aperiodic current pulse of 10 μs/350 μs of artificial lightning generated by the developed and created in 2012 at the Department No. 4 of electromagnetic tests of the Research & Design Institute «Molniya» of the NTU «KhPI» with powerful GCL [6], for the I level of their protection against lightning should be $10 \cdot 10^6$ J/Ω ± 35 %.

With the electrical current loading of the tested objects, it is necessary to register and monitor the ATP of the lightning current component used in the online mode. Typically, similar electrotechnological procedures are performed using measuring means, such as high-voltage high-current measuring shunts (HHMSs) with coaxial cable communication lines operating in a matched wave mode [3, 4], and digital storage oscilloscopes (DSO). As a rule, HHMSs are special non-standardized measuring tools, which are not produced by industry due to their insignificant quantitative need and absence from businessmen for such products of commercial interest. Therefore, domestic high-voltage electrical engineers, together with engineers-metrologists, have to solve their own engineering and technical problems for their development and production with subsequent state metrological certification.

1. The state of the engineering task. In [7], the design and technical characteristics of a measuring coaxial shunt of the ШК-300 type were described to determine the ATP pulses of artificial lightning current generated in high-current discharge circuits of the geological and technical measures in accordance with the requirements of normative documents [1, 2]. The structure of this shunt includes a manganin measuring disk with a thickness $h_s \approx 0.3$ mm with an external diameter $D_{se} \approx 80$ mm, which determines the impulse resistance of the shunt, which is approximately $R_S \approx 0.185$ mΩ ± 1% [3, 7]. The practice of operating the ШК-300 shunt in laboratory conditions showed its insufficient electrothermal and electrodynamic stability in the high-current discharge circuit of the GCL which reproduces the pulsed current $i_L(t)$ of artificial lightning on the active-inductive load ($R_l \approx 0.1$ Ω, $L_l \approx 1$ μH) with an action integral equal to about $J_L \approx 2 \cdot 10^6$ J/Ω ± 20% [1, 2]. After approximately 100 specified high-current discharges of GCL for the test load and a measuring shunt of the ШК-300 type, the latter loses its metrological characteristics and becomes unsuitable for its further use. According to [5], according to [5], for the aperiodic current pulse of 15 μs/315 μs of an artificial lightning with an amplitude $I_{mL} \approx 184$ kA ($J_L \approx 7.88 \cdot 10^6$ J/Ω) according to [5], the shunt was destroyed by an internal impulse gas-dynamic pressure in a few hundred atmospheres due to the electric explosion (sublimation) of a part of the material of its thin measuring manganin disk [8]. As we see, when using high-voltage pulse technology with discharge currents of capacitor batteries GCL in hundreds of kA to the choice of the design of the corresponding measuring shunt, higher requirements for its electrothermal lightning resistance should be presented.

In [9], the design of a shunt shunt for the measurement of pulsed currents of microsecond duration with amplitude of up to 75 kA was presented. As a high-resistance measuring element in this shunt structure, parallel-connected straight-line segments of nichrome wire were placed along the circumference between two massive coaxial cylindrical electrodes of the shunt - internal brass and outer duralumin [9]. The ends of each piece of nichrome wire placed parallel to the longitudinal axis of the shunt were soldered to two parallel massive brass disks, between which was a cylindrical ceramic insulator. With a shunt sensitivity of about 350 mV/kA, it allowed reliably to measure only large microsecond pulses the currents of a high-voltage electrophysical installation (amplitude not exceeding 75 kA) and transmit without distortion the current pulse front up to 0.6 μs [9].

The goal of the paper is the development and creation at the Research & Design Institute «Molniya» of the NTU «KhPI» of a coaxial disk shunt of the ШК-300М2 type which makes it possible to reliably measure the ATP of current pulses of artificial lightning in wide amplitude and time ranges with an action integral up to $15 \cdot 10^6$ J/Ω.

2. Problem definition. The operational experience of the high-voltage high-current ШК-300 type high-current measuring shunt accumulated in the Department No. 4 of electromagnetic testing of the Research & Design Institute «Molniya» of the NTU «KhPI» demonstrates that, taking into account the state of the high-voltage impulse technique of the actual task of metrological support of tests on [1, 2, 5] of domestic aviation and rocket and space technology, as well as electric power facilities for lightning in this shunt construction improvement must be subject to: first, a thin

measuring manganin disk; secondly, the insulation between the massive internal brass and massive outer brass cylindrical electrodes. These two positions are the «weak links» in the design of the ШК-300 measuring shunt with its intended application as part of measuring instruments designed to implement technical tasks in accordance with the stringent requirements of [1, 2, 5].

It is required to rationally select the geometry and material of the measuring disk, as well as the insulation between the main brass electrodes in the measuring coaxial shunt, which, after the improvement, has acquired the name ШК-300М2, is required within the applied engineering and technical approach. In addition, after the modernization of the measuring coaxial disk shunt, it is necessary to perform its practical testing and testing of the operability in the high-current discharge circuit of the current high-power high-voltage GCL according to [3].

3. Calculation evaluation of some parameters of the measuring coaxial disk shunt of the ШК-300М2 type. As the material of the measuring disk of a coaxial shunt of the type ШК-300М2, we chose the stainless steel 12Х18Н10Т of domestic production widely used in engineering and everyday life [10]. The average thickness h_{sm} of the measuring disk wall of the investigated high-current high-voltage coaxial shunt of the ШК-300М2 type in the adiabatic mode of its operation on the basis of the known laws of electrical and thermal physics can be estimated from the following relationship:

$$h_{sm} \approx (\pi D_{sm})^{-1}\left[(J_L \rho_s)/(c_s \Delta T_s d_s)\right]^{1/2}, \qquad (1)$$

where $D_{sm} \approx D_{se}/2$; ρ_s, c_s, d_s are the specific electrical resistance, specific heat and density of the disk material at ambient temperature T_0 equal to room temperature 20 °C, respectively; $\Delta T_s=(T_s-T_0)$ is the ermissible short-term overheating of the material of the shunt disk with its current temperature T_s caused by the current flowing through it.

For design reasons, we assume that the outer diameter of the measuring steel disk in a ШК-300М2 shunt is $D_{se} \approx 80$ mm, and its internal diameter is $D_{si} \approx 10$ mm. Then, from (1) with $D_{sm} \approx 40$ mm, $J_L \approx 15 \cdot 10^6$ J/Ω, $\Delta T_s \approx 100$ °C and the initial data known for [10] for 12Х18Н10Т stainless steel ($\rho_s \approx 72{,}5 \cdot 10^{-8}$ Ω·m; $c_s \approx 462$ J/(kg·°C); $d_s \approx 7900$ kg/m^3), we obtain that the radial averaged wall thickness of the measuring steel disk will be numerically equal to $h_{sm} \approx 1.4$ mm. Taking into account a certain reserve in thickness h_{sm} and taking into account our very limited technological possibilities in the selection of materials, we choose the thickness of the wall of the measuring disk of stainless steel 12Х18Н10Т equal to $h_{sm} \approx 2$ mm.

Note that in (1) for a shunt of the ШК-300М2 type studied, the value of the short-term superheating ΔT_s of the material of the measuring disk, occurring during the time of the current $i_L(t)$ no more than 1000 ms in practically adiabatic mode, is limited by the type of solid insulation used to separate it from main brass electrode shunt. When using fluoroplastic insulation, the value of overheating ΔTs for reliable operation of ШК-300М2 shunt in the GCL composition should not be more than 100 °C [3, 4]. At $\Delta T_s \approx 50$ °C and the initial data taken above for the integral of the action J_L of the pulsed lightning current, the geometric, electrical, and thermophysical characteristics of the steel shunt disk from (1), it follows that the h_{sm} thickness of the disk is exactly about 2 mm.

The active resistance R_{S0} of the measuring steel disk of the coaxial shunt ШК-300М2 in the quasi-stationary mode, which practically corresponds to the regime of DC current flowing through it, can be approximated by the following formula [11]:

$$R_{S0} \approx 0.5\,(\pi h_{sm})^{-1} \rho_s \ln(D_{se}/D_{si}). \qquad (2)$$

From (2) at $h_{sm} \approx 2$ mm, $\rho_s \approx 72.5 \cdot 10^{-8}$ Ω·m, $D_{se} \approx 80$ mm and $D_{si} \approx 10$ mm it follows that the sought value of RS0 is approximately equal to 0.12 mΩ. Measurement of the shunt of the ШК-300М2 shunt type, almost equal to the R_{S0} value, carried out by metrologists in a highly stable scheme of 19 A a DC generator showed that in this experimental case $R_{S0} \approx 0.094$ mΩ. It can be seen that the difference between the calculated and experimental data for R_{S0} in our case does not exceed 22 %.

4. Practical implementation of the measuring coaxial disk shunt type ШК-300М2. Fig. 1, 2, respectively, are a general view and a schematic arrangement of a measuring coaxial disk shunt of the type ШК-300М2. The weight of this measuring shunt is about 3.2 kg, and its overall dimensions do not exceed 90×95 mm.

Fig. 1. General view of a coaxial shunt type ШК-300М2 designed to measure on the screens of the DSO in an agreed mode of operation of its coaxial cable communication line of powerful current pulses of artificial lightning in a high-current discharge circuit of a high-voltage GCL with an integral of their action up to $15 \cdot 10^6$ J/Ω

From the data in Fig. 2, it can be seen that a measuring steel disk 5 of thickness $h_{sm} \approx 2$ mm is tightly clamped between its massive disks 6 and 7 with a thickness of 10 mm, made of a sheet of fluoroplastic

insulation. Between the massive brass cylindrical electrodes 1 and 4 of the shunt through which the measured current pulse $i_L(t)$ of artificial lightning flows from the GCL capacitors, insulating sleeves 2 and 3 with a thickness of 3 mm are installed, also made of fluoroplastic insulation.

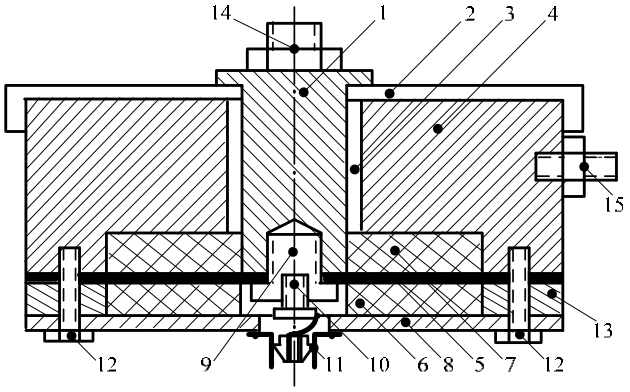

Fig. 2. Elements of the structure of a coaxial disk shunt of the ШК-300М2 type in its longitudinal axial section (1 – massive internal cylindrical electrode, 2,3 – insulating sleeves, 4 – massive outer cylindrical electrode, 5 – high-resistance steel measuring disk, 6,7 – massive insulation disks, 8 – a shroud disk, 9,10,12 – fastening screws, 11 – CP-75 output coaxial connector, 13 – massive clamping ring, 14, 15 – respectively input (potential) and output (earthed) bolted shunt connecting elements to high-current discharge circuit of the GCL)

These bushings significantly increase the electrical strength of the insulating gaps between the live parts of the high-voltage high-current shunt of the ШК-300М2 type, which positively affects the reliability of its functioning as part of a powerful GCL. The increased electrodynamic resistance of the shunt under investigation is provided by a massive pressure brass ring 13 with a thickness of 7 mm, a brass shroud disk 8 with a thickness of 5 mm and steel screws of fixation 12 in quantity of 8 pieces evenly distributed along the outer circular perimeter of the massive brass electrode 4 of the shunt.

A measuring coaxial disk shunt of the type ШК-300М2 is connected in the rupture of a high-current high-voltage discharge circuit of a powerful GCL of one or another version [3, 5]. Moreover, the inner cylindrical brass electrode 1 with diameter of 29 mm of the shunt is connected by means of the bolted joint elements 14 to the potential part of the high-current discharge circuit of the GCL, and its outer cylindrical brass electrode 4 with a diameter 80 mm with the help of the 15 bolt connection elements - to the grounded part of the discharge circuit of the GCL (usually to the metal grounded collector of the high-power capacitor bank of the generator).

5. Results of experimental approbation of a measuring coaxial disk shunt of ШК-300М2 type in a high-current circuit of high-voltage GCL. Fig. 3 shows an oscillogram of the pulsed *A*- component of artificial lightning current obtained by means of a measuring coaxial disk shunt of the type ШК-300М2, included in the discharge circuit of a powerful GCL [3] reproducing according to the requirements of normative documents [1, 2] on the active-inductive load ($R_l \approx 0.1$ Ω, $L_l \approx 1.5$ μH) pulses of artificial lightning current.

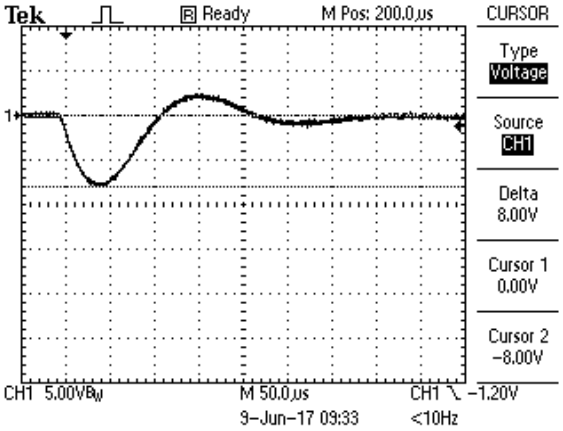

Fig. 3. The oscillogram of the pulsed *A*- component of the artificial lightning current with normalized ATPs in the high-current discharge circuit of the GCL [3] obtained with the help of a measuring coaxial disk shunt of the type ШК-300М2 ($I_{mA1} \approx -200$ kA; $t_{mA1} \approx 38$ μs; $J_A \approx 2.39 \cdot 10^6$ J/Ω; $U_{cA} \approx -29.7$ кV; $S_{SA} \approx 25 \cdot 10^3$ A/V; scale on the vertical – 125 kA/cell; scale on the horizontal – 50 μs/cell)

In the course of experimental studies of the behavior of the improved design and characteristics of a ШК-300М2 shunt in the discharge circuit GCL [3] whose capacitor bank, when forming the one shown in Fig. 3 components of the lightning current were charged to a constant voltage $U_{cA} \approx -29.7$ kV, it was found that its impulse resistance R_S takes a numerical value equal to about $R_S \approx 0.08$ mΩ ± 1%. This experimental R_S value under flow conditions along the measuring steel shunt disk shown in Fig. 3 pulsed current $i_L(t)$ of artificial lightning differs from the active resistance $R_{S0} \approx 0.094$ mΩ of the shunt in question by no more than 15% in direct current. It should be noted that the indicated values of the active resistances R_S and R_{S0} are in good agreement with the results of previous studies of transient electromagnetic processes and the penetration depths of the pulsed electromagnetic field in conducting non-magnetic media on the sections of the first three half-waves of the decaying sinusoidal current pulse acting on them [4]. Due to the peculiarities of the distribution in the metal of the measuring disk of the shunt of the pulsed electromagnetic field from the measured pulsed current $i_L(t)$ of the simulated lightning, its impulse resistance R_S will always be less than the active resistance of the R_{S0} disk measured at constant current [4].

It is known that the value of the impulse active resistance R_S of the shunt measuring disk in the coordinated mode of connecting its coaxial cable communication line to the DSO determines its conversion coefficient S_S having the dimension A/B and calculated by the ratio $S_S \approx 2/R_S$. In this case, the value of the S_S parameter is numerically equal to the current flowing through the shunt disk when a voltage of 1 V is applied to its input. In this connection, the ATP, measured with a

coaxial ШК-300М2 shunt of the pulse current $i_L(t)$ of artificial lightning in the discharge chains of a powerful GCL will be determined by the following relationship:

$$i_L(t) \approx S_S U_{LO}(t), \quad (3)$$

where $U_{LO}(t)$ is the pulse voltage recorded by means of a measuring shunt on the screen of the DSO.

Taking into account the presented results, we find that the conversion coefficient SS of the measuring shunt of the ШК-300М2 type for the recording mode according to them [1, 2] of the *A*- and *D*- components of the pulsed current of artificial lightning, and also according to [5] 10 μs/350 μs will be $S_{SA} \approx 2/R_S \approx 25 \cdot 10^3$ A/B. When using a shunt made at the end of a coaxial cable line of a shunt made on the basis of an PK 75-7-11 radio frequency cable with a 75-Ω impedance matching voltage divider [3, 7], the S_S conversion coefficient of the investigated shunt-type shunt of the ШК-300М2 type in mode of registration of the intermediate *B*-, long *C*- and shortened long *C**- component of the artificial lightning current will be equal to $S_{SC} \approx 1/R_S \approx 12{,}5 \cdot 10^3$ A/V. This MVD is implemented with two output coaxial connectors 1:1 (for S_{SA}) and 1:2 (for S_{SC}) based on three 110 Ω resistors and placed in a separate shielded housing [3, 7].

Fig. 4 shows the oscillogram of the shortened long-time *C**- component of the current of artificial lightning in a high-current discharge circuit of the GCL [3] which follows in time immediately after the pulsed *A*- current component of the lightning and simultaneously fixed on the DSO screen by means of a measuring coaxial disk shunt of type ШК-300М2. We will point out that in the conducted experiments the DSO Tektronix TDS 1012 series were used in a buried measuring bin and remote from the GCL discharge circuits at a distance of approximately 70 m.

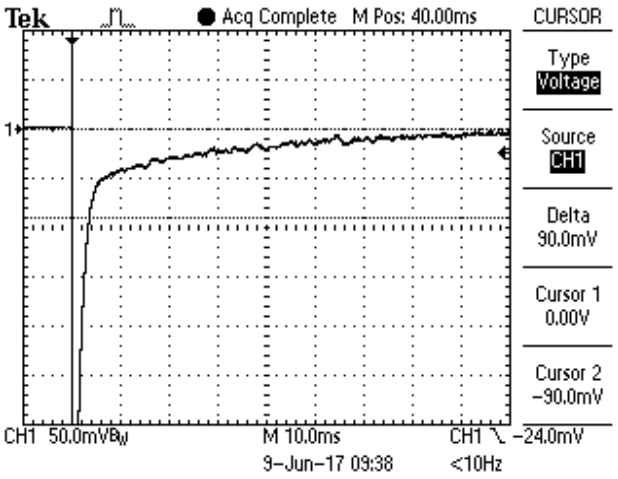

Fig. 4. The oscillogram of the shortened long *C**- component of the artificial lightning current with normalized ATPs in the discharge circuit of the GCL [3] obtained simultaneously with the current *A*- component flowing before it with the aid of a measuring coaxial disk shunt of the type ШК-300М2 ($I_{mC*} \approx -750$ A; $t_{mC*} \approx 5$ ms; $\tau_{pC*} \approx 15$ ms; $q_{C*} \approx -18.1$ C; $S_{SC*} \approx 12.5 \cdot 10^3$ A/B; $U_{cC*} \approx -4$ kV; scale on the vertical – 625 A/cell; scale on the horizontal – 10 ms/cell)

The charging voltage of the negative polarity of the capacitor bank GCL [3] which forms on the active-inductive load ($R_l \approx 0.1$ Ω; $L_l \approx 1.5$ μH) the shortened *C** - current component of the simulated lightning applied to the data in Fig. 4 was $U_{cC*} \approx -4$ kV. Note that the ones shown in Fig. 3 and 4 ATPs of the pulsed *A*- and shortened long-time *C**- current component of a lightning simulated in the laboratory conditions correspond to the current requirements of normative documents [1, 2].

Conclusions.

1. The developed and created at the Department No. 4 of electromagnetic tests of the Research & Design Institute «Molniya» of the NTU «KhPI» measuring coaxial disk shunt of type ШК-300М2 developed and created allows for its direct placement in a high-current high-voltage discharge circuit of a powerful GCL by means of one additional shielded coaxial cable communication line up to 70 m and a few located in remote from the GCL buried deep shielded bunker DSO in an agreed mode of their operation simultaneously and repeatedly measured on the active-inductive load of the tested object, the main components of artificial lightning current with normalized ATPs in accordance with the requirements of US regulations SAE ARP 5412: 2013 and SAE ARP 5416: 2013 with their amplitude up to ±220 kA and the action integral up to $2.4 \cdot 10^6$ J/Ω.

2. The measuring coaxial disk shunt of the ШК 300М2 type is capable of repeatedly recording on the active-inductive load and transmitting in a coordinated mode along the coaxial cable communication line to the DSO the aperiodic pulses of a time current of 10 μs/350 μs of a short stroke of an artificial lightning generated in a high-current high-voltage discharge circuit of a powerful GCL with standardized ATPs according to the requirements of the International Standard IEC 62305-1: 2010 with their amplitude up to ±220 kA and the action integral up to $13.5 \cdot 10^6$ J/Ω.

3. The high-current experiments on a high-power high-voltage GCL were carried out in June 2017 at the Experimental and Test Site of the Research & Design Institute «Molniya» of the NTU «KhPI» in accordance with the requirements of the US regulations SAE ARP 5412: 2013 and SAE ARP 5416: 2013 of the measuring coaxial disk shunt type ШК-300М2 which passed the state metrological certification at the state enterprise «Kharkivstandartmetrologiya» (certificate of conformity No. 06/0206 of 19.07.2017).

REFERENCES

1. SAE ARP 5412: 2013. Aircraft Lightning Environment and Ralated Test Waveforms. SAE Aerospace. USA, 2013. − pp. 1-56.

2. SAE ARP 5416: 2013. Aircraft Lightning Test Methods. SAE Aerospace. USA, 2013. − pp. 1-145.

3. Baranov M.I., Koliushko G.M., Kravchenko V.I., Nedzel'skii O.S., Dnyshchenko V.N. A Current Generator of the Artificial Lightning for Full-Scale Tests of Engineering Objects. *Instruments and Experimental Technique*, 2008, no.3, pp. 401-405. **doi: 10.1134/s0020441208030123**.

4. Baranov M.I. *Izbrannye voprosy elektrofiziki. Tom 2, Kn. 2: Teoriia elektrofizicheskikh effektov i zadach* [Selected topics of Electrophysics. Vol.2, Book 2. A theory of electrophysical effects and tasks]. Kharkiv, Tochka Publ., 2010. 407 p. (Rus).
5. IEC 62305-1: 2010 «Protection against lightning. Part 1: General principles». Geneva, IEC Publ., 2010.
6. Baranov M.I., Koliushko G.M., Kravchenko V.I., Rudakov S.V. A generator of aperiodic current pulses of artificial lightning with a rationed temporal form of 10 μs/350 μs with an amplitude of ±(100–200) kA. *Instruments and Experimental Techniques*, 2015, vol.58, no.6, pp. 745-750. **doi: 10.1134/s0020441215060032.**
7. Dnyshchenko V.N., Eremeev V.O., Nedzelsky O.S., Ponudzhaeva E.G. SC-300 measuring shunt for determining the amplitude-time parameters of the simulated lightning current pulse. *Bulletin of NTU «KhPI». Series: Technique and electrophysics of high voltage*, 2007, no.20. pp. 75-79. (Rus).
8. Baranov M.I., Kniaziev V.V., Rudakov S.V. Calculation and experimental estimation of results of electro-thermal action of rationed by the international standard IEC 62305-1-2010 impulse current of short blow of artificial lightning on the thin-walled coverage from stainless steel. *Electrical engineering & electromechanics*, 2017, no.1, pp. 31-38. (Rus). **doi: 10.20998/2074-272X.2017.1.06.**
9. Donets S.E., Ledenev V.V., Litvinenko V.V. Rod shunt to measure strong currents of microsecond duration. *Bulletin of NTU «KhPI». Series: Technique and electrophysics of high voltage*, 2008, no.44. pp. 34-44. (Rus).
10. Available at: http://prom.ua/p19700265-pischevaya-nerzhaveyuschaya-stal.html (accessed 12 June 2014). (Rus).
11. Baranov M.I., Belyi I.V., Khimenko L.T. Equivalent electrical parameters of coaxial systems of various shapes with a homogeneous azimuthal magnetic field in the gap. *Theoretical electrical engineering*, 1976, no.20, pp. 67-74. (Rus).

Received 09.08.2017

M.I. Baranov[1], *Doctor of Technical Science, Chief Researcher,*
V.V. Kniaziev[1], *Candidate of Technical Science, Senior Research Scientist,*
S.V. Rudakov[2], *Candidate of Technical Science, Associate Professor,*
[1] Scientific-&-Research Planning-&-Design Institute «Molniya», National Technical University «Kharkiv Polytechnic Institute», 47, Shevchenko Str., Kharkiv, 61013, Ukraine,
phone +380 57 7076841,
e-mail: baranovmi@kpi.kharkov.ua, knyaz2@i.ua
[2] National University of Civil Protection of Ukraine, 94, Chernyshevska Str., Kharkiv, 61023, Ukraine,
phone +380 57 7073438,
e-mail: serg_73@i.ua

How to cite this article:
Baranov M.I., Kniaziev V.V., Rudakov S.V. A coaxial disk shunt for measurement in the high-current circuit of high-voltage generator of storm discharges of pulses of current of artificial lightning with the integral of action up to $15 \cdot 10^6$ J/Ohm. *Electrical engineering & electromechanics*, 2017, no.5, pp. 45-50. **doi: 10.20998/2074-272X.2017.5.07.**

UDC 621.319 **doi: 10.20998/2074-272X.2017.5.08**

G.V. Bezprozvannych, I.A. Mirchuk

THE EVALUATION OF POSSIBILITY OF NORMAL OPERATION OF CABLES BASED ON TWISTED PAIRS WITH PVC JACKET UNDER THE CONDITIONS OF HIGH HUMIDITY AND TEMPERATURE

Introduction. Development of cables for structured cabling systems based on twisted pairs for shipbuilding is carried out in two main directions: increasing the fire safety of cables and increasing the long-term permissible operating temperature by using new, more heat-resistant, electrical insulating materials. Purpose. Substantiation of the possibility of unshielded cables on the basis of unshielded twisted pairs with thermoplastic polyethylene insulation in PVC protective jacket in conditions of high humidity and high operating temperatures on the basis of the results of accelerated aging. Methodology. The cycle of aging under conditions of increased humidity is performed for 336 hours. Then the sample was under natural drying conditions for 1440 hours. Thermal aging in a thermostat at 90 °C was carried out in two stages: first – for 206 hours, the second – for 260 hours. In the initial state and after accelerated aging, measurements of the capacitance and tangent of the dielectric loss angle of all the insulating gaps at frequencies of 100 Hz, 1 and 10 kHz were performed. Results. According to the results of accelerated aging under conditions of high humidity and temperature, it is established that the design of an unshielded cable based on unshielded twisted pairs with thermoplastic polyethylene insulation in a protective coating based on PVC-plastic is resistant to external influencing factors. Practical value. The prolonged holding at temperature of 90 °C is equivalent to operation at temperature of 40 °C for 6.8 years. At higher operating temperatures, the lifetime of the cable is significantly reduced. References 5, tables 1, figures 5.

Key words: **cables based on twisted pairs for shipbuilding, accelerated aging, hygroscopic moistening, thermal aging, partial capacitance, tangent of the dielectric loss angle, service life.**

Представлены результаты ускоренного старения в условиях повышенной влажности и температуры образца неэкранированного кабеля на основе витых пар с полиэтиленовой термопластичной изоляцией в защитной оболочке на основе поливинилхлоридного пластиката. Оценка устойчивости кабеля к действию внешних воздействующих факторов выполнена по частичным емкостям и тангенсу угла диэлектрических потерь изоляционных промежутков между жилами. Конструктивная особенность кабеля приводит к группированию частичных емкостей в четыре характерные области. Установлена динамика изменений диэлектрических параметров в процессе гигроскопического увлажнения, естественной сушки и теплового старения при температуре 90 ^{o}C образца кабеля. Определены коэффициенты парной корреляции между диэлектрическими параметрами в исходном состоянии и после внешних воздействующих факторов. Показано, что конструкция кабеля устойчива к действию повышенной влажности и температуры. Библ. 5, табл. 1, рис. 5.

Ключевые слова: **кабели на основе витых пар для судостроения, ускоренное старение, гигроскопическое увлажнение, тепловое старение, частичные емкости, тангенс угла диэлектрических потерь, срок службы.**

Introduction. The development of the shipbuilding infrastructure includes the presence of modern branched structured control systems with high-speed data transmission.

Shipboard cables have higher requirements for electrical, installation characteristics, resistance to external factors (temperature, humidity, vibration, solar radiation, etc.) than to cables for general industrial use. Cables for the industrial interface must meet the safety criteria and technical requirements, primarily fire and explosion safety [1, 2].

It should be noted that about 60-70 % of the total number of electrical cables on the ships are cables of control, signaling and communication systems. Development of cables for structured cabling systems based on twisted pairs for shipbuilding is carried out in two main directions: increasing the fire safety of cables and increasing the long-term permissible operating temperature by using new, more heat-resistant, electrical insulating materials. It is shown in [3] that cables of general industrial use on the basis of twisted pairs of category 5e can operate under conditions of increased radiation situation.

The goal of the paper is substantiation of the possibility of operation in conditions of high humidity and high operating temperatures of unshielded cable based on unshielded twisted pairs with thermoplastic polyethylene insulation in a protective polyvinylchloride (PVC) jacket according to the results of accelerated aging.

Characteristic areas of partial capacitances of insulating gaps. The evaluation of the cable's resistance to the action of external factors acting on partial capacitances and the tangent of the dielectric loss angle of the insulation gaps between the wires. Shrinkage of insulation in the process of thermal aging or swelling during prolonged hygroscopic moistening leads to a change in the characteristics of the insulation gaps of the cable.

For cables based on twisted pairs, a random orientation of the pairs is characteristic. The twisting steps of unshielded twisted pair (UTP) are different to provide the required noise immunity: as a result, the distances between the wires are averaged, which causes the number of groups of partial capacitances to decrease. For example, in a 4-pair UTP-based cable (Fig. 1, 2), the

distance between wires 1 and 3 is on the average the same as between wire 1 and any other – 4, 5, 6, 7 or 8. As a result, all partial capacity between the 8-th wires (and there are as many such capacitances as the sides of the 8-gon, i.e. $N=\frac{n(n-1)}{2}=\frac{8(8-1)}{2}=28$) are grouped in only 4 regions – Fig. 3.

The first area is the capacitance between the contacting wires of the same pair (***i-j*** – intervals: 1 – 2, 3 – 4, 5 – 6, 7 – 8, Fig. 1); the second one is the capacitance between the wires of the contacting pairs (***i-k*** – intervals, for example: 1 – 7, 1 – 8, 2 – 7, 2 – 8, Fig. 1); the third one is the capacitance between the wires of non-contiguous pairs (***i-l*** – intervals: 1 – 5, 1 – 6, 2 – 5, 2 – 6, etc., Fig. 1). The fourth group can be measured according to the «wire – versus all others» scheme (***i-s*** – area of insulation of the wires, for example, 1 – 2, 3, 4, 5, 6, 7, 8, Fig. 1).

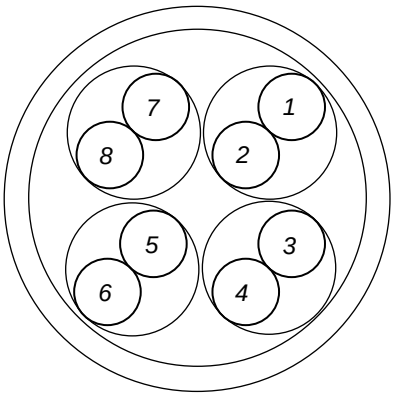

Fig. 1. Scheme of an unshielded twisted-pair cable (UTP): 4 twisted pairs, with different twisting steps (the case of the same orientation of twisted pairs, possible on separate sections of the cable)

The regulatory characteristics of the insulation gaps are determined on the basis of the calculation of the electrostatic field. Fig. 2 shows the lines of the electric field with different schemes for feeding the potential to the conductors: to the second wire of the first pair (Fig. 2,*a*); to the second wire of the first and eighth wire of the fourth pair (Fig. 2,*b*); to the second wire of the first, the eighth wire of the fourth and third wire of the second pair (Fig. 2,*c*); to the second wire of the first, the eighth wire of the fourth, the third wire, the second and fifth wire of the third pair (Fig. 2,*d*); to the second wire of the fourth pair (Fig. 2,*e*), respectively. Based on the calculation of the electrostatic field, the linear capacitances (C) and the fraction of the stored energy (η) [4] of the potential wires are determined with respect to the total energy stored in the cable (Fig. 3): C = 53.0 pF / m; η = 0.506 – for one internal (Fig. 2,*a*); C = 37.7 pF / m; η = 0.473 – for one external (Fig. 2,*e*); C = 101.9 pF / m; η = 0.524 – for two internal (Fig. 2,*b*); C = 114.2 pF / m; η = 0.571 – for four internal (Fig. 2,*d*); C = 6.214 pF / m; η = 0.0085 – for eight wires together. The share of energy stored in the solid insulation of the wires is about 50 %. Consequently, the dielectric losses in the insulating gaps (such as «solid phase-air») should also be about 50 % of the losses in the solid dielectric itself.

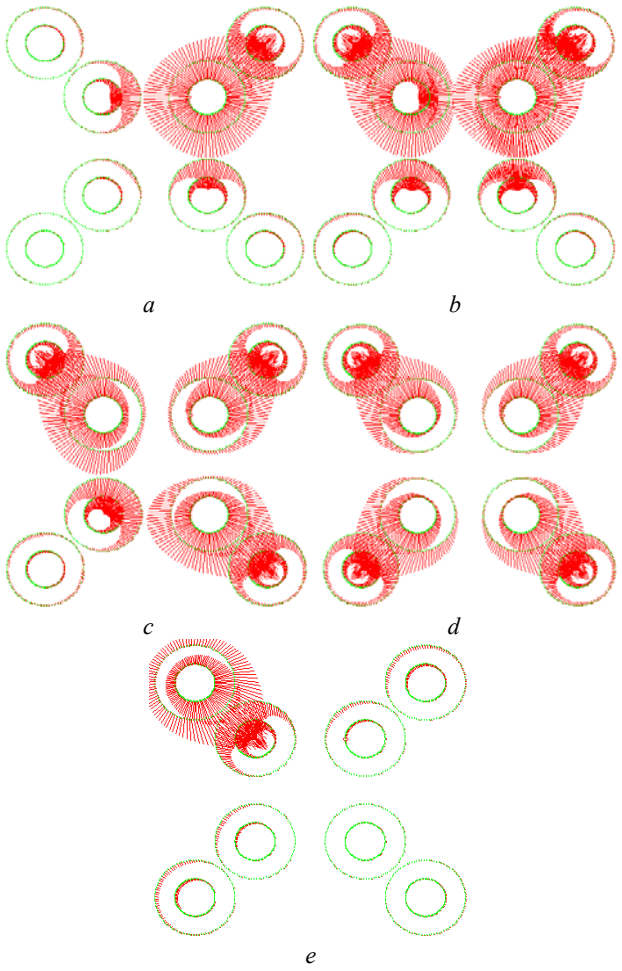

Fig. 2. Pictures of electric field lines in the cross-section of UTP-cable with different orientation of pairs at different schemes of potential supply to the conductors

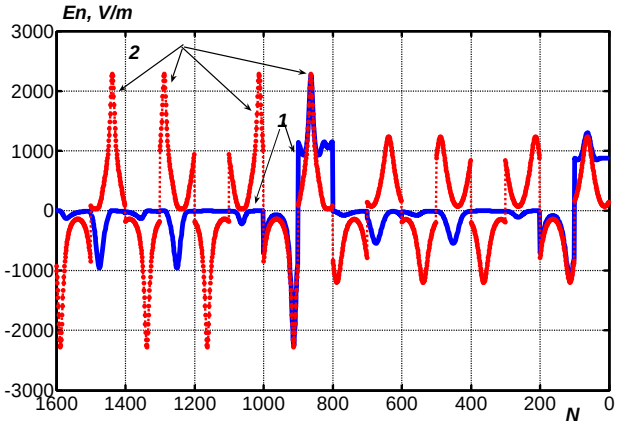

Fig. 3. The distribution of the electric field strength when the potential is to applied one (curve *1*) and four (curve *2*) internal wires of twisted pairs in the UTP-cable (the number of main nodes is N = 2500, that is, the order of the system of linear algebraic equations)

Dynamics of changes in the parameters of insulation gaps as a result of accelerated aging. Experimental studies were performed on a UTP-cable of category 5e sample of length of 1.8 m. Their purpose is to check the stability of the cable of the basic design with thermoplastic solid polyethylene insulation in a protective shell based on polyvinyl chloride plastic to the effect of high

humidity and temperature. The cycle of aging under conditions of increased 100 % humidity in a desiccator (hygroscopic moistening of the sample-through unsealed ends) was performed for 336 hours. Then the sample was under natural drying conditions for 1440 hours. The thermal aging in a thermostat at 90 °C was carried out in two stages: the first – for 206 hours, the second – for 260 hours.

In the initial state and after accelerated aging, measurements of the capacitance and tangent of the dielectric loss angle of all the insulating gaps at frequencies of 100 Hz, 1 and 10 kHz were performed.

Fig. 4,*a* shows the parameters of the insulation gaps of a UTP-cable of category 5e sample in the initial state. For the «wire-wire of the same pair» intervals, the lowest levels of tgδ are observed, with tgδ falling with increasing frequency.

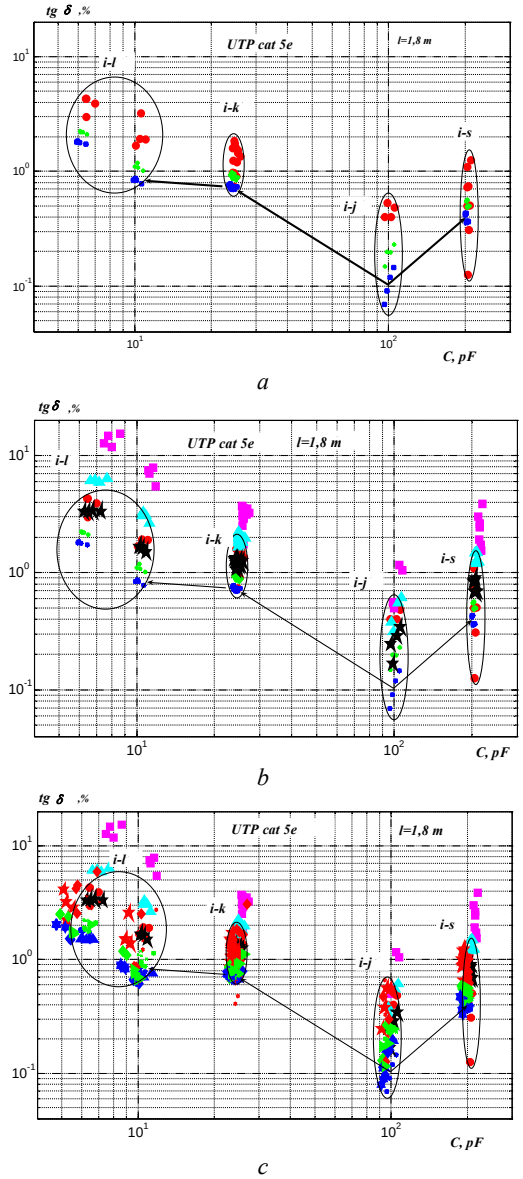

Fig. 4. Dynamics of changes in partial capacitances and tangent of the dielectric loss angle in the process of accelerated aging under conditions of high humidity and temperature

External influence – hygroscopic moistening – leads to a strong change in the parameters of only some regions – Fig. 4,*b* (the experimental points lie outside the selected regions). This is a consequence of the appearance of moisture in the capillaries formed by contacting insulated cores [5]. Fig. 5,*b* shows the parameters of the insulating gaps in the initial state and after a two-week exposure (336 hours) in the desiccator. The capacitances of the gaps have increased little, but tgδ has grown significantly more, and to a greater extent for wires distant from each other (the region of small partial capacitances, the left part of Fig. 4,*b*). After extraction from the desiccator and natural drying for two months (1440 hours), a decrease in tgδ is observed due to the removal of moisture from the surface of the isolated wires and a decrease in partial capacities due to swelling of the insulation (diffusion of moisture into the thickness of the insulation).

As a result of thermal aging at temperature of 90 °C, the decrease in tgδ continues due to the removal of moisture from the insulation layer and the growth of partial capacities due to shrinkage of insulation. Drying the cable at a temperature of 90 °C for 260 hours resulted in an almost complete restoration of the electrical characteristics of all its insulating gaps (see Fig. 4,*c*). In this case, the PVC jacket slightly changed in color, lost its shine, but retained its elasticity.

There is a positive correlation, both for partial capacitance and for the tangent of the dielectric loss angle (Table 1).

Table 1

Coefficients of mutual pair correlation between the capacitance in the initial state and the capacity after accelerated aging (r_C), between the tangent of the dielectric loss angle in the initial state and after accelerated aging ($r_{tg\delta}$)

Frequency of measurements *f*, kHz	Conditions of accelerated aging			
	336 hours under conditions of 100 % humidity	1440 hours At normal conditions	206 hours of heat aging at temperature 90 °C	456 hours of heat aging at temperature 90°C
	r_C			
0.1	0.9998	0.9998	0.9999	0.9998
	$r_{tg\delta}$			
	0.9001	**0.8176**	**0.8578**	**0.7876**
1	r_C			
	1.0000	0.9999	0.9999	0.9999
	$r_{tg\delta}$			
	0.9810	0.9909	0.9876	0.9622
10	r_C			
	1.0000	1.0000	0.9999	0.9999
	$r_{tg\delta}$			
	0.9111	0.9966	0.9942	0,9904

The values of the selective linear paired coefficient of K. Pierson correlation *r* are large for partial capacitances and, in practice, vary only slightly at different frequencies (see Table 1). For the tangent of the dielectric loss angle, the more pronounced frequency dependence $r_{tg\delta}$ is characteristic: the pair correlation coefficient has large values at the frequency 1 kHz and 10 kHz, which is associated with both the polarization processes and the electrical conductivity in the insulation.

As an adequate lifetime of the cable sample, the estimated service life, obtained on the basis of parameters of the accelerated aging regime, adequate to the aging of the cables under operating conditions (Fig. 5) is taken. The normal operation time of the cable is 1.14 years and 6.8 years at an operating temperature of 60 °C and 40 °C, respectively.

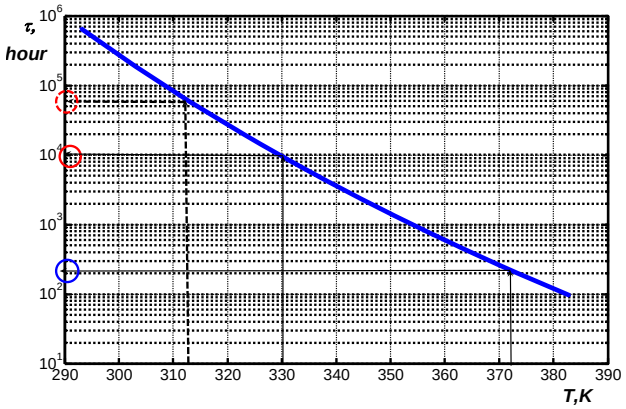

Fig. 5. To assess the life of the cable under normal operating conditions

Conclusions. The results of accelerated aging of unshielded cable based on unshielded twisted pairs with thermoplastic polyethylene insulation in a protective jacket based on PVC-plastic material in conditions of high humidity and temperature show that the design is resistant to external influencing factors. The prolonged holding at 90 °C is equivalent to operation at temperature of 40 °C for 6.8 years. At higher operating temperatures, the lifetime of the cable is significantly reduced.

REFERENCES

1. IEC 60092-359:2014, Electrical Installations In Ships – Part 359: Sheathing Materials For Shipboard Power And Telecommunication Cables By IEC TC/SC 18A. 50 p.

2. IEC 60332-1-2:2004, Tests on electric cables under fire conditions – Part 1: Test on a single vertical insulated wire or cable.

3. Bezprozvannych G.V., Naboka B.G., Morozova E.V. Radiating resistance of common commercial cables of internal laying. *Electrical engineering & electromechanics*, 2006, no.3, pp. 82-86. **doi: 10.20998/2074-272X.2006.3.16.** (Rus).

4. Bezprozvannych A.V., Naboka B.G., Moskvitin E.S. Examination of the three-phase insulation of cables in a metal shell. *Electricity*, 2010, no.1, pp. 48-54. (Rus).

5. Bezprozvannych A.V. The electrical scanning of the transverse structure by multicore cables by the method of cumulative measurements. *Tekhnichna elektrodynamika*, 2008, no.3, pp. 30-36. (Rus).

Received 25.08.2017

G.V. Bezprozvannych[1], *Doctor of Technical Science, Professor,*
I.A. Mirchuk[2], *Postgraduate Student,*
[1] National Technical University «Kharkiv Polytechnic Institute»,
2, Kyrpychova Str., Kharkiv, 61002, Ukraine,
phone +380 57 7076010,
e-mail: bezprozvannych@kpi.kharkov.ua
[2] Private Joint Stock Company «Ukraine Scientific-Research Institute of Cable Industry»,
2-P, Promychlennaya Str., Berdyansk, Zaporozhye Region, 71101, Ukraine,
phone +380 66 8288554,
e-mail: garik710@ukr.net

How to cite this article:
Bezprozvannych G.V., Mirchuk I.A. The evaluation of possibility of normal operation of cables based on twisted pairs with PVC jacket under the conditions of high humidity and temperature. *Electrical engineering & electromechanics*, 2017, no.5, pp. 51-54. **doi: 10.20998/2074-272X.2017.5.08.**

UDC 53.082.73 **doi: 10.20998/2074-272X.2017.5.09**

V.G. Zhekul, O.P. Smirnov, E.I. Taftaj, O.V. Khvoshchan, I.S. Shvets

PIEZOELECTRIC WAVEGUIDE SENSOR FOR MEASURING PULSE PRESSURE IN CLOSED LIQUID VOLUMES AT HIGH VOLTAGE ELECTRIC DISCHARGE

Purpose. Investigations of the characteristics of pressure waves presuppose the registration of the total profile of the pressure wave at a given point in space. For these purposes, various types of «pressure to the electrical signal» transmitters (sensors) are used. Most of the common sensors are unsuitable for measuring the pulse pressure in a closed water volume at high hydrostatic pressures, in particular to study the effect of a powerful high-voltage pulse discharge on increasing the inflow of minerals and drinking water in wells. The purpose of the work was to develop antijamming piezoelectric waveguide sensor for measuring pulse pressure at a close distance from a high-voltage discharge channel in a closed volume of a liquid. Methodology. We have applied the calibration method as used as a secondary standard, the theory of electrical circuits. Results. We have selected the design and the circuit solution of the waveguide pressure sensor. We have developed a waveguide pulse-pressure sensor DTX-1 with a measuring loop. This sensor makes it possible to study the spectral characteristics of pressure waves of high-voltage pulse discharge in closed volumes of liquid at a hydrostatic pressure of up to 20 MPa and a temperature of up to 80 °C. The sensor can be used to study pressure waves with a maximum amplitude value of up to 150 MPa and duration of up to 80 μs. According to the results of the calibration, the sensitivity of the developed sensor DTX-1 with a measuring loop is 0.0346 V/MPa. Originality. We have further developed the theory of designing the waveguide piezoelectric pulse pressure sensors for measuring the pulse pressure at a close distance from a high-voltage discharge channel in a closed fluid volume by controlling the attenuation of the amplitude of the pressure signal. Practical value. We have developed, created, calibrated, used in scientific research waveguide pressure pulse sensors DTX-1. We propose sensors DTX-1 for sale in Ukraine and abroad. Sensors DTX-1 can be used to study pressure waves with a maximum amplitude value of up to 150 MPa in closed fluid volumes at a hydrostatic pressure of up to 20 MPa and a temperature of up to 80 °C. References 10, figures 7.

Key words: **piezoelectric sensor, pulse pressure, electrical characteristics, high-voltage discharge, closed volume of liquid.**

На основании проведенного анализа рынка приборов, измеряющих импульсное давление, выбрана конструкция и схемное решение помехоустойчивого волноводного датчика давления, обеспечивающего стабильность и достоверность показаний на близком расстоянии от канала высоковольтного электрического разряда в замкнутом объеме жидкости. Разработан волноводный датчик импульсного давления ДТХ-1 с измерительным шлейфом, позволяющий исследовать спектральные характеристики волн давления в закрытых объемах жидкости при гидростатическом давлении до 20 МПа и температуре до 80 °С. Датчик может быть применен для изучения волн давления с максимальным амплитудным значением до 150 МПа и длительностью до 80 мкс. Согласно результатам тарировки с использованием вторичного эталона, чувствительность датчика ДТХ-1 с измерительным трактом – 0,0346 В/МПа. Библ. 10, рис. 7.

Ключевые слова: **пьезоэлектрический датчик, импульсное давление, электрические характеристики, высоковольтный разряд, замкнутый объем жидкости.**

Introduction. A lot of modern technologies (in particular, electric discharge) use a pressure wave as the determining factor of the impact on the object being processed. The study of the spectral characteristics of such waves is of great interest and is an urgent task for any industrialized country with a developed scientific potential.

Investigations of the characteristics of pressure waves, which are generated, for example, by an electric discharge in a liquid, involve recording the total profile of the pressure wave at a given point in the volume of the liquid. For these purposes, various kinds of pressure sensors to the electric signal have been used for a long time [1-6]. Sensors based on natural (quartz, tourmaline, lithium niobate, etc.), artificially created and specially polarized in the electric field piezomaterials (piezoceramics such as barium titanate, lead titanate, lead zirconate, piezoceramics, etc.) are the most widely used in measuring the pulse pressures.

At the Institute of Impulse Processes and Technologies (IIPT) of the National Academy of Sciences of Ukraine, which is engaged in the development and implementation of various electric discharge technologies, various means of recording pulsed pressures have been used for many years in carrying out research. Among them are piezoelectric pressure sensors by the known in the field of creating measuring acoustic equipment the Danish Company «Brüel & Kjær» [7]. In addition, the IIPT developed and manufactured its own pressure sensors based on various types of piezoceramics [5, 8]. Most of the earlier studies were related to the measurement of pressures in open volumes of liquid at considerable distances from the discharge channel. This circumstance significantly reduced the requirements for the design of the sensor and some of its parameters (the amplitude of the measured pulse pressure, the level of permissible static liquid pressure, etc.).

Within the framework of this work, it was necessary to develop a pressure sensor for measuring the impulse pressure in a closed water volume with increased hydrostatic pressures. One of the applications of such a sensor is to study the effect of a high-voltage pulse discharge on increasing the inflow of minerals and drinking water in wells [9]. A high-pressure discharge chamber was used to calibrate and test the developed sensor (Fig. 1) which allows maintaining high hydrostatic pressure and proximity of the receiving part of the sensor

to the discharge channel (source of hydrodynamic perturbation-pressure waves). The internal diameter of the discharge chamber is 120 mm.

The proximity to the source of the pulsed pressure, the need for galvanic isolation of the sensor piezoelectric element and the circuit of the electrical circuit through which a pulsed current reaches tens of kA, the presence of a rigid reflecting wall of the chamber on which the sensor is to be mounted increases the level of its requirements, making it impossible to use most available pressure sensors, including, hydrophones of the company «Brüel & Kjær».

The conducted marketing researches made it possible to draw a conclusion on the principle possibility of using two pulse pressure sensors in such conditions: DPX 101-5K by OMEGA Company (USA) with a sensitivity of 0.1552 V/MPa, permissible pulse pressure amplitude up to 100 MPa and PS-02 by the GlobalTest Ltd (Russia) with sensitivity of 0.0735 V/MPa, permissible amplitude of impulse pressure up to 250 MPa.

Fig. 1. High-pressure discharge chamber

During the tests of the acquired sensors, carried out by low-power electric discharges in the high-pressure discharge chamber, their significant sensitivity to the «current interference» arising due to electromagnetic interference from the high-voltage circuit was detected. Such a term for this interference is introduced due to its time and phase correlation with the oscillogram of the current flowing in the discharge circuit.

All attempts to reduce the level of interference due to additional measures (bringing of discharge and measurement circuits to one ground point, use of double screens in measurement paths, high-frequency filtering on ferrite rings) did not have a positive effect.

Oscillograms with «current guidance» are shown in Fig. 2. Due to the low sensitivity of the quartz sensors of these sensors, the amplitude of the useful signal was measured in units of volts. The amplitude of the «current guide» actually read on the oscillograms was in the range of units of volts, and was commensurable or even exceeded the useful signal from the pulse pressure sensor. This led to the conclusion that these sensors of standard design can not be used in the conditions of strong electromagnetic fields that accompany the discharge.

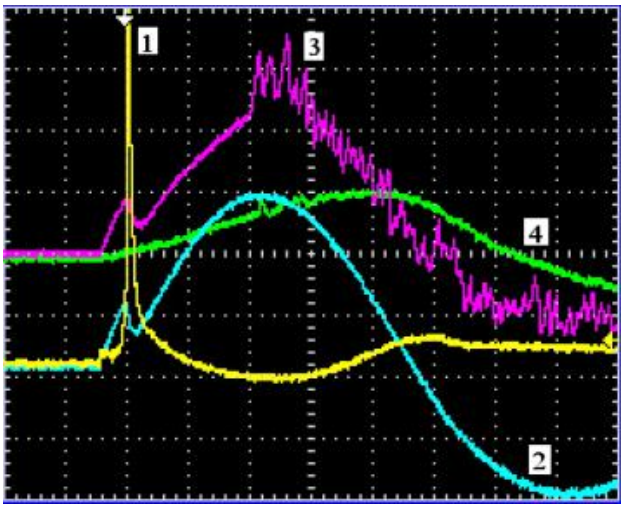

Fig. 2. The oscillogram of the pressure pulse and electrical characteristics with an electrical discharge initiated by a thin conductor: 1 – voltage across the discharge gap; 2 – current in the discharge channel; 3 – pressure wave generated by an electrical discharge in a liquid measured with a sensor pressure DPX 101-5k; 4 – pressure wave generated by an electric discharge in a liquid, measured with the help of a pressure sensor PS-02

Proceeding from the foregoing, there is a need to develop a pressure sensor that ensures the reliability of the obtained measurement results and reliability of operation in conditions of high electromagnetic fields.

The goal of the work is the development of an interference-resistant piezoelectric waveguide sensor for measuring pulsed pressure at a close distance from a high-voltage discharge channel in a closed fluid volume.

Results of sensor design. When designing a pressure sensor that meets the above requirements, a waveguide pressure sensor ВДД [5], developed earlier in the IIPT, was used as a prototype.

A distinctive feature of the developed pressure sensor should be high sensitivity, due to which the sensor generates useful signal amplitude from tens to hundreds of volts. However, a signal of this amplitude is dangerous both for the recording oscilloscope and for the transducer element of the sensor.

To reduce the level of the measuring signal, a measuring path was developed, the electrical circuit of which is shown in Fig. 3.

When a pressure wave P hits the sensor, an electric charge Q_1 is induced on its piezoceramic element with electrical capacitance C_1, and the potential difference U_1 on its plates is determined by the relation

$$U_1 = Q_1/C_1. \quad (1)$$

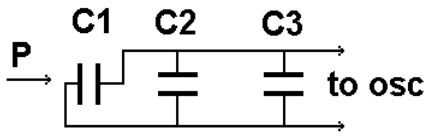

Fig. 3. Electrical circuit of the measuring path: C1 – electrical capacitance of the measuring element (piezoceramics) of the pressure sensor; C2 – electrical capacitance of the measuring coaxial cable; C3 – electrical capacitance of the additional condenser; P – wave pressure generated by an electric discharge in the liquid; to osc – to the oscilloscope

In the case of a capacitor with C_2 capacitance and an additional capacitor of capacitance C_3 connected to the sensor plates, the same electric charge Q_2 will provide a potential difference at the output of the U_{osc} circuit, determined by the ratio

$$U_{osc} = Q_1/(C_1+C_2+C_3). \quad (2)$$

The coefficient k expressing the degree of attenuation of the useful signal and interference from the sensor is defined as the ratio

$$k = U_1/U_{osc} = (C_1+C_2+C_3)/C_1. \quad (3)$$

The analysis showed that the use of the ЦТС -19 piezoceramic sensor as a transducer element makes it possible to provide acceptable values of U_{osc} in the pulse pressure measurement range up to 150 MPa at a value of $k = 450$.

The carried out complex of investigations made it possible to propose the design of a waveguide pressure sensor DTX-1 [10] shown in Fig. 4.

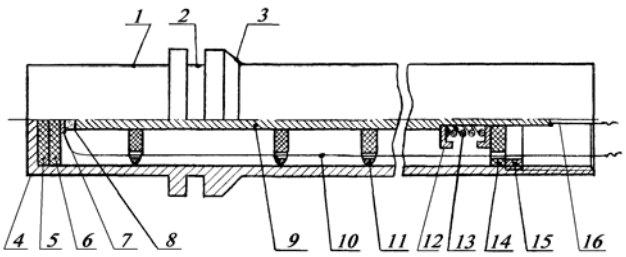

Fig. 4. Waveguide pressure sensor ДТХ-1 design

The piezoelectric waveguide pulse pressure sensor ДТХ-1 consists of a metal casing 1, on which there is a groove 2 under the sealing ring, a stop surface 3, a receiving bottom-membrane 4, gaskets from the vibration damping material 5, gaskets made of dielectric material with high electrical strength 6, 7, a piezoelectric element 8, a copper waveguide 9, conductors 10, 16, rubber shock absorbers 11, washers 12, springs 13, an insulating washer 14, nuts 15.

The pulse pressure sensor operates as follows.

With the help of additional fastening elements, the sensor is placed in a special opening of the process chamber coaxially with the direction of passage of the pressure wave under study. The metal housing 1 of the sensor makes contact with the chamber by mechanically applying the fastening elements to the abutment surface 3, and the sealing rubber ring in the groove 2 allows measurement in a chamber filled with liquid both at atmospheric and increased hydrostatic pressure.

The release of energy in the liquid during certain technological operations (for example, in discharge-pulse technologies) leads to the appearance of hydrodynamic perturbation and propagation of pressure waves. The pressure wave alternately passes through the liquid layer in the process chamber, the receiving bottom-membrane 4 of the sensor, the gasket from the vibration damping material 5, the gasket from the dielectric material with high electrical strength 6, the current collector 7, the piezoelectric cell 8, the copper waveguide 9.

The choice of the thickness and type of the gasket material from the vibration damping material 5 makes it possible to weaken the amplitude of the pressure wave and increase the upper limit of the pressure sensor measurement. The presence of a gasket made of a dielectric material with a high electrical strength 6 avoids an electrical contact between the housing 1 and the receiving membrane-side 4 and the piezoelectric element 8.

When a pressure wave is applied to the piezoelectric element 8, a potential difference appears at its ends due to the phenomenon of the piezoelectric effect. Voltage with the help of soldered to a piezoelectric element 8 of a copper waveguide 9, a current collector 7 and conductors 10, 16 is fed to the measuring path. The length of the copper waveguide 9 is chosen from the condition that there are no effects on the piezoelectric element of 8 pressure waves reflected from its end, which allows us to investigate pressure waves with duration of up to 80 μs.

The alignment of the waveguide 9 in the cylindrical body 1 is carried out by rubber shock absorbers 11. The density of the abutment of the receiving base-membrane 4, the gaskets 5 and 6, the current collector 7 ensures the mechanical action of the spring 13 by means of a washer 12, an insulating washer 14 and nuts 15.

As a material of insulating gaskets used paronite ПМБ (State Standard 481-80) and polyethylene terephthalate ПЭТ-Э (State Standard 24234-80) was used, as a piezoelement material – ЦТС-19 (State Standard 13927-74).

The external view of the waveguide pressure sensor ДТХ-1 is shown in Fig. 5.

Fig. 5. The external view of the waveguide pressure sensor ДТХ-1

The waveguide pressure sensor ДТХ-1 has a significantly higher sensitivity (about two orders of magnitude) compared to the DPX 101-5K and PS-02 pressure sensors, due to this the level of the useful signal is more than an order of magnitude higher than the current-induced level. For example, in Fig. 6 shows the oscillogram of the current, voltage and signal from the

sensor ДТХ-1 in the electric explosion of a copper conductor with a diameter of 0.14 mm in water.

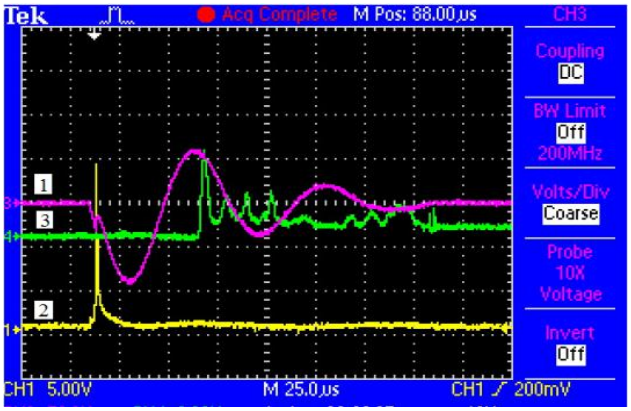

Fig. 6. Oscillogram of the pressure pulse and electrical characteristics during electrical explosion of a copper conductor (conductor diameter – 0.14 mm, length – 0.038 m; charging voltage – 10 kV; stored energy – 1 kJ; hydrostatic pressure – 20 MPa): 1 – current in the discharge channel (inverted); 2 – voltage across the discharge gap; 3 – signal from the sensor ДТХ-1

Calibration of the waveguide pressure sensor. The calibration of the ДТХ-1 sensor was performed by comparing the calibration (reference) pressure pulses with the signals obtained with the ДТХ-1 sensor. Based on the results of the comparison, the sensitivity factor of the sensors was calculated.

As pressure calibration pulses, the data obtained with the help of a secondary reference (pressure sensor DPX 101-5K) were used with the following installation parameters: charging voltage of the capacitor bank – 15 kV; capacitance of the capacitor bank – 2.26 uF; the inductance of the circuit is 4.29 μH. With these loop parameters, it was possible to separate in time the «current jamming» and the useful signal of the DPX 101-5K sensor.

The initiation of the discharge was carried out with a copper conductor of 0.14 mm in diameter and 50 mm in length, which increased the stability of the amplitude of the pressure wave. The hydrostatic pressure in the chamber was maintained at 10 MPa. The pressure sensor ДТХ-1 fixed pulses from five digits. The obtained results were subjected to statistical processing, the average value was found, according to which the sensitivity of the calibrated sensor was determined.

ДТХ-1 calibration was performed in conjunction with the measuring path (see Fig. 3), which has the following parameters:

• electrical capacitance of the manufactured pressure sensor ДТХ-1 C1 – 150 pF;

• electrical capacitance of measuring cable РК 50-2-16 S2 with length of 10 m – 1166 pF;

• electrical capacitance of the load capacitor C3 – 66340 pF.

Thus, the calibration of the sensor with the path consisted in determining its sensitivity when subjected to a pressure pulse of known amplitude (obtained on a certified sensor).

Fig. 7 shows the combined time profiles of the reference pulse (1) and the pulse profile recorded by the waveguide sensor ДТХ-1 (2). For convenience of comparison of the oscillograms, the amplitudes of both signals are reduced to one value. The above results (see Fig. 7) showed that the coincidence of the signals, both along the rising edge of the pressure pulse, and in the duration of its decrease is satisfactory.

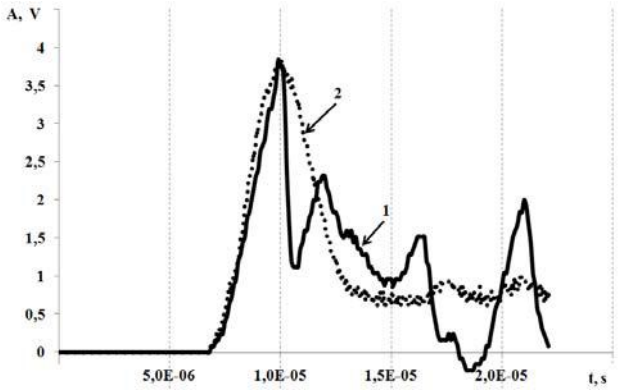

Fig. 7. Pulse wave pressure profiles:
1 – reference pressure pulse;
2 – pulse of the waveguide pressure sensor ДТХ-1

According to the calibration results, the sensitivity of the developed sensor ДТХ-1 with the measuring path is 0.0346 V/MPa.

The conducted laboratory tests showed the stability of the sensitivity of the sensor when measuring pressure waves with amplitude of up to 150 MPa and long-term operation in the range of hydrostatic pressures (0.1-20 MPa), temperatures (10-80) °C.

The developed pressure sensors ДТХ-1 were used to record the impulse pressures when performing a number of scientific research works at the IIPT of the National Academy of Sciences of Ukraine, a prototype was delivered to the research center in France.

Conclusions.

1. A design and circuit solution of an interference-resistant waveguide pressure sensor for electrical discharge technologies providing stability and reliability of indications at a close distance from a high-voltage discharge channel in a closed fluid volume are proposed.

2. A waveguide pulse pressure sensor ДТХ-1 with a measuring loop has been developed which makes it possible to investigate the spectral characteristics of pressure waves in a high-voltage electric discharge in closed fluid volumes at a hydrostatic pressure of up to 20 MPa and a temperature up to 80 °C.

3. According to the calibration results, the sensitivity of the developed sensor ДТХ-1 with the measuring path is 0.0346 V/MPa.

REFERENCES

1. Sharapov V.M., Polishchuk E.S., Koshevoi N.D. *Datchiki: spravochnoe posobie* [Sensors: a reference book]. Moscow, Tekhnosfera Publ., 2012. 624 p. (Rus).

2. Fomin N.A. Diagnostics of Rapidly Proceeding Processes in Fluid and Plasma Mechanics. *Journal of Engineering Physics and Thermophysics*, 2008, vol.81, no.1, pp. 68-81. **doi: 10.1007/s10891-008-0010-y.**

3. Panich A.E. *P'ezoelektricheskoe priborostroenie: sbornik v 3 tomakh* [Piezoelectric instrument making: a collection in 3 volumes]. Rostov-na-Donu, SKNTs VSh Publ., 2006. (Rus).
4. Shamrakov A.L. Prospects for the development of piezoelectric sensors for fast-changing, pulsed and acoustic pressures. *Sensors and systems*, 2005, no.9, pp. 4-8. (Rus).
5. Beskaravainyi N.M., Pozdeev V.V. *Teoreticheskie osnovy izmereniia impul'snykh davlenii v zhidkikh sredakh* [Theoretical basis for measuring pulsed pressures in liquid media]. Kiev, Naukova Dumka Publ., 1981. 190 p. (Rus).
6. Elkarous L., Robbe C., Pirlot M., Golinval J.-C. Dynamic calibration of piezoelectric transducers for ballistic high-pressure measurement. *International Journal of Metrology and Quality Engineering*, 2016, vol.7, no.2, p. 201. **doi: 10.1051/ijmqe/2016004.**
7. Available at: https://www.bksv.com/en (accessed 22 July 2016).
8. Poklonov S.G., Zhekul V.G., Smirnov A.P. Technique and results of experimental investigations of the influence of the elastic barrier on pressure wave parameters in electric discharge in water. *Surface Engineering and Applied Electrochemistry*, 2007, vol.43, no. 5, pp. 350-353. **doi: 10.3103/S1068375507050079.**
9. Shvets I., Zhekul V., Poklonov S., Smirnov O., Mel'kher Ju., Litvinov V., Konotop S., Khvoshchan O., Zaloga Je. Electro-discharge method of restoration of productivity of artesian well. *Ukrainian Black Sea region agrarian science*, 2013, no.3, pp. 200-205. (Ukr).
10. Taftaj E.I., Zhekul V.G., Smirnov O.P., Khvoshchan O.V., Shvets I.S. *P`jezoelektrychnyj hvylevidnyj datchyk impul'snogo tysku* [Piezoelectric waveguide impulse pressure sensor] Patent UA, no. u 2016 11774, 2017. (Ukr).

Received 03.08.2017

V.G. Zhekul[1]*, Candidate of Technical Science, Senior Research Scientist,*
O.P. Smirnov[1]*, Candidate of Technical Science, Senior Research Scientist,*
E.I. Taftaj[1]*, Research Scientist,*
O.V. Khvoshchan[1]*, Candidate of Technical Science,*
I.S. Shvets[1]*, Candidate of Physics and Mathematics Sciences,*
[1] Institute of Pulse Processes and Technologies (IPPT) of NAS of Ukraine,
43-A, Bohoyavlensky Ave., Mykolayiv, 54018, Ukraine,
phone +380 512 224113,
e-mail: Smirnovap1978@gmail.com, Khvoshchan@gmail.com

How to cite this article:
Zhekul V.G., Smirnov O.P., Taftaj E.I., Khvoshchan O.V., Shvets I.S. Piezoelectric waveguide sensor for measuring pulse pressure in closed liquid volumes at high voltage electric discharge. *Electrical engineering & electromechanics*, 2017, no.5, pp. 55-59. **doi: 10.20998/2074-272X.2017.5.09.**

UDC 621.3.013:621.311 **doi: 10.20998/2074-272X.2017.5.10**

V.Yu. Rozov, D.Ye. Pelevin, K.D. Pielievina

EXTERNAL MAGNETIC FIELD OF URBAN TRANSFORMER SUBSTATIONS AND METHODS OF ITS NORMALIZATION

Purpose. Research of external magnetic field of urban transformer substations and the methods it reduction to the standard level in the living quarters of nearby. Methodology. Experiment based on the actual values the measuring magnetic flux density of the alternating magnetic field. Theories of electromagnetic field on quasi-static formulation is basis of external magnetic field of urban transformer substations description. Results. We have made comprehensive experimental researches the magnetic field of a 50 Hz through model urban transformer substations on the external environment. For calculating the external magnetic field of transformer substations the mathematical model of multi-dipole is proposed. It practical uses for induction external magnetic field of calculating created in nearby built in house transformer substations power 715 kVA is proposed. Comparison of results calculation and experiment was conducted. Originality. We have established that magnetic flux density of the magnetic field does not exceed standard level in the living quarters of nearby (0.5 μT) if quarters the location distances of more than 8 m from the transformer substation on the first time. Transformer substations in the built-in houses can create the dangerous to public health magnetic field which induction 1.5-7 μT in neighboring living quarters. It exceeds the normative level in 3-14 times. Practical value. We have proposed normalization methods of the external magnetic field built-in transformer substations. Methods are based on improving construction transformer substations. And methods of external passive and active shielding are considered. References 22, figures 9.

Key words: **transformation substation, external magnetic field, living spaces, multi-dipole model, methods of normalization.**

Целью работы является исследование внешнего магнитного поля городских трансформаторных подстанций (ТП) и методов его уменьшения в близлежащих жилых помещениях до нормативного уровня. Выполнены комплексные экспериментальные исследования магнитного поля частотой 50 Гц, создаваемого типовыми городскими ТП во внешней среде. Показано, что индукция магнитного поля в близлежащих жилых помещениях не превышает нормативного уровня (0,5 мкТл), если помещения расположены на расстояниях более 8 м от корпуса ТП. Предложена мультидипольная математическая модель для расчета внешнего магнитного поля ТП и приведен пример ее практического использования для расчета индукции внешнего магнитного поля, создаваемого в близлежащем жилом помещении ТП мощностью 715 кВА, встроенной в жилой дом. Приведено сравнение результатов расчета и эксперимента. Показано, что встроенные в жилые дома ТП могут создавать в соседних жилых помещениях опасное для здоровья населения магнитное поле с индукцией 1,5-7 мкТл, что в 3-14 раз превышает его нормативный уровень. Предложены методы нормализации внешнего магнитного поля встроенных ТП, основанные на совершенствовании конструкции ТП, а также методах внешнего пассивного и активного экранирования (компенсации). Библ. 22, рис. 9.

Ключевые слова: **трансформаторная подстанция, внешнее магнитное поле, жилые помещения, мультидипольная модель, методы нормализации.**

Introduction. The magnetic field (MF) of the industrial frequency of 50 Hz is the most dangerous for people's health even with its weak but long-lasting effect [1]. The main sources that create such MF inside residential premises are power facilities located in residential areas – air and cable transmission lines (TL), as well as urban transformer substations (TS).

The maximum permissible level (MPL) of magnetic flux density of MF 50 Hz for the population created by electrical installations is regulated in [2] and is 10 μT in the residential area and 0.5 μT within the residential premises.

The most acute problem of the normalization of the external magnetic field (EMF) of the TS is in residential buildings with integrated TS [2, 6], when the distance between the TS and living quarters is reduced to several meters. Such houses (Fig. 1) are quite widespread in Ukraine and other countries. In addition, built-in TS began to be widely used in the world to supply sections of 10-20 floors in modern high-rise residential buildings [7] in order to reduce power losses. The problem of normalizing their MF also needs to be solved.

At present, the MF of the TLs have been most thoroughly studied and the methods of its reduction to a safe level for the population have been determined [3-5]. At the same time, the study of the EMF of the TS was not given due attention, although in some cases – when the TS approached the living quarters, their MF may exceed the MPL.

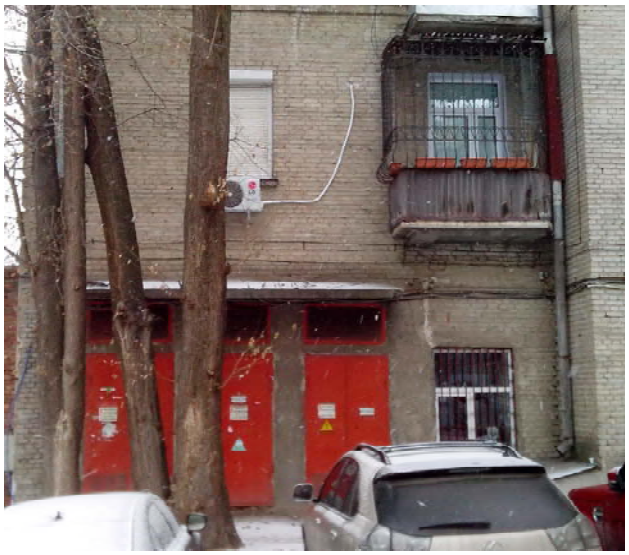

Fig. 1. A typical residential building with built-in TS (Kharkiv, Danilevsky Str., 19)

Thus, the EMF of the TS is currently not sufficiently investigated, which makes it difficult to solve the actual and socially significant problem of the normalization of the MF at frequency of 50 Hz in the premises of apartment houses located near the TS.

The goal of the work is investigation of the EMF of urban TS and methods for reducing it to the normative level in nearby residential premises.

TS as a source of the MF. Urban TSs provide electricity for residential buildings. They perform the functions of converting three-phase high voltage of 6 (10) kV into voltage of 0.38 kV and distributing electric energy of 380 V (220 V) to end users [2, 6]. Typical urban TS (Fig. 2) have power from 100 kVA to 1400 kVA and are equipped with one or two lowering three-phase transformers with grounded neutral. TS contain partitioned switchgears (SG) from current conductors (buses, cables) with the necessary switching, protective and measuring equipment.

a

b

Fig. 2. Design of urban TS (*a*) and its SG (*b*)

The main sources of the EMF of the TS are three-phase current conductors of the SG, each of which, with a symmetrical load of different phases, generally forms three current circuits [5, 8, 9], creating the MF.

Three-phase transformers of the SG have a symmetrical design theoretically excluding the creation of the EMF [8]. In practice, they create the EMF caused by technological deviations from symmetry [8, 10]. The magnetic flux density of this MF is insignificant and does not exceed 10 % of the total EMF of the TS. The EMF of the transformer has a dipole character [9], rapidly decays when removed from the TS (Fig. 3) and is not taken into account in further analysis.

The other elements of the SG, including switchgear, protective and measuring equipment of the TS, as well as input and output twisted three-phase cables, also practically do not affect the EMF of the TS [9].

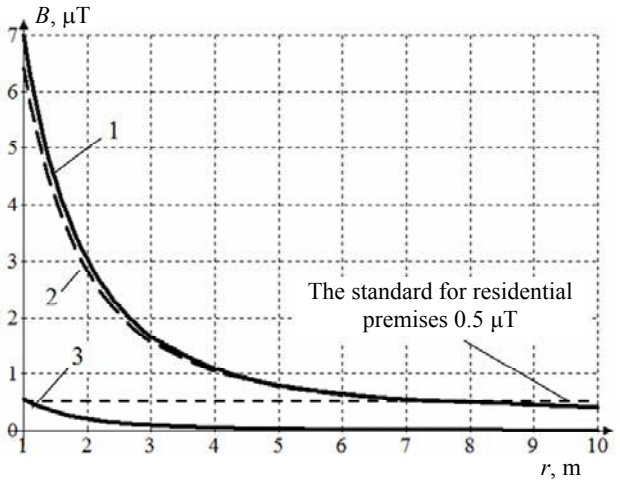

Fig. 3. Characteristic decrease in magnetic flux density of the MF of the TS of type K-42-630 at removal from distance *r* from its housing (1 – total MF of the TS, 2 – MF of current conductors, 3 – MF of the transformer)

Thus, the EMF of the TS is determined by the MF of three-phase current conductors of the TS which can be represented in accordance with Fig. 4.

Experimental investigations of the EMF of the TS. Experimental investigations of the EMF of the TS have been performed for 42 TS of city of Kharkiv with nominal power (S_{nom}) from 100 to 1260 kVA. 36 TS located in separate buildings (inside microdistricts) and 6 TS built into residential buildings were investigated.

The research is based on direct measurements of the effective value of the magnetic flux density of alternating MF in a limited number of points using a Magnetoscop 1.069 magnetometer by Foerster Company (magnetic flux density measurement range 0-600 μT, relative error 2.5 %) and EMF-828 (magnetic flux density measurement range 0-2000 μT, relative error 4 %).

The magnetic flux density of the MF at the *i*-th point of the measurement was determined from the measurements of the magnetic flux density of the MF in the three orthogonal positions of the magnetometer sensor using formula

$$B_i = \sqrt{B_{xi}^2 + B_{yi}^2 + B_{zi}^2}\,, \qquad (1)$$

where B_{xi}, B_{yi}, B_{zi} are the measured effective values of the spatial components of the magnetic flux density of the MF at the *i*-th measurement point along the axes of the magnetometer sensors *X*, *Y*, *Z*.

The beginning of the coordinate grid was combined with the surface of the TS housing. MF measurements were carried out at the distance from the TS in the

horizontal (vertical) direction corresponding to the maximum values of the MF with the fixation of the actual currents in the current conductors of the TS. The resulting magnetic flux density value of the MF of the TS was reduced to the rated power of the TS.

In the residential zone, the measurement points were located on lines perpendicular to the walls of the building, in increments of 1 m height of 1 m. When measuring MF in nearby residential premises, the measurement points were located in the nodes of a spatial grid parallel to the walls of the premises. The basic grid of measurements had a step of 0.5 m and was located in a horizontal plane, at an altitude of 0.5 m from the floor of the room.

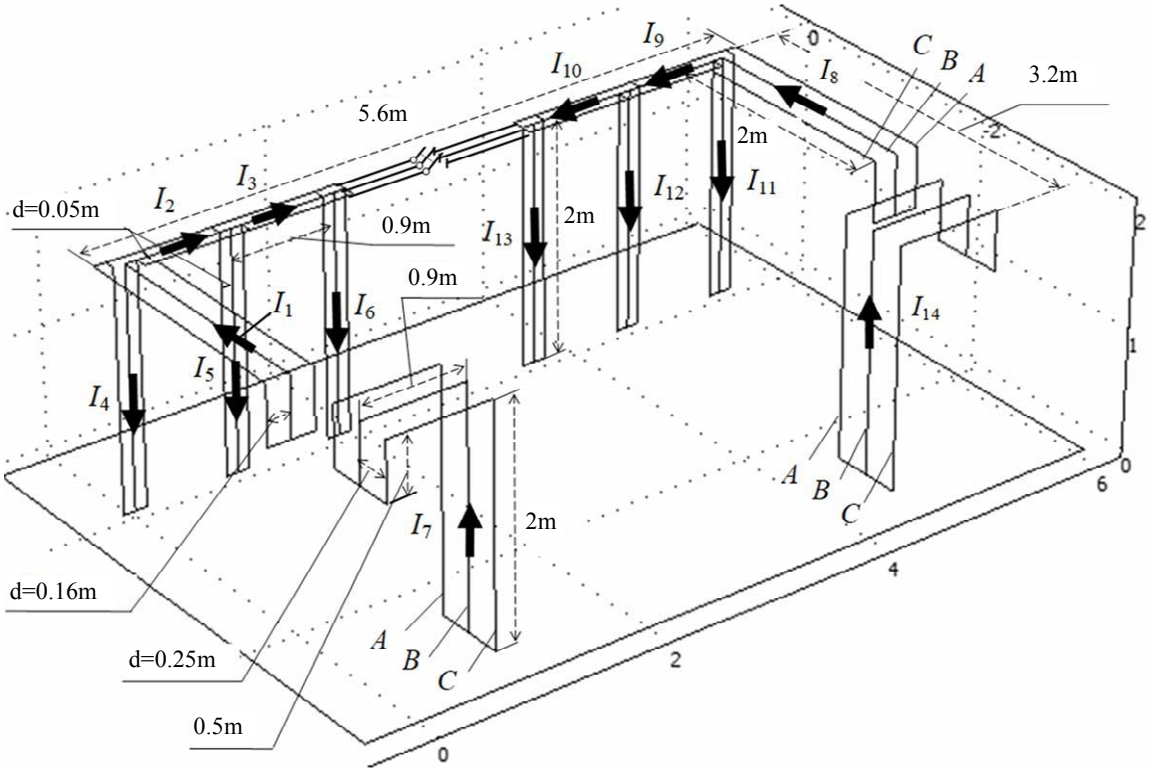

Fig. 4. Configuration of the current conductors of the considered two-transformer TS of power of 715 кVA

The generalized results of measurements of the magnetic flux density of the MF of the TS of different power are shown in Fig. 5 where the value of the magnetic flux density near the external wall of the room of the TS corresponds to r = 2 m, the distance between which and the housing of freestanding TS is 2 m.

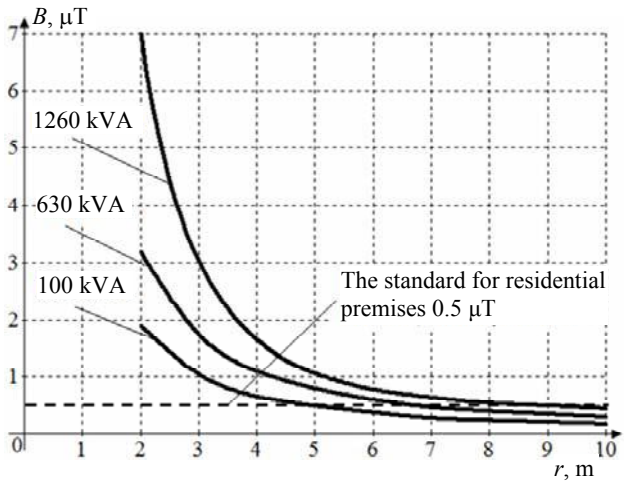

Fig. 5. Experimental values of the magnetic flux density of the EMF of stand-alone TS of various power reduced to their nominal load when removing the measuring point from their housing (r is the distance of the TS housing to the point of observation)

An analysis of the results of experimental investigations shows the following. The magnetic flux density of the EMF of the TS falls to the MPL (0.5 μT) at the distance of 8 m from the TS of maximum power (1260 kVA). At the minimum power of the TS (100 kVA), its EMF drops to the MPL at the distance of 5 m.

Since all stand-alone TS are located more than 15 m from residential buildings, they do not represent the dangers for its residents.

The maximum magnetic flux density of the EMF of the TS under consideration (Fig. 5) occurs near the outer walls of their premises and is 7 μT which does not exceed the MPL for the residential development area (10 μT) in accordance with [2].

Therefore, urban TS do not pose a public health hazard when they are located at the distance of more than 8 m from residential buildings. However, this condition is violated for in-built TS when the distance between the TS housing and living quarters is reduced to several meters.

Thus, Fig. 6 shows the magnetic flux density distribution of the MF built from the results of measurements in a residential building located on the first floor of the house (Fig. 1) above the built-in two-transformer TS with power of 715 kVA. The distance

from the TShousing to the floor of a residential building on the first floor is 1.85 m. The actual load of the TS during the measurements was 45 % of the nominal ($0.45 \cdot S_{nom}$).

The results of the measurements are shown in Fig. 6. Their analysis shows that the maximum level of the magnetic flux density of the MF in a residential building above the built-in TS even at the reduced load of the TS ($0.45 \cdot S_{nom}$) is 1.6 μT which is more than 3 times than the MPL. With larger installed power of the TS operating at the rated load mode, the magnetic flux density value of the MF in accordance with Fig. 5 can reach 7 μT.

Thus, the built-in TS can create in the adjacent residential premises the MF with magnetic flux density in 3-14 times exceeding the MPL which poses a danger to public health and requires taking measures to normalize their EMF.

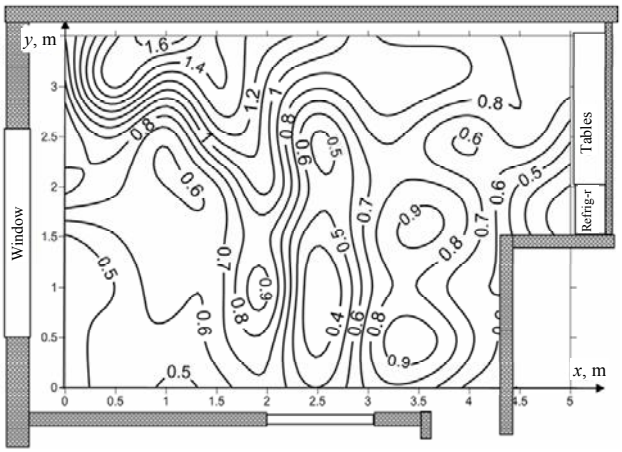

Fig. 6. Experimental values of the magnetic flux density distribution of the MF (μT) at an altitude of 0.5 m from the floor of the living space located above the built-in TS of power of S_{nom} = 715 kVA at the actual load $0.45 \cdot S_{nom}$

Modeling of the EMF of the TS. The analysis shows that the EMF of the TS is normalized in the outer region of space – at points remote by the distance R_o from the TS housing. This distance is at least 2 m and considerably exceeds the distance d between the axes of the phase conductors of the TS (0.05-0.5 m) [6] that creates the conditions for the application of the multi-dipole mathematical model in the calculation of the EMF of the TS [8, 11, 12]. This model, with a large number of current conductors with a complex configuration, which is characteristic for TS, allows us to simplify the calculation of the EMP of the TS with the limited methodological error (less than 10 %) in comparison with the Biot-Savart method and numerical methods [3, 8]. In addition, the multi-dipole model has a clear physical interpretation, which makes it easier to synthesize the means of reducing the MF based on it [3].

In order to build a multi-dipole model of the EMF of the TS, the approach realized in [3] can be used when each linear circuit with current I of the TS (Fig. 4) with the length L and the width d is arbitrarily divided into N elementary microcontours with areas $S_i = a_i \cdot d$ characterized by dipole magnetic moments $\dot{\vec{m}}_i$ (Fig. 7). In this case, it is necessary to satisfy the following conditions [3, 8]:

$$R_0 > 2d \; ; \; R_0 > 2a \; ; \; a = \frac{L}{N} < 0{,}5R_0 \, . \qquad (2)$$

In this case, the magnetic flux density of the MF $\dot{\vec{H}}_k(P)$ produced by a single rectilinear single-phase current loop (Fig. 7) at the observation point P can be determined by the expressions [3, 8]

$$\dot{\vec{H}}_k(P) = -\sum_{i=1}^{N} \nabla \left[\frac{\left(\dot{\vec{m}}_i, \vec{R}_i \right)}{4\pi R_i^3} \right]; \qquad (3)$$

$$\dot{\vec{m}}_i = \dot{I} \cdot \vec{S}_i = \dot{I} \cdot e^{-j\varphi} \cdot a_i \cdot d \cdot \vec{n} \, , \qquad (4)$$

where N is the number of microcontours in a rectangular contour of the TS; $\vec{S}_i$ is the vector of the square of the i-th microcontour; $\vec{n}_i$ is the unit vector normal to S_i; $\vec{R}_i$ is the radius-vector from the geometrical center of the i-th microcontour to the observation point P; φ is the phase of the current $\dot{I}$.

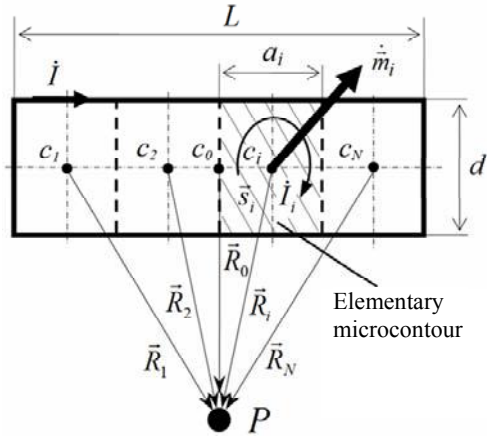

Fig. 7. Multidipole representation of the elementary contour with alternating current $\dot{I}$ as a source of the MF

Then the magnetic flux density $\dot{\vec{B}}_{TS}$ of the EMF of the TS (Fig. 4), containing K three-phase rectilinear TS contours, can be defined as

$$\dot{\vec{B}}_{TS}(P) = -\sum_{l=1}^{K} \sum_{\alpha=1}^{3} \sum_{i=1}^{N} \nabla \left[\frac{\mu_0 \left(\dot{\vec{m}}_{l\alpha i}, \vec{R}_{l\alpha i} \right)}{4\pi R_{l\alpha i}^3} \right], \qquad (5)$$

where α is the TS current conductor phase number (α = 1…,3); l is the TS contour number (l = 1, …, K); μ_0 is the magnetic constant.

We use the proposed multi-dipole model (5) to calculate the magnetic flux density of the EMP of the built-in TS. The calculation will be carried out for a real urban 2-transformer TS with power of 715 kVA built into the residential house (Fig. 1). In the calculation, we assume that the currents in the phases of all the TS circuits are sinusoidal, shifted by 120 el. degrees and form a symmetrical system. Current conductors of the TS are current threads. The external environment does not

contain sources of the MF. The effect on the EMP of the metal parts of the TS housing and the walls of the apartment house in accordance with [9, 13] is neglected.

The calculation scheme of the TS corresponds to Fig. 4 and contains 18 rectilinear three-phase current contours (K = 18) with shown in Fig. 4 dimensions and actual currents, determined experimentally under TS load $0.45 \cdot S_{nom}$: I_1 = 312 A; I_2 = 208 A; I_3 = 108 A; I_4 = 104 A; I_5 = 100 A; I_6 = 108 A; I_7 = 21 A; I_8 = 174 A; I_9 = 114 A; I_{10} = 62 A; I_{11} = 60 A; I_{12} = 52 A; I_{13} = 62 A; I_{14} = 12 A.

The results of calculating the flux density of the MF in a horizontal plane located at an altitude of 2.35 m above the TS were performed in accordance with (5) and are shown in Fig. 8.

Comparison of the calculation results (Fig. 8) with the results of the experiment (Fig. 6) shows that the maximum calculated magnetic flux density value of MF (1.7 μT) with an error of less than 10 % coincides with the experimental results (1.6 μT). This confirms the correctness of the proposed methodology for calculating the magnetic flux density of the EMF of the TS and the assumptions made above.

Methods of normalization of the EMF of the TS. As follows from the above analysis, the normalization of the EMF is required for TS built in residential houses, when the distance between the TS housing and the residential space is less than 8 m. The main methods of normalizing the EMF of the TS are shown in Fig. 9.

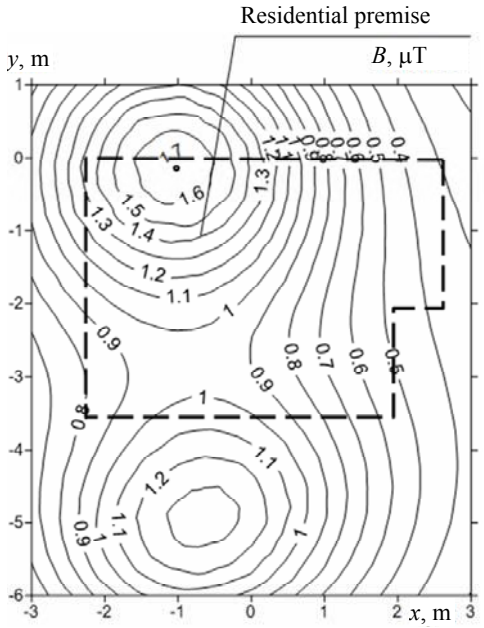

Fig. 8. Calculated values of the magnetic flux density distribution of the MF (μT) at an altitude of 0.5 m from the floor of the living space (Fig. 1) located above the built-in TS of power of S_{nom} = 715 kVA at the actual load $0.45 \cdot S_{nom}$

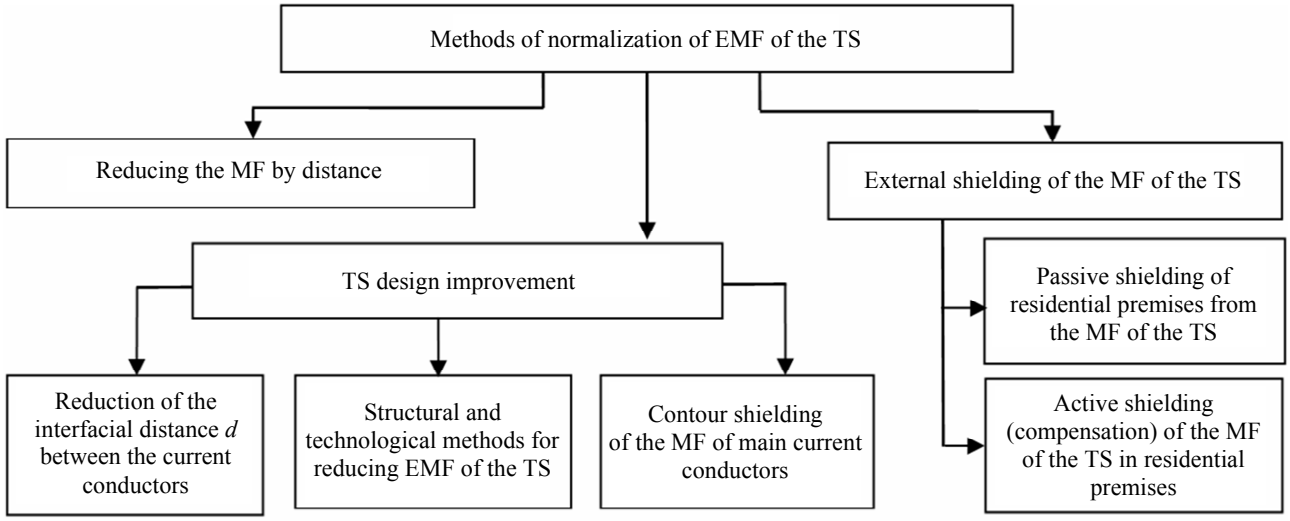

Fig. 9. Classification of methods of normalization of EMF created by the TS in nearby residential premises

The EMF of the TS falls off intensely as a function of the distance (Fig. 5) which allows to significantly reduce the MF when removing the TS from residential premises. However, the implementation of this method is possible only in the presence of free space which limits its use.

A significant decrease in the EMF of the TS is possible due to its special design of the TS. Thus, the constructive and technological methods proposed in [8, 9] (symmetrization, transposition, splitting of current conductors, local active and passive shielding of the MF) allow to reduce the EMF of the TS by an order of magnitude or more. A promising method of reducing the EMF of the TS is the contour shielding of its current leads in accordance with [5, 9]. However, the change in the design of existing TS is technically difficult and has legal limitations, and the industrial release of TS in a special design requires significant investment.

Therefore, methods of external shielding of the MF of the TS are more preferable for practical implementation. Passive shielding is carried out with the help of electrically conductive (ferromagnetic) materials placed on walls and ceilings located near the TS of residential premises [14, 15]. This method is universal but

at a low frequency of 50 Hz its implementation requires substantial material means.

Of great interest from the point of view of the cost of realization for high efficiency are the methods of active shielding of the MF [4, 8, 9, 16-22]. However, they require their development in relation to the MF which is the subject of further research.

Conclusions.

1. Complex experimental investigations of the distribution of the flux density of the external magnetic field with frequency of 50 Hz, created by 42 typical urban transformer substations (TS) with installed power from 100 kVA to 1260 kVA are performed for the first time. It is shown that the flux density of the magnetic field in nearby residential premises does not exceed the regulatory level (0.5 μT), provided that the TS is removed from residential premises over the distance of more than 8 m.

2. A multi-dipole mathematical model for calculating the external magnetic field of the TS is proposed and experimentally justified making it possible to simplify the calculation with a limited error (10 %) and having a clear physical interpretation. The model is built on the basis of dipole sources of the magnetic field, characterized by the magnetic moments of independent elementary microcontours $d \times a_i$ into which all the linear sections of three-phase current conductors of the TS with interphase distance d are arbitrarily divided. The magnetic field at the observation point distant by more than $2d$ $(2\,a_i)$ is defined as the superposition of the magnetic field created by the magnetic moments of the elementary microcontours of all the linear sections of the TS current conductors.

3. It is theoretically substantiated and experimentally confirmed that the greatest danger to public health is TP built into homes that can create in a neighboring residential area a magnetic field with the flux density of 1.5-7 μT, which is 3-14 times higher than the normative level.

4. The methods of normalizing the external magnetic field of the TS in residential premises are considered based on the improvement of the TS design, the use of external shielding (compensation) of the TS magnetic field, and the prospects for the development of methods for external active shielding of the magnetic field are substantiated.

REFERENCES

1. Serdiuk A.M., Dumanskiy V.Yu., Bitkin S.V., Didyk N.V., Dumanskiy Yu.D. Hygienical ground of requirements to placing and exploitation of cable busses of electricity transmission and their equipment in the conditions of modern municipal building. *Hygiene of populated places*, 2015, no.66, pp. 20-29. (Ukr).

2. *Pravyla ulashtuvannja elektroustanovok 5-te vyd., pererobl. j dopovn. (stanom na 22.08.2014)* [Electrical Installation Regulations. 5 edition, Revised and enlarged]. Kharkiv, Fort Publ., 2014. 800 p. (Ukr).

3. Rozov V.Yu., Reutskyi S.Yu., Pelevin D.Ye., Pyliugina O.Yu. The magnetic field of power transmission lines and the methods of its mitigation to a safe level. *Tekhnichna elektrodynamika*, 2013, no.2, pp. 3-9. (Rus).

4. Kuznetsov B.I., Nikitina T.B., Voloshko A.V., Bovdyj I.V., Vinichenko E.V., Kobilyanskiy B.B.. Synthesis of an active shielding system of the magnetic field of power lines based on multiobjective optimization. *Electrical engineering & electromechanics*, 2016, no.6, pp. 26-30. (Rus). **doi: 10.20998/2074-272X.2016.6.05.**

5. Rozov V.Yu., Dobrodeyev P.N., Kvytsynskyi A.A. Double-circuit passive shielding of the magnetic field of high-voltage cable lines in junction zones. *Tekhnichna Elektrodynamika*, 2017, no.1, pp. 23-28. (Rus).

6. Opoleva G.N. *Skhemy i podstantsii elektrosnabzheniia. Spravochnik* [Schemes and substations of power supply. Directory]. Moscow, Forum-Infra Publ., 2006. 480 p. (Rus).

7. Alotto P., Guarnieri M., Moro F., Turri R. Mitigation of residential magnetic fields generated by MV/LV substations. *Universities Power Engineering Conference, 42nd International.* 2007, pp. 832-836. **doi: 10.1109/UPEC.2007.4469057.**

8. Rozov V.Yu. *Vneshnie magnitnye polia silovogo elektrooborudovaniia i metody ikh umen'sheniia* [External magnetic fields of power electrical equipment and methods for reducing them]. Kiev, The Institute of Electrodynamics Publ., 1995, no.772. 42 p. (Rus).

9. Rozov V. Yu., Erisov A.V., Lupikov V.S. *Osobennosti snizheniia vneshnikh magnitnykh polei raspredelitel'nykh ustroistv i poluprovodnikovykh preobrazovatelei* [Features of reducing external magnetic fields of switchgears and semiconductor converters]. Kiev, The Institute of Electrodynamics Publ., 1996, no.791. 46 p. (Rus).

10. Zautner F.L., Pilyugina O.Yu., Rozov V.Yu. Probabilistic method for predicting electromagnetic interference of electrical equipment in the low-frequency range. *Tekhnichna Elektrodynamika*, 1994, no.1, pp. 3-6. (Rus).

11. Rozov V.Yu. Construction of systems for automatic compensation of external magnetic fields of mobile objects containing ferromagnetic masses. *Tekhnichna Elektrodynamika. Thematic issue «Problems of modern electrical engineering»*, 2002, no.2, pp. 9-14. (Rus).

12. Rozov V.Yu., Getman A.V., Petrov S.V., Ericov A.V., Melanchenko A.H., Horoshilov V.S, Shmidt I.R. Magnetism of spacecraft. *Tekhnichna Elektrodynamika. Thematic issue «Problems of modern electrical engineering»*, 2010, no.2, pp. 144-147. (Rus).

13. Rozov V.Yu., Grinchenko V.S., Pelevin D.Ye., Chunikhin K.V. Simulation of electromagnetic field in residential buildings located near overhead lines. *Tekhnichna Elektrodynamika*, 2016, no.3, pp.6-9. (Rus).

14. Szabó J., Jánossy G., Thuróczy G. Survey of residential 50 Hz EMF exposure from transformer stations. *Bioelectromagnetics*, 2007, vol.28, no.6, pp. 48-52. **doi: 10.1002/bem.20264.**

15. Burnett J., Du Yaping P. Mitigation of extremely low frequency magnetic fields from electrical installations in high-rise buildings. *Building and Environment*, 2002, vol.37, no.8-9, pp. 769-775. **doi:10.1016/S0360-1323(02)00043-4.**

16. Shidlovskij A.K., Rozov V.Yu. Automatic compensation systems for external magnetic fields of energy-saturated objects. *Tekhnichna Elektrodynamika*, 1996, no.1, pp.3-9. (Rus).

17. Rozov V.Yu., Assuirov D.A., Reuckij S.Ju. Closed systems for compensation of the magnetic field of technical objects with different methods of feedback formation. *Tekhnichna Elektrodynamika. Thematic issue «Problems of modern electrical engineering»*, 2008, no.4, pp. 97-100. (Rus).

18. Rozov V.Yu., Assuirov D.A. The method of active shielding of the external magnetic field of technical objects. *Tekhnichna Elektrodynamika. Thematic issue «Problems of modern electrical engineering»*, 2006, no.3, pp. 13-16. (Rus).

19. Voloshko A.V. Synthesis of active shielding systems of power transmission lines magnetic field. *Visnyk Nac. Akad. Nauk Ukr.,* 2017, no.7, pp. 64-73. (Ukr). **doi: 10.15407/ visn2017.07.064.**

20. Cruz P., Riquelme J.M., de la Villa A., Martínez J.L. Ga-based passive loop optimization for magnetic field mitigation of transmission lines: neural network applications in electrical engineering. *Neurocomputing*, 2007, vol.70, no.16-18, pp. 2679-2686. **doi:10.1016/j.neucom.2006.05.016.**

21. del-Pino-López J.C., Giaccone L., Canova A., Cruz-Romero P. Design of active loops for magnetic field mitigation in MV/LV substation surroundings. *Electric Power Systems Research*, 2015, vol.119, pp. 337-344. **doi: 10.1016/j.epsr. 2014.10.019.**

22. Garzia F., Geri A. Active shielding design of indoor MV/LV substations using genetic algorithms optimization. *IEEE Symposium on Electromagnetic Compatibility*, 2003, vol.1, pp.197-202.

Received 12.08.2017

V.Yu. Rozov[1]*, Doctor of Technical Science, Corresponding member of NAS of Ukraine,*
D.Ye. Pelevin[1]*, Candidate of Technical Science,*
K.D. Pielievina[1]*, Postgraduate Student,*
[1] State Institution «Institute of Technical Problems of Magnetism of the NAS of Ukraine»,
19, Industrialna Str., Kharkiv, 61106, Ukraine,
phone: +380 572 992162,
e-mail: pelevindmitro@ukr.net

How to cite this article:
Rozov V.Yu., Pelevin D.Ye., Pielievina K.D. External magnetic field of urban transformer substations and methods of its normalization. *Electrical engineering & electromechanics*, 2017, no.5, pp. 60-66. **doi: 10.20998/2074-272X.2017.5.10.**

UDC 621.31 **doi: 10.20998/2074-272X.2017.5.11**

Yu.L. Sayenko, T.K. Baranenko, D.N. Kalyuzhniy

FEATURES OF SELECTION OF CAPACITOR BANKS IN ELECTRIC NETWORKS WITH INTERHARMONIC SOURCES

Purpose. Development of a methodology for selecting capacitor bank parameters designed to compensate for reactive power, if there are sources of interharmonics in the electrical network. Development of a methodology for selecting the parameters of capacitor banks that are part of resonant filters of higher harmonics and interharmonics. Methodology. For the research, we used the decomposition of the non-sinusoidal voltage (current) curve into the sum of the harmonic components with frequencies as multiple of the fundamental frequency - higher harmonics, and not multiple fundamental frequencies - interharmonics. Results. Expressions are obtained for checking the absence of inadmissible overloads of capacitor banks by voltage and current in the presence of voltage (current) in the curve, along with higher harmonics, of the discrete spectrum of interharmonics. When selecting capacitor banks, both for reactive power compensation and for filter-compensating devices, the necessity of constructing the frequency characteristics of the input and mutual resistances of the electrical network for analyzing possible resonant phenomena is confirmed. Originality. The expediency of simplified calculation of the voltage variation at the terminals of the banks of the capacitors of the higher harmonics filters and interharmonics due to the presence of the reactor in the filters is substantiated. Practical value. The use of the proposed approaches will make it possible to resolve a number of issues related to the choice of parameters of capacitor banks in networks with nonlinear loads, including: ensuring reliable operation of capacitor banks when their parameters deviate from their nominal values, as well as deviations in the parameters of the supply network and sources of harmonic distortion; ensuring the absence of resonant phenomena at frequencies of both higher harmonics and interharmonics. References 10.

Key words: **capacitor bank, reactive power compensation, filter-compensating device, higher harmonics, interharmonics**.

Разработана методика выбора батарей конденсаторов, применяемых как в качестве компенсаторов реактивной мощности при наличии источников интергармоник, так и в составе фильтров высших гармоник и интергармоник. Получены выражения для проверки отсутствия недопустимых перегрузок батарей конденсаторов по напряжению и по току при наличии в кривой напряжения (тока), наряду с высшими гармониками, дискретного спектра интергармоник. Обоснована целесообразность упрощенного учета изменения напряжения на зажимах батарей конденсаторов фильтров высших гармоник и интергармоник за счет наличия реактора в составе фильтров. Использование предложенных подходов позволит комплексно решать ряд вопросов, связанных с выбором параметров батарей конденсаторов в электрических сетях с нелинейными нагрузками. Библ. 10.

Ключевые слова: **батарея конденсаторов, компенсация реактивной мощности, фильтро-компенсирующее устройство, высшие гармоники, интергармоники.**

Introduction. Rational application of compensating devices in power supply systems allows to reduce power losses in the electric network (EN), to ensure the proper quality of the consumed electricity due to the normalization of voltage levels and, on the whole, allows achieving high technical and economic performance of electrical installations. Thus, the solution of the issues of reactive power compensation (RPC) is one of the aspects of both energy saving in EN and reliability of power supply to industrial enterprises [1-4].

Some of the most commonly used in power supply systems for various purposes of RPC devices are capacitor banks (CB), as they have a number of characteristic advantages: insignificant specific losses of active power, absence of rotating parts, simplicity of installation and operation, relatively low cost, low weight, time of work, the possibility of implementing an individual RPC [5, 6].

However, in modern EN there is a tendency to increase the number and power of nonlinear electric receivers. This is primarily a variety of frequency converters, rectifiers, inverters, DC drives and other semiconductor devices. Sharply varying loads are not only sources of voltage fluctuations, but also harmonic distortions of the current and voltage curves. In the presence of higher harmonics (HG) in the voltage curve, the aging process of the dielectric of capacitors proceeds more intensively than in the case when the capacitors operate at a sinusoidal voltage. This is explained by the fact that the physicochemical processes in dielectrics, which cause their aging, are significantly accelerated at high frequencies of the electric field. Analogously, the additional heating caused by the current of the HG current is affected. Depending on the frequency characteristics of the power supply systems, the CBs may be in a mode close to the resonance of the currents at the frequency of any of the HG [6-8]. Due to the overloads of the CB, they fail in the HG current. It should be noted that, depending on sources of distortion, a significant spectrum of interharmonics (IG) can be generated along with the HG, which, in accordance with the IEC standard, include harmonic oscillations with frequencies not multiples of the frequency of the supply network [6]. IG have a negative influence on the power supply systems [9]. Thus, the choice of CB parameters for non-sinusoidal modes should consist in preventing resonance modes at both the HG and IG frequencies and ensuring acceptable voltages on the capacitors and their allowable current loading. However, the question of the choice of CB parameters in the presence of IG is insufficiently investigated.

The goal of investigation is the development of a technique for selecting parameters of capacitor banks used both as reactive power compensators in the presence of sources of discrete spectrum of interharmonics, and in the composition of higher and interhamonic filters.

Statement of the main material. The technical conditions for the operation of the CB provide for limiting the excess of voltage and current above nominal values by certain values of c_u and c_i (in fractions of nominal values). So, according to international standards, capacitors must withstand the increased voltage of the network, which operates for a certain period of time. For example, the EN-60831-1/2 Standard specifies the requirements according to which at the industrial frequency the capacitor must withstand a voltage of $1.1U_{nom}$ up to 8 hours per day. In addition, the capacitors must be designed for continuous operation at current not exceeding $1.3I_{nom}$. Thus, the values of c_u and c_i are 1.1 and 1.3, respectively.

Then, if there are HG in the voltage curve a condition of absence of unacceptable overload of the CB by voltage [6]:

$$\frac{\sqrt{U_{CB}^2+\sum_{n=2}^{\infty}U_{nCB}^2}}{U_{nom,CB}}\le c_u, \qquad (1)$$

where U_{CB} is the voltage at the terminals of the CB at the industrial frequency (main harmonic voltage), in calculations it is allowed to use the nominal voltage of the CB $U_{nom,CB}$ as U_{CB}; n is the number of the harmonic component; U_{nCB} is the voltage of the n-th harmonic on capacitors.

The condition for excluding unacceptable overload of the CB by current:

$$\frac{\sqrt{I_{CB}^2+\sum_{n=2}^{\infty}I_{nCB}^2}}{I_{nom,CB}}\le c_i, \qquad (2)$$

where I_{CB} is the current of the industrial frequency in the CB (main harmonic current), as in the case of voltage, it is allowed in the calculations to use the rated current $I_{nom,CB}$ as I_{CB}; I_{nCB} is the current of the n-th harmonic flowing through CB.

If the discrete spectrum of the IG is present in the current and voltage curves, conditions (1) and (2) take the following form:

$$\frac{\sqrt{U_{CB}^2+\sum_{\substack{k=1\\ \nu_k\ne 1}}^{\infty}U_{\nu_k CB}^2}}{U_{nom,CB}}\le c_u; \qquad (3)$$

$$\frac{\sqrt{I_{CB}^2+\sum_{\substack{k=1\\ \nu_k\ne 1}}^{\infty}I_{\nu_k CB}^2}}{I_{nom,CB}}\le c_i, \qquad (4)$$

where k is the number of the harmonic component of the voltage and current curves, respectively; ν_k is the relative frequency of the k-th harmonic component (the value of ν_k at some k can coincide with the relative HG frequency n); $U_{\nu_k CB}$ is the voltage of the ν_k-th harmonic on capacitors; $I_{\nu_k CB}$ is the current of the ν_k-th harmonic flowing through CB.

For the practical application of the condition for the absence of unacceptable overloads of the CB by voltage and current, in the presence of a discrete spectrum of the IG along with the HG, it is advisable to reduce it to the following:

$$\sqrt{1+\frac{1}{U_{nom,CB}^2}\sum_{\substack{k=1\\ \nu_k\ne 1}}^{N}U_{\nu_k CB}^2}\le c_u; \qquad (5)$$

$$\sqrt{1+\frac{1}{I_{nom,CB}^2}\sum_{\substack{k=1\\ \nu_k\ne 1}}^{N}I_{\nu_k CB}^2}\le c_i, \qquad (6)$$

there N is the number of last harmonic taken into account.

In expressions (5) and (6), the number N should be determined by the frequency range, where the harmonics have the most significant amplitudes. In the general case, the values of N and ν_N will depend on the source of the IG.

Considering that the excess voltage at the terminals of the CB is allowed up to a value of cu (not more than 8 hours every 24 hours), and the permissible current overload to the value c_i=1.3; It is more convenient to transform (5) and (6) to the following form:

$$U_{nom,CB}\ge 2.2\sqrt{\sum_{\substack{k=1\\ \nu_k\ne 1}}^{N}U_{\nu_k CB}^2}; \qquad (7)$$

$$I_{nom,CB}\ge 1.2\sqrt{\sum_{\substack{k=1\\ \nu_k\ne 1}}^{N}I_{\nu_k CB}^2}. \qquad (8)$$

Verification of the absence of resonant modes during the operation of the CB connected to a network with non-sinusoidal sources can be performed by analyzing the frequency characteristics of the corresponding EN. Frequency characteristics of EN can be obtained both experimentally and by calculation. The method for calculating the resonant modes in EN involves the construction of a circuit for replacing the network under consideration, determining the parameters of the replacement circuit at harmonic frequencies and calculating the frequency characteristics of the input and mutual resistances (or conductances) of network nodes at harmonic frequencies [10].

On the basis of the obtained replacement scheme, a matrix of nodal conductivities of the EN at the frequency of the n-th harmonic is formed:

$$Y_{yn}=\begin{bmatrix} Y_{11n} & Y_{12n} & \cdots & Y_{1mn}\\ Y_{21n} & Y_{22n} & \cdots & Y_{2mn}\\ \vdots & & & \vdots\\ Y_{m1n} & Y_{m2n} & \cdots & Y_{mmn}\end{bmatrix}. \qquad (9)$$

Each of the diagonal elements of this matrix corresponds to a specific node of the system and is equal to the sum of the conductivities of all branches directly connected to this node. The off-diagonal elements are equal to the conductivities of the corresponding branches connecting the given pair of nodes taken with the minus sign. In the absence of such branches, the off-diagonal element is assumed to be zero.

The input resistance of the EN on the side of the node with the number i at the frequency of the n-th harmonic can be found as [10]

$$Z_{iin} = \frac{A_{iin}}{D_n}, \quad (10)$$

where D_n is the determinant of the matrix of nodal conductances (9) at the frequency of the n-th harmonic; A_{iin} is the algebraic complement of the determinant D_n.

Mutual (transfer) resistance of the i-th and j-th nodes of the EN at the frequency of the n-th harmonic is

$$Z_{ijn} = \frac{A_{ijn}}{D_n}, \quad (11)$$

where A_{ijn} is the algebraic complement of the determinant D_n.

Algebraic complements A_{iin} and A_{ijn} can be found as

$$A_{iin} = D_{iin}; \quad (12)$$

$$A_{ijn} = (-1)^{i+j} D_{ijn}, \quad (13)$$

where D_{iin} is the minor obtained from the determinant D_n deleting the i-th row and the i-th column; D_{ijn} is the the minor obtained from the determinant D_n deleting the i-th row and the j-th column.

At frequencies corresponding to the frequencies of the resonances of the currents, the values of the input and mutual resistances of the nodes will tend to infinity (if the active resistances are neglected). At resonances of currents, a relatively small harmonic current, whose frequency coincides with the resonance frequency, causes considerable stresses at the network nodes (due to large input and mutual resistances of the nodes). This leads to the flow of significant currents in the branches of the network and the overload of the CB.

Due to the fact that changes in the EN occur in the frequency characteristics of the input and mutual resistances caused by changes in the resistance of the mains power, the capacities and modes of the connected loads, and possible switchings in the circuit, it is necessary to take into account these factors and determine possible ranges of changes in the resonance frequencies.

The approach taken to the choice of CB parameters used for RPC is also valid for the selection of the CB that are part of the filter-compensating devices (FCD) used to reduce the voltage nonsinusoidal and, at the same time, the RPC.

The presence of the reactor in the composition of the filter changes the voltage at the terminals of the CB by a value that depends on the frequency of the filter setting ν [6],

$$U_{CB} = a_\nu U_{en}, \quad (14)$$

where U_{en} is the linear (phase) voltage of the electric network; a_ν is the voltage change coefficient.

Without account of the active resistance of the filter circuit

$$a_\nu = \frac{\nu^2}{\nu^2 - 1}. \quad (15)$$

Since all elements of the filter circuit have active resistance (terminals of capacitors, reactors, bus bars, cables, etc.), then taking into account the active resistance, the voltage change coefficient is determined by the expression [6]

$$a_\nu = \frac{\nu^2 tg\varphi_r}{\sqrt{tg^2\varphi_r\left(\nu^2 - 1\right)^2 + 1}}, \quad (16)$$

where $tg\varphi_r = x_r/R_f$; x_r is the filter reactor's resistance depending from the resonant condition; R_f is the total active resistance of the filter circuit.

The ratio x_r/R_f is the Q of the contour. Thus, we can write $tg\varphi_r = Q$. For the FCD of the HG $Q \geq 10$ [10], according to the investigations carried out for the FCD IG, especially installed in the low-frequency band, the inequality $Q \geq 10$ is also satisfied.

Calculations have shown that the determination of the coefficient a_ν from expression (15) gives an error in the direction of increase, in comparison with the coefficient a_ν determined by the expression (16), by not more than 1 % at Q=10, with the exception of the range $0.55 \leq \nu \leq 0.7$. In the indicated range, the maximum error for $\nu = 0.7$ is 1.9 %. As the quality factor increases, the error decreases significantly. So, for example, even at Q=20, the error of calculating a_ν from expression (15) for all frequencies entering the possible zones of the FCD IG unit is less than 1 %.

Thus, when choosing the nominal voltage of the CB of the IG filters, the coefficient a_ν should be determined in accordance with (15). In this case, a slight overestimation of the rated voltage is possible, which is preferable from the point of view of reliable operation of the CB filters when they are detuned.

Taking into account the expressions (5) and (14), the condition for the absence of an unacceptable overload of the CB of the FCD tuned to the frequency ν, by voltage:

$$\sqrt{a_\nu^2 k_U^2 + \frac{1}{U_{nom,CB}^2}\sum_{\substack{k=1 \\ \nu_k \neq 1}}^{N} U_{\nu_k CB}^2} \leq c_u = 1.1, \quad (17)$$

где $k_U = \frac{U_{en}}{U_{nom,CB}}$.

The CB current I_{CB} is proportional to the voltage on the bank U_{CB}, therefore we can write [10]

$$I_{CB} = I_{nom,CB} a_\nu k_U. \quad (18)$$

Substituting (18) into (6), after the transformations, we obtain the condition for the absence of an unacceptable overload of the CB of the FCD by current:

$$\sqrt{a_\nu^2 k_U^2 + \frac{1}{I_{nom,CB}^2}\sum_{\substack{k=1 \\ \nu_k \neq 1}}^{N} I_{\nu_k CB}^2} \leq c_i = 1.3. \quad (19)$$

Conclusions. When choosing capacitor banks for both reactive power compensation and filter-compensating devices, it is necessary to build the frequency characteristics of the input and mutual resistances of the electrical network for analyzing possible resonant phenomena, both in the node with the source of the interharmonics, and in all other nodes of the network. When building frequency characteristics, it is necessary to take into account the active resistances of the elements of the electrical network, which have

a significant effect on the impedance at resonance of currents.

When choosing the parameters of the filter capacitor banks, a complex solution of a whole range of issues is necessary including ensuring their reliable operation when the parameters of both the filters themselves and the power supply network are disturbed, sources of harmonic distortion from nominal ones; the absence of resonant phenomena at the frequencies of both higher harmonics and interharmonics. The solution of these questions requires: calculation of the spectral composition of the currents of the sources of higher harmonics and interharmonics, rational selection of the zone(s) for the installation of the filter-compensating device, as accurate as possible calculation of the actual frequency of the filter adjustment and the possible range of its deviations.

REFERENCES

1. Zaytsev I. M. On compensation of reactive power of electrical equipment. *Energy saving. Power engineering. Energy audit*, 2010, no.11, pp. 66-69. (Ukr).

2. Omelchuk A.O., Skripnik A.M., Trondyuk V.S. Concerning the balance of reactive power in power grids in the new normative conditions of jet energy flows in Ukraine. *Scientific Herald of National University of Life and Environmental Sciences of Ukraine. Series: Technique and energy of APK*, 2011, no. 161, pp. 111-119. (Ukr).

3. Seema Dudhe. Reactive Power Compensation Techniques in Transmission lines. *International Journal on Recent and Innovation Trends in Computing and Communication (IJRITCC)*, 2015, vol. 3, iss. 5, pp. 3224-3226.

4. Dixon J., Moran L., Rodriguez J., Domke R. Reactive Power Compensation Technologies: State-of-the-Art Review. *Proceedings of the IEEE*, 2005, vol.93, iss.12, pp. 2144-2164. **doi: 10.1109/JPROC.2005.859937**.

5. Davidov O.Yu., Byalobrzheskiy O.V. Analysis of reactive power compensation systems in electrical engineering systems. *Transactions of Kremenchuk Mykhaylo Ostrogradskiy State University*, 2010, no.3(62), pp. 132-136. (Ukr).

6. Zhezhelenko I.V., Saenko Yu.L. *Kachestvo elektroenergii na promushlennukh predpriiatiiakh* [Power quality in industrial plants]. Moscow, Energoatomizdat Publ., 2005. 261 p. (Rus).

7. Attachie J.C., Amuzuvi C.K. Using a Fixed and Switched-Capacitor Bank to Investigate Harmonic Resonance and Capacitor Bank Switching in a Distribution Network. *Research Journal of Applied Sciences, Engineering and Technology*, 2014, vol.7, iss.9, pp. 1900-1909. **doi: 10.19026/rjaset.7.480.**

8. Wilsun Xu, Xian Liu, Yilu Liu. Assessment of harmonic resonance potential for shunt capacitor applications. *Electric Power Systems Research*, 2001, vol.57, iss.2, pp. 97-104, **doi: 10.1016/S0378-7796(01)00092-X**.

9. Saenko Yu.L., Baranenko T.K., Baranenko E.V. Reduction of levels of harmonic distortions in electric networks with sources of interharmonics. *Electrification of transport*, 2012, no.3, pp. 78-83. (Ukr).

10. Zhezhelenko I.V., Saenko Yu.L., Baranenko T.K., Gorpinich A.V., Nesterovich V.V. *Izbrannye voprosy nesinusoidal'nykh rezhimov v elektricheskikh setiakh predpriiatii* [Selected issues of non-sinusoidal regimes in electric networks of enterprises]. Moscow, Energoatomizdat Publ., 2007. 296 p. (Rus).

Received 19.08.2017

Yu.L. Sayenko[1], *Doctor of Technical Science, Professor,*
T.K. Baranenko[1], *Candidate of Technical Science, Associate Professor,*
D.N. Kalyuzhniy[2], *Candidate of Technical Science, Associate Professor,*
[1] Pryazovskyi State Technical University,
7, Universytets'ka Str., Mariupol, 87500, Ukraine,
phone +380 629 446551,
e-mail: yls62@i.ua, tbaranenko@gmail.com
[2] O.M. Beketov National University of Urban Economy in Kharkiv,
12, Revolution Str., Kharkiv, 61002, Ukraine,
phone +380 57 7073117,
e-mail: KalyuzhniyDN@gmail.com

How to cite this article:
Sayenko Yu.L., Baranenko T.K., Kalyuzhniy D.N. Features of selection of capacitor banks in electric networks with interharmonic sources. *Electrical engineering & electromechanics*, 2017, no.5, pp. 67-70. **doi: 10.20998/2074-272X.2017.5.11.**

Матеріали приймаються за адресою:
Кафедра "Електричні апарати", НТУ "ХПИ", вул. Кирпичова, 21, м. Харків, 61002, Україна
Електронні варіанти матеріалів по e-mail: a.m.grechko@gmail.com

Довідки за телефонами: +38 050 653 49 82 Клименко Борис Володимирович
+38 067 359 46 96 Гречко Олександр Михайлович